

EFFICACY OF SOLIDWORKS FLOW SIMULATION
FOR USE IN THERMAL MANAGEMENT AND
PROPULSION SYSTEMS COOLING OF UNMANNED
AIRCRAFT SYSTEMS

By

KARIS L. REAVIS

Bachelor of Science

Oklahoma State University

Stillwater, Oklahoma

2017

Submitted to the Faculty of the
Graduate College of the
Oklahoma State University
in partial fulfillment of
the requirements for
the Degree of
MASTER OF SCIENCE
May 2021

EFFICACY OF SOLIDWORKS FLOW SIMULATION
FOR USE IN THERMAL MANAGEMENT AND
PROPULSION SYSTEMS COOLING OF UNMANNED
AIRCRAFT SYSTEMS

Thesis Approved:

DR. ANDREW ARENA

Thesis Adviser

DR. RICHARD GAETA

DR. JOSEPH CONNER

Name: Karis L. Reavis

Date of Degree: May 2021

Title of Study: EFFICACY OF SOLIDWORKS FLOW SIMULATION FOR USE IN
THERMAL MANAGEMENT AND PROPULSION SYSTEMS
COOLING OF UNMANNED AIRCRAFT SYSTEMS

Major Field: Mechanical and Aerospace Engineering

Abstract: As the capabilities of unmanned aircraft systems (UAS) expand, optimizing the thermal management designs become increasingly important. SOLIDWORKS Flow Simulation is a powerful and accessible tool that has the potential to accelerate prototyping for thermal management systems. This paper begins with analyzing a simple, flat plate, forced convection heat transfer problem using the software, and compares it to theoretical and experimental data. Once the baseline settings are determined, increasingly complex parameters needed to analyze an UAS are tested. The analysis proved to be capable of providing good qualitative results that predicted physical phenomena seen in experimental data given a fine enough mesh. However, there are many shortcomings and pitfalls in the software that a user must beware. Furthermore, good 3D analysis was difficult to achieve. Either providing only qualitatively good results or outright failing depending on the other settings. Therefore, it was determined that the software, if used carefully, is capable of analyzing certain 2D heat transfer problems, but further investigation is needed before using the software to analyze 3D models and eventually an UAS.

TABLE OF CONTENTS

Chapter	Page
I. INTRODUCTION	1
Evolution of UAS	1
Motivation	2
Objective	3
II. REVIEW OF LITERATURE	4
Flat Plate Forced Convection	4
Heat Transfer Coefficients	7
CFD Analysis	13
Summary	15
III. METHODOLOGY	16
Software	16
Problem Description	20
Settings	26
Result Processing	32
IV. FINDINGS	38
Settings	38
Fluid Flow and Heat Transfer	55
V. CONCLUSION.....	69
Suggestions and Future Work	71
VI. REFERENCES	73

Chapter	Page
VII. APPENDICES	78

LIST OF TABLES

Table	Page
Table 1: Summary of Literature Review	12
Table 2: Summary of flow types	22
Table 3: Summary of Flow Type test cases.....	23
Table 4: Test Case Matrix.....	23
Table 5: Dry air properties at 298.3 K and 1 atm.....	26
Table 6: Initial general settings	27
Table 7: Initial computational domain settings	28
Table 8: Final refinement settings summary	40
Table 9: Increase in cell count with Initial Refinement Level and Global Domain Level	42
Table 10: Final computational domain settings summary	45
Table 11: Final general settings summary	45
Table 12: General simulation results	79
Table 13: Flat plate parameters by simulation number.....	80
Table 14: Computational domain settings by simulation number	82
Table 15: Global Mesh settings by simulation number	84z

Table	Page
Table 16: Refinement settings by simulation number	87
Table 17: General settings by simulation number part 1	89
Table 18: General settings by simulation number part 2	93
Table 19: General solid settings by simulation number	98
Table 20: Comparison of predicted heat transfer coefficients for 2D-External-Constant Temperature	99
Table 21: Comparison of predicted heat transfer coefficients for 2D-External-Constant Heat Flux case.....	99
Table 22: Comparison of predicted heat transfer coefficients for 2D-Internal-Constant Temperature case	99
Table 23: Comparison of predicted heat transfer coefficients for 3D-Internal-Constant Temperature case	100

LIST OF FIGURES

Figure	Page
Figure 1: Boundary layer transition from laminar to turbulence transition and its effect on h	5
Figure 2: Initial Refinement Level of 1 (Left) versus Initial Refinement Level of 7 (Right)	17
Figure 3: Cell sizes ranging from zero refinements to four.....	18
Figure 4: Cell Count versus number of Refinements at Constant Global Domain Level .	19
Figure 5: Convergence of heat transfer coefficient.....	20
Figure 6: Plate Dimensions.....	24
Figure 7: Plate thickness effect on cell count.....	24
Figure 8: Overview of the Problem.....	25
Figure 9: Flat plate coordinate system	27
Figure 10: Initial refinement settings	28
Figure 11: Tunnel design for internal flow test case.....	30
Figure 12: Constant heat flux settings change.....	31
Figure 13: Changing analysis type from 2D to 3D	32

Figure	Page
Figure 14: Surface parameter used to obtain average heat transfer coefficient	33
Figure 15: XY Plot of the local heat transfer coefficient along the length of the plate	34
Figure 16: Pressure increase at leading edge of the plate	35
Figure 17: Equations used to calculate Shape Factor	36
Figure 18: Sketch used to obtain boundary layer velocities	36
Figure 19: Results summary where Total Cells was obtained	37
Figure 20: Convergence of the heat transfer coefficient with increase in Initial Refinement Level and Global Domain Level	39
Figure 21: Final Global mesh not including refinements during calculation	40
Figure 22: Convergence of heat transfer coefficient with increase in computational domain size in y+ and y- directions.....	43
Figure 23: Convergence of heat transfer coefficient with increase in computational domain size in y- direction.....	44
Figure 24: Thin airfoil leading edge separation bubble primary and secondary bubbles..	46
Figure 25: Primary and secondary leading-edge separation bubbles for laminar case at Re = 8.00E+04.....	47
Figure 26: Leading-Edge dimensions to keep flow from separating	48
Figure 27: Leading- Edge streamlines after altering the leading edge	48
Figure 28: Sketch of line along top surface	49
Figure 29: SOLIDWORKS Flow Simulation termination during 3D External Flow case	51

Figure	Page
Figure 30: Mesh refinement of External vs Internal Flow leading edge mesh	52
Figure 31: Cell Refinement in spanwise direction for 2D computational domain	53
Figure 32: Heat transfer coefficient along plate at $Re_L = 3.20 \times 10^5$ for 2D-Internal- Constant Temperature case	54
Figure 33: Average heat transfer coefficient's percent difference from theoretical predictions by Reynolds number	56
Figure 34: Average heat transfer coefficient's percent difference from experimental data by Reynolds number	57
Figure 35: Heat transfer coefficient along plate at $Re_L = 9.60 \times 10^6$ for 2D-External- Constant Temperature case	58
Figure 36: Heat transfer coefficient along plate at $Re_L = 5.60 \times 10^6$ for 2D-Internal- Constant Heat Flux case	59
Figure 37: Heat transfer coefficient along plate at $Re_L = 1.28 \times 10^6$ for 2D-External- Constant Temperature case	60
Figure 38: Shape factor along plate at $Re_L = 1.28 \times 10^6$ for 2D-External-Constant Temperature case	61
Figure 39: Heat transfer coefficient along plate at $Re_L = 8.00 \times 10^4$ for 2D-External- Constant Temperature case	62
Figure 40: Shape factor along plate at $Re_L = 8.00 \times 10^4$ for 2D-External-Constant Temperature case	63

Figure	Page
Figure 41: Heat transfer coefficient along plate at $Re_L = 1.28 \times 10^6$ for 2D-Internal-Constant Heat Flux case	64
Figure 42: Heat transfer coefficient along plate at $Re_L = 9.60 \times 10^6$ for 2D-External-Constant Temperature case	64
Figure 43: Average heat transfer coefficient's percent difference from theoretical predictions by Reynolds number for 3D-Internal-Constant Temperature case	65
Figure 44: Average heat transfer coefficient's percent difference from experimental data by Reynolds number for 3D-Internal-Constant Temperature case.....	66
Figure 45: Heat transfer coefficient along plate at $Re_L = 3.20 \times 10^5$ for 3D- Internal - Constant Temperature case	67
Figure 46: Heat transfer coefficient along plate at $Re_L = 5.60 \times 10^6$ for 3D-Internal-Constant Temperature case	67
Figure 47: Heat transfer coefficient along plate at $Re_L = 8.00 \times 10^4$ for 2D-Internal-Constant Heat Flux case	100
Figure 48: Heat transfer coefficient along plate at $Re_L = 3.20 \times 10^5$ for 2D-Internal-Constant Heat Flux case	101
Figure 49: Heat transfer coefficient along plate at $Re_L = 9.60 \times 10^6$ for 2D-Internal-Constant Heat Flux case	101
Figure 50: Heat transfer coefficient along plate at $Re_L = 3.20 \times 10^5$ for 2D-External-Constant Temperature case	102

Figure	Page
Figure 51: Heat transfer coefficient along plate at $Re_L = 5.60 \times 10^6$ for 2D-External- Constant Temperature case	102
Figure 52: Heat transfer coefficient along plate at $Re_L = 8.00 \times 10^4$ for 2D-Internal- Constant Temperature case	103
Figure 53: Heat transfer coefficient along plate at $Re_L = 1.28 \times 10^6$ for 2D-Internal- Constant Temperature case	103
Figure 54: Heat transfer coefficient along plate at $Re_L = 5.60 \times 10^6$ for 2D-Internal- Constant Temperature case	104
Figure 55: Heat transfer coefficient along plate at $Re_L = 9.60 \times 10^6$ for 2D-Internal- Constant Temperature case	104
Figure 56: Heat transfer coefficient along plate at $Re_L = 8.00 \times 10^4$ for 3D-Internal- Constant Temperature case	105
Figure 57: Heat transfer coefficient along plate at $Re_L = 3.20 \times 10^6$ for 3D-Internal- Constant Temperature case	105
Figure 58: Heat transfer coefficient along plate at $Re_L = 1.28 \times 10^6$ for 3D-Internal- Constant Temperature case	106
Figure 59: Heat transfer coefficient along plate at $Re_L = 5.60 \times 10^6$ for 3D-Internal- Constant Temperature case	106
Figure 60: Heat transfer coefficient along plate at $Re_L = 9.60 \times 10^6$ for 3D-Internal- Constant Temperature case	107

Figure	Page
Figure 61: Temperature along plate at $Re_L = 8.00 \times 10^4$ for 2D-Internal-Constant Heat Flux case.....	107
Figure 62: Temperature along plate at $Re_L = 3.20 \times 10^5$ for 2D-Internal-Constant Heat Flux case.....	108
Figure 63: Temperature along plate at $Re_L = 1.28 \times 10^6$ for 2D-Internal-Constant Heat Flux case.....	108
Figure 64: Temperature along plate at $Re_L = 5.60 \times 10^6$ for 2D-Internal-Constant Heat Flux case.....	109
Figure 65: Temperature along plate at $Re_L = 9.60 \times 10^6$ for 2D-Internal-Constant Heat Flux case.....	109
Figure 66: Shape factor along plate at $Re_L = 3.20 \times 10^5$ for 2D-External-Constant Temperature case	110
Figure 67: Shape factor along plate at $Re_L = 5.60 \times 10^6$ for 2D-External-Constant Temperature case	110
Figure 68: Shape factor along plate at $Re_L = 9.60 \times 10^6$ for 2D-External-Constant Temperature case	111
Figure 69: Shape factor along plate at $Re_L = 8.00 \times 10^4$ for 2D-External-Constant Temperature case	111
Figure 70: Shape factor along plate at $Re_L = 3.20 \times 10^5$ for 2D-External-Constant Temperature case	112

Figure	Page
Figure 71: Shape factor along plate at $Re_L = 5.60 \times 10^6$ for 2D-Internal-Constant Temperature case	112
Figure 72: Shape factor along plate at $Re_L = 5.60 \times 10^6$ for 2D-Internal-Constant Temperature case	113
Figure 73: Shape factor along plate at $Re_L = 9.60 \times 10^6$ for 2D-Internal-Constant Temperature case	113
Figure 74: Shape factor along plate at $Re_L = 8.00 \times 10^4$ for 2D-External-Constant Heat Flux case.....	114
Figure 75: Shape factor along plate at $Re_L = 3.20 \times 10^5$ for 2D-External-Constant Heat Flux case.....	114
Figure 76: Shape factor along plate at $Re_L = 1.28 \times 10^6$ for 2D-External-Constant Heat Flux case.....	115
Figure 77: Shape factor along plate at $Re_L = 5.60 \times 10^6$ for 2D-External-Constant Heat Flux case.....	115
Figure 78: Shape factor along plate at $Re_L = 9.60 \times 10^6$ for 2D-External-Constant Heat Flux case.....	116
Figure 79: Shape factor along plate at $Re_L = 8.00 \times 10^4$ for 3D-Internal-Constant Temperature case	116
Figure 80: Shape factor along plate at $Re_L = 3.20 \times 10^5$ for 3D-Internal-Constant Temperature case	117

Figure	Page
Figure 81: Shape factor along plate at $Re_L = 1.28 \times 10^6$ for 3D-Internal-Constant	
Temperature case	117
Figure 82: Shape factor along plate at $Re_L = 5.60 \times 10^6$ for 3D-Internal-Constant	
Temperature case	118
Figure 83: Shape factor along plate at $Re_L = 9.60 \times 10^6$ for 3D-Internal-Constant	
Temperature case	118

CHAPTER I

INTRODUCTION

EVOLUTION OF UAS

Although there has been an explosion in unmanned aircraft usage in military application in recent decades: one of the first recorded uses is over a century ago. In July of 1849 Austrian forces, attempting to capture Venice, launched 200 balloons carrying explosives over the city. This early UAS was not particularly successful however, as the winds changed after launch resulting in most balloons detonating outside the city. However, as technology has improved the interest in and success of UAS has increased significantly.

The more modern roots of UAS appears more recently with the U.S drone program beginning in 1936 after U.S. Admiral William Harrison Standley watched the Queen Bee, a military drone designed for target practice by the British, fly and saw its potential in warfare. However, the primary use of these early unmanned aircraft was for target practice. It was not until the late 1960s and early 1970s when the U.S realized that the unmanned aircraft would be particularly useful for reconnaissance missions. This led to the development of the Ryan Model 137 “Lightning Bug”, which saw great success in the Vietnam War. [1]

The 1980s and 1990s saw advances in technology that drastically improved the reliability and performance of UAS with faster communication speed and Global Positioning System (GPS).

Now, data could be gathered even if the UAS was unable to return to the base, faster video speeds meant that pilots could more easily control the aircraft, and GPS drastically extended the range of the aircraft's missions. This led to enormous growth of UAS during the 2000's, and between 2002 and 2008 the Department of Defense (DoD) grew the number of unmanned aircraft from 167 to over 6,000. [1]

The 2010s saw an increased interest in recreational and commercial use of UAS with talk of large corporations using them for delivery, agriculture, construction, and more. [2] Today there are over 11,000 military drones [3] and 800,000 UASs registered with the FAA [4], but the increased use of drones looks to continue. Non-military UAS applications are expected to triple from 2019 through 2029 and around \$455 million was invested into companies developing the technology in 2018 alone. [5] In military applications the UAS research budget was over \$4 billion in 2017, and some expect the budget to increase to \$13 billion by 2027.

The need for UAS is large and growing. Many important uses for them are already known, but there may be more undiscovered. To push the boundaries of what is possible for these devices, there is a lot of research left to be done over many fields of study. This makes being able to rapidly prototype and test invaluable for developing new UAS.

MOTIVATION

Thermal management is a field of study within UAS that will continually need improved as engineers push the boundaries of UASs. Increasing the aircraft's capabilities with more electronics, more powerful engines, desire for smaller inlets to reduce drag, and methods to lower noise are all important to the success of the UAS but are at odds with the thermal management system. [6]

Failure to properly cool the aircraft can result in reduced engine efficiency, electronics malfunction, or even engine failure. While obviously undesirable, determining whether the thermal management system is properly optimized during the design phase is difficult. Furthermore, many applications desire rapid prototyping and testing such as in academic research and the best solution for cooling the system can vary greatly depending on the size, shape, and performance of the aircraft. SOLIDWORKS may be particularly helpful in academic research into UASs as well since it is commonly taught for 3D modeling as part of undergraduate curriculum, and many engineers are already familiar with the software. Also, the model can be easily reused for other things such as manufacturing or structural analysis.

The use of CFD for thermal management analysis has high potential because many different variations can be tested quickly and cheaply and it has already revolutionized much of the aircraft design process such as for airfoils, turbine blades, and aircraft bodies. [7] It is highly likely that some CFD software is already being used to solve similar problems, but this paper specifically evaluates SOLIDWORKS CFD software called SOLIDWORKS Flow Simulation.

OBJECTIVE

This paper aims to validate the use of SOLIDWORKS Flow Simulation for qualitatively or quantitatively analyzing the thermal management systems of an UAS. Since analyzing a full UAS is very complex and can't be easily compared to known benchmarks, the software will first be validated against basic heat transfer problems with experimental and theoretical data to compare against. Once the optimal settings are found and the data is validated against the benchmarks, another slightly more complex problem is then analyzed. Finally, the results will be analyzed to determine whether the software adequately evaluates the problem or where it fails.

CHAPTER II

REVIEW OF LITERATURE

FLAT PLATE FORCED CONVECTION

To fully analyze SOLDIWORKS ability to capture the physical mechanisms of the flow, three different flow types must be considered: laminar, turbulent, and mixed. In laminar flow, the fluid moves as a uniform sheet with little vertical motion or vorticity. This results in a small amount of heat transfer when compared to turbulent flow. Turbulent flow is characterized by randomness and vorticity, resulting in more interaction between the heated plate and the fluid. The increase in interaction between the plate and fluid results in a higher heat transfer coefficient. Since the Reynolds number at the start of the plate is 0 and increases along the length of the plate, there will always be some amount of laminar flow. However, if the flow is turbulent for the 90% of the plate then it will be analyzed as fully turbulent. The case where the flow has significant portions of both laminar and turbulent flow is considered mixed flow. Reynolds number is the ratio of inertial forces to viscous force, which is why it is often used to predict when the flow will transition from laminar to turbulent flow.

The faster the fluid velocity the greater the influence the inertial forces take over and the greater the likelihood of the flow transitioning to turbulent flow. The change is not instantaneous, there is a period between laminar and turbulent where the flow is in transition. In this transition

phase, the heat transfer coefficient quickly rises to that of turbulent flow. This change usually starts occurring at a Reynolds number of around 10^5 and does not typically become fully turbulent until a Reynolds number of 3×10^6 . The characteristics of the transition from laminar to turbulent are hard to predict and so for general analysis on flat plate flow, 5×10^5 is often used as the critical Reynolds number or the Reynolds number at which the flow becomes turbulent. [8]

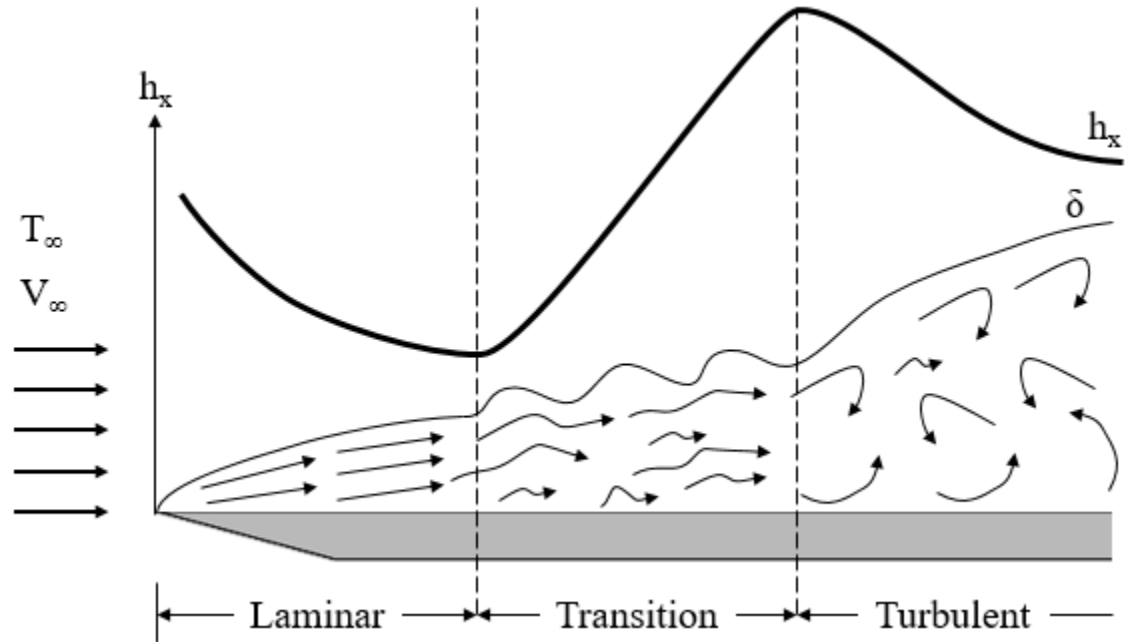


Figure 1: Boundary layer transition from laminar to turbulence transition and its effect on h

Figure 1 shows the transition from laminar flow to turbulent flow. For heat transfer, the transition to turbulent flow results in a sharp increase in the heat transfer coefficient. In the results examination, regions where the heat transfer coefficient increases dramatically will be assumed to be transitioning to turbulent flow.

The equation used to calculate Reynolds number at a point, x , along a flat plate is shown below. In this equation, V_∞ is the freestream velocity, x is the distance along the length of the plate, and ν is the kinematic viscosity at the film temperature.

$$Re_x = \frac{V_\infty x}{\nu}$$

The film temperature, T_{film} , is the average of the temperature of the plate, T_{plate} , and of the freestream air, T_∞ . It is commonly used to determine what air property values to use when predicting convective heat transfer. The equation is shown below.

$$T_{film} = \frac{T_{plate} + T_\infty}{2}$$

The properties of air that are taken at the film temperature for calculations are the kinematic viscosity, ν , the Prandtl number, Pr , and the thermal conductivity, k . These properties will be needed in order to calculate the heat transfer coefficient using the equations for Nusselt number describes in the following section. The equations to get the local and average heat transfer coefficients are shown below.

$$h_x = \frac{Nu_x k}{x}$$

$$h = \frac{Nu k}{L}$$

The process used to calculate the average convective heat transfer coefficient of the constant temperature flat plate used to validate SOLIDWORKS Flow Simulations is as follows:

1. Calculate the film temperature
2. Look up properties of air at 1 atm pressure and the film temperature

3. Calculate the Reynolds number
4. Approximate the Nusselt number using the equations discussed in the following section
5. Calculate the heat transfer coefficient

The process used to calculate the average convective heat transfer coefficient of the constant heat flux flat plate is similar, but since the temperature of the plate is not known beforehand to obtain the film temperature, the temperature of the plate needs to be estimated, then validated once the heat transfer coefficient is obtained. Thus, the steps for the process are as follows:

1. Estimate the temperature of the plate
2. Calculate the film temperature using the estimated plate temperature
3. Look up the properties of air at 1 atm pressure and the film temperature
4. Calculate the Reynolds number
5. Approximate the Nusselt number using the equations discussed in the following section
6. Calculate the heat transfer coefficient
7. Calculate the temperature along the plate and verify that it is near the estimated temperature

HEAT TRANSFER COEFFICIENTS

Analysis of convective heat transfer over an isothermal flat plate is split into three categories: laminar, turbulent, and mixed. Laminar describes smooth flow, moving parallel in layer. Turbulent describes flow that is full of energy and vorticity, whose motion appears random. Mixed describes flow that starts laminar and transitions into turbulent.

According to Cengel and Ghajar, the flow over a flat plate can be considered laminar when the Reynolds number is below 5×10^5 , which is known as the critical Reynolds number. [8] Other articles analyzed use different critical Reynolds number; however, the actual transition number is very case dependent and tend to be relatively close together. In experimental cases, the flow tends to transition earlier since the environment is not perfectly controlled and there is some inherent turbulence.

In Cengel and Ghajar's book, the energy equation is solved using boundary layer approximations and a similarity variable to obtain a local Nusselt number for laminar and turbulent flow. The equations are shown below.

$$Nu_x = \frac{h_x x}{k} = 0.332 Re_x^{\frac{1}{2}} Pr^{\frac{1}{3}}$$

$$Nu_x = \frac{h_x x}{k} = 0.0296 Re_x^{0.8} Pr^{\frac{1}{3}}$$

The equation for laminar flow is valid when the Prandtl number is greater than 0.6. The equation for turbulent flow is valid when the Prandtl number is greater than 0.6 and less than 60 and for Reynolds numbers between 5×10^5 and 10^7 . [8]

If the average heat transfer coefficient can be found, h, then then the average Nusselt number can be determined. The average Nusselt number equations for laminar and turbulent flow are shown below.

$$Nu = \frac{hx}{k} = 0.664 Re_L^{\frac{1}{2}} Pr^{\frac{1}{3}}$$

$$Nu = \frac{hx}{k} = 0.037 Re_L^{0.8} Pr^{\frac{1}{3}}$$

These equations are valid for the same Prandtl number and Reynolds number regimes their local counterparts are valid for.

If the flow is mixed, meaning it contains both laminar and turbulent flow, the equations can be combined to form the following equation.

$$Nu = \frac{hx}{k} = (0.037Re_L^{0.8} - 871)Pr^{\frac{1}{3}}$$

This equation is valid when the Prandtl number is greater than 0.6 and less than 60 and for Reynolds numbers between 5×10^5 and 10^7 . This equation ignores the phase of the flow where it transitions from laminar to turbulent, assuming the transition is instantaneous. [8]

Whenever the plate is kept at a constant heat flux instead of temperature, laminar and turbulent local Nusselt number equations then respectively become:

$$Nu_x = \frac{h_x x}{k} = 0.453Re_x^{\frac{1}{2}}Pr^{\frac{1}{3}}$$

$$Nu_x = \frac{h_x x}{k} = 0.0308Re_x^{0.8}Pr^{\frac{1}{3}}$$

The average Nusselt numbers for laminar and turbulent flow can then be calculated to be the following: [8]

$$Nu = \frac{hx}{k} = 0.906Re_L^{\frac{1}{2}}Pr^{\frac{1}{3}}$$

$$Nu = \frac{hx}{k} = 0.0385Re_L^{0.8}Pr^{\frac{1}{3}}$$

Jurges found that the average heat transfer coefficient for a 0.5 m x 0.5 m copper flat plate could be calculated using the following equation. [9]

$$h = 5.7 + 3.8V$$

However, Watmuff et al. proposed that the equation developed by Jurges also included radiation effects, and so gave a new average convective heat transfer coefficient. [10]

$$h = 2.8 + 3.0V$$

Sharples and Charlesworth analyzed the heat transfer properties of a flat plate mounted to the roof of a house that mimicked a solar collector at varying angles of attack. For the purpose of this study only the 0° angle of attack case will be analyzed. The flat plate was electrically heated and 1.81 m x 0.89 m. They found the following correlation for the average convective heat transfer coefficient of a flat plate. [11]

$$h = 9.4V^{0.5}$$

However, Satori analyzed the previous equations and determined that only the equations developed with boundary layer theory should be used to predict the heat transfer coefficient since the experimentally determined equations are not based on the physical processes at hand and only mathematically represent the exact experimental setup tested. Any small changes to the system could have large effects on the flow. [12] This sentiment is supported by Sharples and Charlesworth who also suggest that the data they gathered is only applicable to their experiment. [11]

Edwards and Furber, who were not examined by Satori, account for more of the physical processes in their data gathering. Not only do they suggest equations for both laminar and turbulent flow, they also consider the free stream turbulence up to 5%. They found that up to 5% free stream turbulence had little impact on the convective heat transfer coefficient. They

developed two equations for Nusselt number based on the data they gathered, one for laminar flow, and one for turbulent flow. The Nusselt equations for laminar and turbulent flow are listed below in order. The turbulent case is valid for Reynolds numbers of 1.5×10^5 - 2.5×10^6 and the Laminar case is valid for Reynolds numbers of 6×10^4 - 3×10^5 . [13]

$$Nu_{Laminar} = 0.39Re^{0.535}$$

$$Nu_{Turbulent} = 0.038Re^{0.786}$$

A summary of the results can be found in Table 1. Satori found that if the physical processes were not accounted for, the heat transfer coefficients gathered could only be used for the specific setup and not as a general rule. Therefore, Sharples and Charlesworth, Watmuff et al., and Jurges will not be used in the analysis. However, both the experimental data gathered by Edwards and Furber as well as the theoretical data gathered by Cengal and Ghajar include the physical processes in their analysis and will be used in the final analysis.

CFD Analysis

Literature Review Equation Summary				
Authors	Equation	Theoretical or Experimental	Flow Type	Used in Analysis ?
Cengal and Ghajar	$Nu_x = \frac{h_x x}{k} = 0.332 Re_x^{\frac{1}{2}} Pr^{\frac{1}{3}}$	Theoretical	Laminar	Yes
Cengal and Ghajar	$Nu_x = \frac{h_x x}{k} = 0.0296 Re_x^{0.8} Pr^{\frac{1}{3}}$	Theoretical	Turbulent	Yes
Cengal and Ghajar	$Nu = \frac{hx}{k} = 0.664 Re_L^{\frac{1}{2}} Pr^{\frac{1}{3}}$	Theoretical	Laminar	Yes
Cengal and Ghajar	$Nu = \frac{hx}{k} = (0.037 Re_L^{0.8} - 871) Pr^{\frac{1}{3}}$	Theoretical	Mixed	Yes
Cengal and Ghajar	$Nu = \frac{hx}{k} = 0.037 Re_L^{0.8} Pr^{\frac{1}{3}}$	Theoretical	Turbulent	Yes
Cengal and Ghajar	$Nu_x = \frac{h_x x}{k} = 0.453 Re_x^{\frac{1}{2}} Pr^{\frac{1}{3}}$	Theoretical	Laminar	Yes
Cengal and Ghajar	$Nu_x = \frac{h_x x}{k} = 0.0308 Re_x^{0.8} Pr^{\frac{1}{3}}$	Theoretical	Turbulent	Yes
Cengal and Ghajar	$Nu = \frac{hx}{k} = 0.906 Re_L^{\frac{1}{2}} Pr^{\frac{1}{3}}$	Theoretical	Laminar	Yes
Cengal and Ghajar	$Nu = \frac{hx}{k} = 0.0385 Re_L^{0.8} Pr^{\frac{1}{3}}$	Theoretical	Turbulent	Yes
Jurges	$h = 5.7 + 3.8V$	Experimental	Mixed	No
Watmuff et al.	$h = 2.8 + 3.0V$	Experimental	Mixed	No
Sharples and Charlesworth	$h = 9.4V^{0.5}$	Experimental	Mixed	No
Edwards and Furber	$Nu_{Turbulent} = 0.038 Re^{0.786}$	Experimental	Turbulent	Yes
Edwards and Furber	$Nu_{Laminar} = 0.39 Re^{0.535}$	Experimental	Laminar	Yes

Table 1: Summary of Literature Review

CFD ANALYSIS

CFD is desirable for use in heat transfer analysis since the complexity of most modern designs are complex and difficult to solve accurately without it. However, since CFD can be complex to set up itself and can potentially lead to faulty conclusions if used incorrectly, research was done into examples of using CFD for similar types of problems.

An older example of CFD heat transfer analysis is in Lee's Paper "Application of CFD Technology to Electronic Thermal Management," which used FLOTHERM, a CFD tool, to estimate heat flow of electronic devices. The electronics they analyzed were small electronics that were cooled using free convection. This article looks at two different studies. One study looked at a portable, handheld electronic device and the other looked at a multichip module. The main objective of the article was to test whether the FLOTHERM CFD software was capable of accurately modeling the convective heat transfer of small electronic devices. The software FLOTHERM was built specifically for electronic devices; however, it was not capable of handling complex geometries, and took a very long time to run. [14]

The results of the first study were that the computation temperatures were very close those measured in the experiment. The max temperature calculated by the software was 98.5°C which was only 6.4% away from the measured value of 92.6°C. The velocities of the flow were also calculated, but there were no experimental results to validate against. The author assumed the velocity field to be adequate since the max temperatures were similar. [14]

More recently, CFD heat transfer studies have been performed on aircraft such as in "Simplified Thermo-Fluid Model of an Engine Cowling in a Small Airplane" by Łapka et al. [15] They used the software to simulate the conduction, convection and radiative heat transfer of a

small engine cowling to improve future selection of materials and cooling methods. Although similar studies had been performed, they had assumed that radiation was negligible. Łapka et al.'s study includes radiation in the simulation and aimed to see whether it effected the flow. [15]

The simulation simply consists of the front of the plane, with most of the body and wings left out. The air comes in through two intakes at the front of the nose and through the nose of the aircraft behind the propeller mount, flows over the engine, and exits under the aircraft primarily through the exhaust but through the landing gear area as well.

The results were as expected. The case where air intake was not allowed through the inlets around the propeller mouth and air outlets weren't allowed through the landing gear area resulted in the highest temperatures, whereas when both were allowed resulted in the lowest temperatures. The highest temperature values were located just above the engine and near the covers of the exhaust vane. The study also found that neglecting radiation reduced the temperature of the nacelle by up to 10 K, and thus the author concluded that taking radiation into account was recommended when simulating the model.

Driss et al. used SOLIDWORKS Flow Simulation to model the flow around a small incurved Savonius wind rotor. Savonius rotors are used to harness wind energy in a manner like windmills, but with the advantage of being cheaper and simpler. The goal of the study was to validate analyze incurved Savonius wind rotors. [16] The paper found that the incurved Savonius rotor improved upon the curved Savonius rotor and shows the usefulness and some of the potential of SOLIDWORKS Flow Simulation.

SUMMARY

Although there are many methods for analyzing heat transfer, with many experiments having been performed on flat plates to refine our ability to predict convection heat transfer coefficients, CFD is still necessary due to its ability to solve complex heat transfer systems. It has been used as a tool for a long time, but as technology and software evolves there is continually a need to validate the new software's ability to solve more complex problems more efficiently.

SOLIDWORKS Flow Simulation has been shown to effectively analyze certain fluid flow problems [16], but few studies have analyzed its ability to solve heat transfer problems and specifically those regarding UAVs. Although no direct comparison to a UAV is made in this paper, it aims to fill in that gap in knowledge by comparing SOLIDWORKS Flow Simulation to theoretical and experimental heat transfer data building the foundation so that future papers can adequately validate the software against UAV experiments.

CHAPTER III

METHODOLOGY

SOFTWARE

SOLIDWORKS Flow Simulation solves the flow numerically, using the Favre-Averaged Navier-Stokes equations and the κ - ϵ model, by breaking down the computational domain into finite cells, and solving the flow properties for each cell. Therefore, the smaller the cells, the more accurately the simulation will approximate real-life flow. However, the decreasing cell size exponentially increase the time required to find a solution since the number of cells dramatically increases. In order to maximize the accuracy of the solution while minimizing the time required the mesh can be altered. Decreasing the size of the cells near areas of interest ensures that computational resources are not wasted on areas where a courser mesh is sufficient. This can be done two ways. The first is through setting the level of initial mesh. The level can range from 1 to 7 and defines the initial density of the mesh. 1 resulting in the largest cell size and 7 the smallest. If the analysis type is external, then an additional setting called “Ratio Factor” can be used to decrease the cell size as the mesh approaches the solid model. This results in a courser mesh farther away from the model where the flow is typically more uniform and a finer mesh close to the model where there are more complex flows. However, sometimes sharp gradients in the flow are still not captured accurately enough in the initial mesh. In such a case, the flow can be refined.

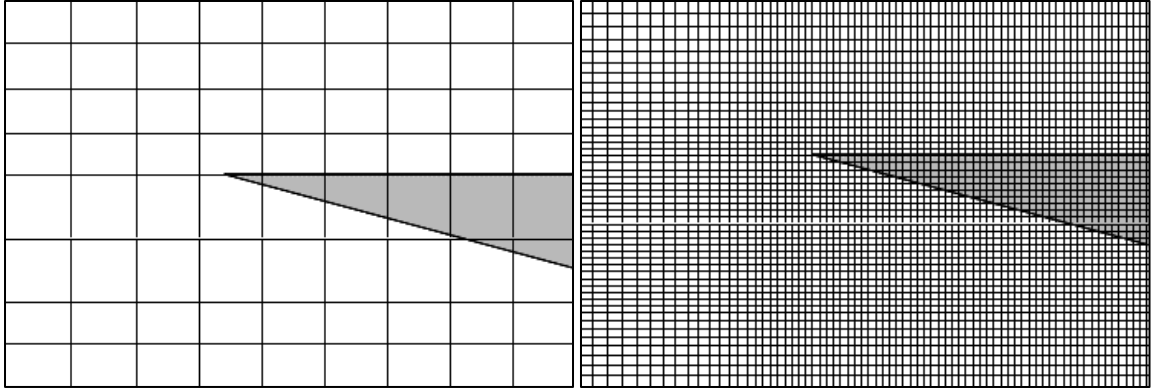


Figure 2: Initial Refinement Level of 1 (Left) versus Initial Refinement Level of 7 (Right)

Figure 2 shows the effect the Initial Refinement Level has on the mesh size. The picture on the left shows the mesh at an Initial Refinement Level of 1. At this point the mesh is still relatively coarse and too small to accurately capture some of the small fluid mechanics that will affect the flow. The Ratio Facto does create a finer mesh near the solid, but this is still not adequate for calculation. The picture on the right shows the maximum Initial Refinement Level of 7. This level makes the mesh much finer but is still likely not fine enough and decreases the cell size in areas of uniform flow where a fine mesh is not needed. However, this can be solved by refining the mesh further during calculation in areas that require a finer mesh.

Since the software is not aware of the flow beforehand, refinements can only occur during the calculation. Refinements divide the cells into eight cells near sharp gradients in the flow where smaller cells are needed. More cell refinements, like the level of initial mesh, exponentially increases the time required to find a solution. Therefore, a balance between accuracy and computation time are also needed here. The number of refinements is defined by the Global Domain Level and the Approximate Maximum Cells. The refinement level can be given a value from 1 to 7 or set to disabled. The number represents the number of times a cell can be divided into eight smaller cells, with the disabled setting resulting in no cell divisions. This is also

capable of producing a mesh far finer than the Initial Refinement Level can produce and is therefore necessary for many flows.

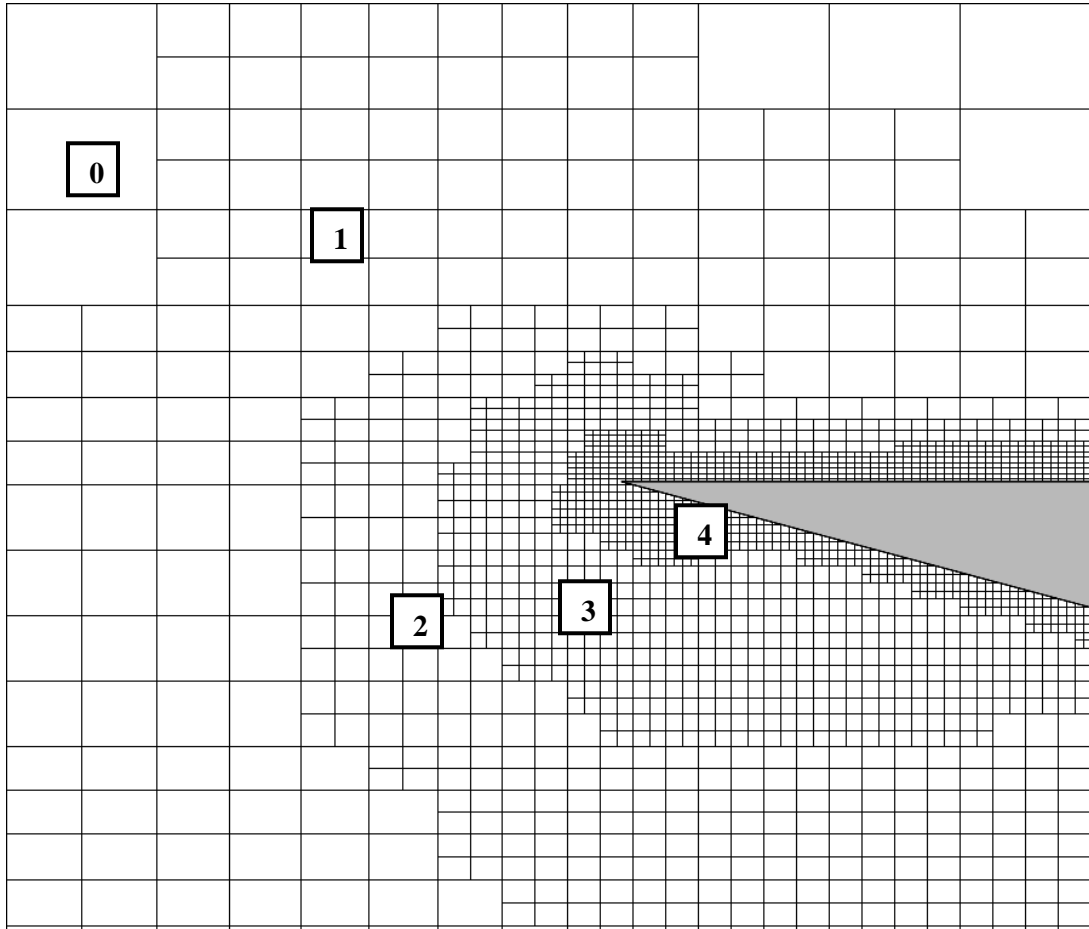


Figure 3: Cell sizes ranging from zero refinements to four

The approximate maximum cells setting does as the name suggests and defines the approximate maximum number of cells in the computational domain. SOLIDWORKS Flow Simulation will then refine the flow to solve resolve the complex areas as best it can, while remaining near or under the approximate maximum cells defined by the user. If the approximate maximum cells setting is exceeded the following refinements will be limited. This can be seen in Figure 3, where the number of cells approaches the Approximate Maximum Cells rather than

growing exponentially. The timing of when the refinement occurs is also important. The software should converge on a solution before refinement so that the refinements can be made where they are most needed. Refinements can be performed manually after the user determines the flow has converged, or a refinement strategy can be defined to run automatically. For this study, an automatic strategy is used. The flow is refined periodically based on the number of travels. There are then two setting that can be adjusted: the travels before the first refinement and the travels between refinements after that. The software should ideally converge on a single solution, or a solution that repeats periodically. To monitor the solution, goals can be chosen and displayed during the calculation process.

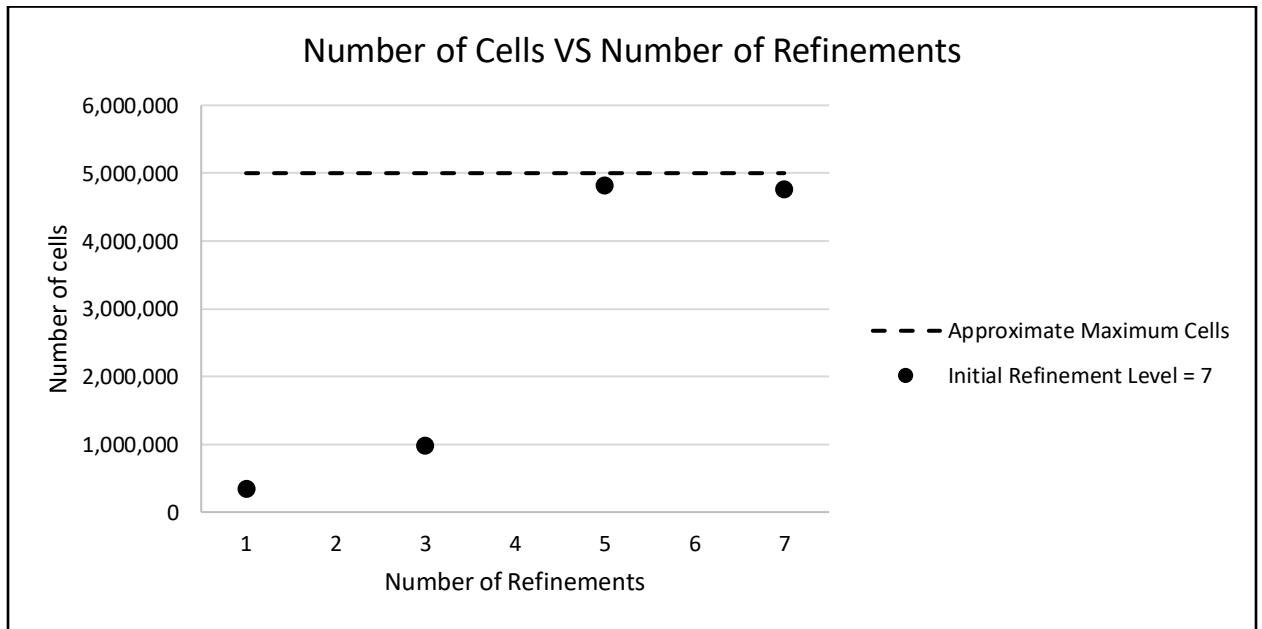


Figure 4: Cell Count versus number of Refinements at Constant Global Domain Level

Monitoring the convergence is important because the small complexities in the flow can have a significant impact on the solution. If software has not been defined well enough to accurately capture these effects of the flow, then the solution has not converged and needs to be

refined further. This can be misleading if not careful as the flow can appear to converge, then upon refinement the results can change since the software is now capturing more of the flow effects. The solution can be considered converged once further refinements of the flow no longer change the result.

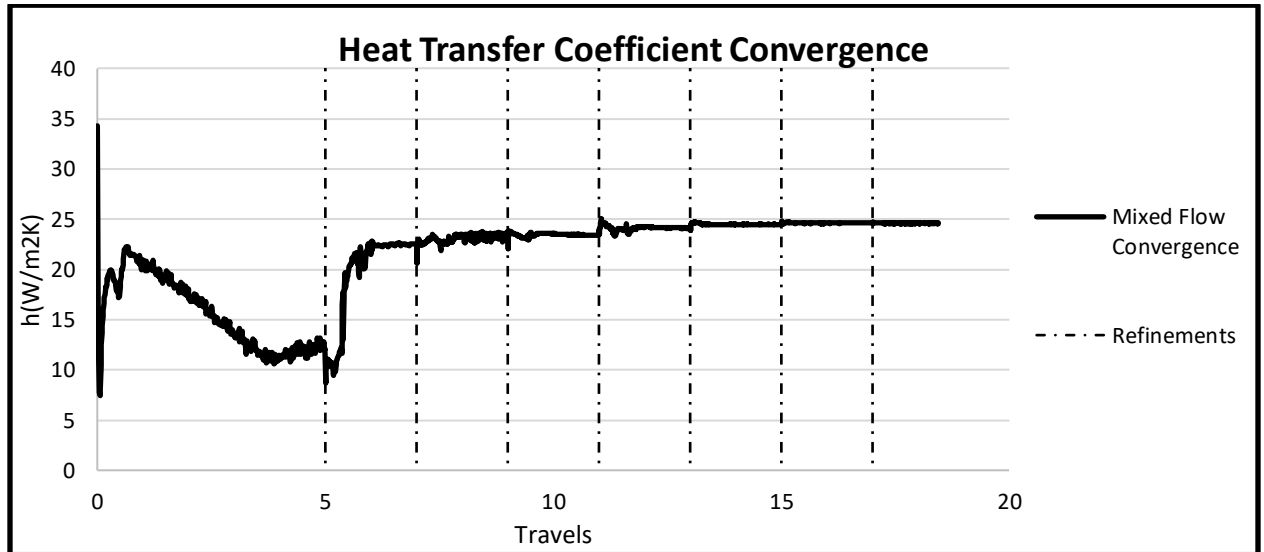


Figure 5: Convergence of heat transfer coefficient

As shown in Figure 5, refining the mesh more accurately captures the effects of the flow and causes the solution to converge. This is because the domain is split into smaller and smaller cells until the smallest flow effects that have a significant effect on the flow are captured.

PROBLEM DESCRIPTION

To fully analyze SOLIDWORKS Flow Simulation's ability to predict heat flow through a UAS, the software should be able to perform the simulation in 3D, with both Internal and External flow analysis, and with the plate at a constant heat flux or constant temperature. Both Internal flow and External Flow will be needed in the UAS analysis, and therefore need analyzed.

However, a 3D Computational Domain is more complicated and computationally expensive, and constant heat flux has less experimental data and theoretical analysis to compare with. To accurately and more easily gather the appropriate settings to run the simulations, the paper starts by analyzing a 2D, external, constant heat flux, heat transfer problem before incorporating the more complex settings one at a time.

The flow type test parameters are designed to test Flow Simulations ability to solve laminar, turbulent, and mixed flow heat transfer. All regimes will be important for testing a UAS since they will all be present in some fashion. While turbulent flow will dominate the outside of the UAS, the inside will have slower laminar flow. It is also important to test how well SOLIDWORKS calculates the transition from turbulent to laminar as it can be difficult to model and can cause problems in the calculation if done poorly. Therefore, the computation settings are set up so that the following flow types can be analyzed.

- 1) Turbulent Flow
- 2) Mixed Flow
- 3) Laminar Flow

A critical Reynolds number of 5×10^5 is assumed here in order to predict the behavior of the flow. Since there is always some laminar flow over the plate, turbulent flow will be said to be turbulent across at least 90% of the plate. 90% is recommended by Cengel and Ghajar to still achieve accurate results when assuming the full plate is turbulent. the Reynolds number across the length of the plate, Re_L , need to be as high as possible for this case, but still kept well under 10^7 . This is the limit of Cengel and Ghajar's heat transfer coefficient equation for turbulent flow. Laminar Flow will be flow that remains fully laminar across the plate and stays well below the

transitional region. For this paper, the Reynolds number across the length of the plate will be kept below 1×10^5 for the Laminar Flow case. For the mixed case, the Reynolds number across the length of the plate will be designed to be approximately 1×10^6 so that the middle of the plate will be around 5×10^5 and will have significant portions of the flow be laminar and significant portions of the flow be turbulent. A summary of the flow types and their Reynolds number ranges is shown below in Table 2.

Flow Type	Reynolds number, Re_L
Turbulent	$5 \times 10^6 \leq Re_L \leq 10^7$
Mixed	$Re_L \approx 1 \times 10^6$
Laminar	$Re_L < 1 \times 10^5$

Table 2: Summary of flow types

The first round of validations will be performed using 2D, external flow, and constant temperature since these conditions are simple, have plenty of experimental data to compare to, and are generally the standard for benchmarking. However, simulations will also be performed in 3D, Internal, and with Constant Heat Flux. This paper is designed to test SOLIDWORKS Flow Simulation for use in UAV which will include three-dimensional, external, and internal flow. Constant Heat Flux convection heat transfer will be tested because it is relatively easy to estimate the heat flux of an engine using power curves and engine efficiencies and will therefore be more practical than the constant temperature analysis.

To gather data across the full spectrum of the flow types, five test cases were designed. Since the turbulent and mixed cases include the transition from laminar to turbulent, there are two cases each to analyze how SOLIDWORKS Flow Simulation solves the heat transfer coefficient at the upper and lower end of the range of Reynolds numbers.

Flow Type Test Cases		
Wind Speed (m/s)	Reynolds number, Re_L	Flow Type
0.5	8.00E+04	Laminar
2	3.20E+05	Mixed
9	1.28E+06	Mixed
35	5.60E+06	Turbulent
60	9.60E+06	Turbulent

Table 3: Summary of Flow Type test cases

Once each of the flow types have been analyzed using External 2D flow, further studies are done to include internal flow, 3D analysis, and constant heat flux. Table 4, shown below, summarizes the general test case settings that will be analyzed.

General Test Cases		
2D or 3D	Computational Domain Type	Heat Transfer Type
2D	External	Constant Temperature
2D	Internal	Constant Temperature
2D	External	Constant Heat Flux
3D	External	Constant Temperature

Table 4: Test Case Matrix

To prevent a blunt leading edge from effecting the flow over the plate and to keep the flow laminar, the leading and trailing edge were chamfered. An example of this can be seen in Figure 6.

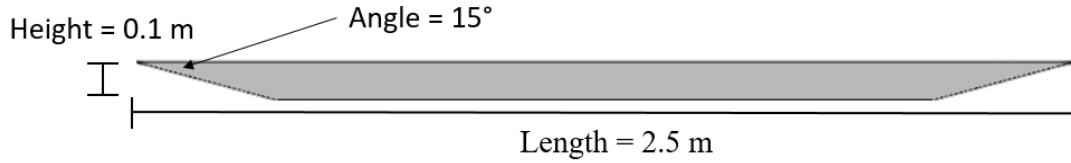


Figure 6: Plate Dimensions

It would be preferable to have the plate as flat as possible to prevent the front edge from effecting the flow on the top of the plate. However, as can be seen in Figure 7, the number of cells drastically increases the smaller the thickness of the plate.

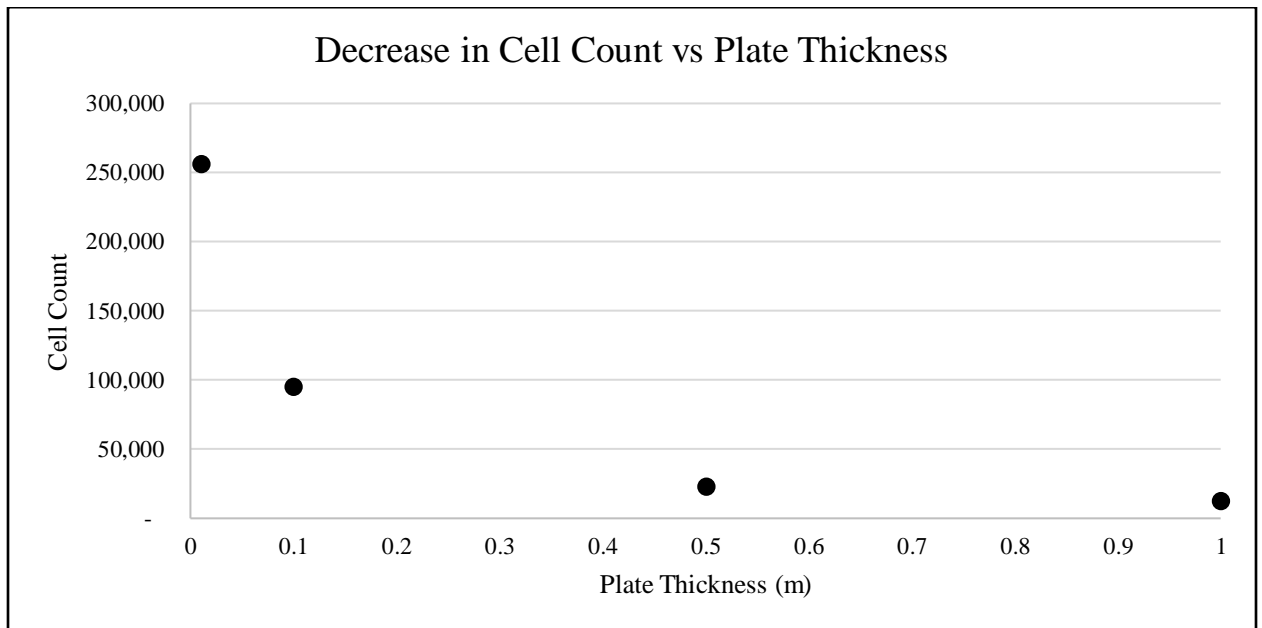


Figure 7: Plate thickness effect on cell count

This increase in cell count occurs because the ratio factor setting decreases the mesh size by requiring at least four cells across the smallest dimension. Therefore, the number of cells increases with a decrease thickness of the plate. For this study, a thickness of 0.1 m was chosen as

it had a relatively low cell count while also minimizing the effect of the plate thickness on the flow.

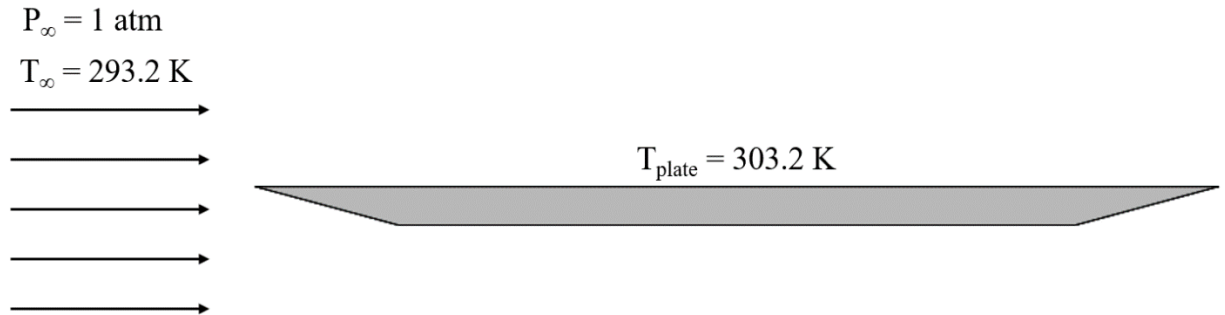


Figure 8: Overview of the Problem

For this validation, the temperature of the flat plate is held at a constant 303.2 K rather than a constant heat transfer rate. This simplifies the problem and aligns it with what was found in the literature review, making it easier and more meaningful to compare data. With the problem set up, it is now possible to solve for the heat transfer coefficients that will be predicted by Cengel and Ghajar, and Edwards and Furber using the methods which were outlined in the Flat Plate Forced Convection section.

The properties are extrapolated using the table for dry air properties in Cengel and Ghajar's book, Heat and Mass Transfer. The values used are show in the table below as they will remain constant for every test case.

Properties of Air at Film Temperature, T_{film}	
Thermal Conductivity, k (W/m*K)	2.55×10^{-2}
Prandtl number, Pr	0.7296
Kinematic Viscosity, ν (m^2/s)	1.56×10^{-5}

Table 5: Dry air properties at 298.3 K and 1 atm

For the internal flow analysis, a circular tunnel was constructed around the plate at the same dimensions that the computational domain was sized to in the external 2D analysis. This meant that most of the settings, theoretical analysis, and experimental analysis could be used to validate the plate for internal flow. In fact, the only settings that needed adjusting were the Initial Refinement Level, and the Global Domain Level.

Because External Flow includes the Ratio Factor setting which automatically decreases the cell size as the computational domain approaches the solid object, the overall cell count was greatly reduced when the same mesh settings were kept. Thus, to maintain consistency across simulations the Initial Refinement Level and Global Domain Level were increased until the cell count was approximately that of the external analysis for 2D flow.

SETTINGS

There must be a starting point for the settings before they can all be tested to determine the most appropriate settings. A table displaying the initial general settings is shown in Table 6. Any settings not shown is either kept as default or described by the problem description. Most of the general settings will be held constant as changing them fundamentally changes the problem description; however, both the turbulence intensity will be tested as turbulence modeling can have a large effect on the accuracy of the simulation.

Initial General Settings							
Analysis Type	Fluids			Wall Settings		Turbulence Parameters	
	Project Fluids	Flow Type	Fluid Temperature	Default Wall Thermal Condition		Intensity	Length (m)
External	Air	Laminar and Turbulent	293.2 K	Wall Temperature	303.2 K	0.100%	0.01

Table 6: Initial general settings

For this paper, the problem is based off the constant temperature flat plate heat transfer study performed in Flow Simulation 2018 Validation Examples; however, this study will look at the problem more in depth and include turbulent flow in the analysis. Also, in the Flow Simulation 2018 Validation Examples, the flow was modeled as internal whereas this study is external. The problem was modeled as 2D originally instead of 3D to keep the cell count down further. SOLIDWORKS solves the problems the same, but 2D assumes the flow is infinite in the Spanwise direction.

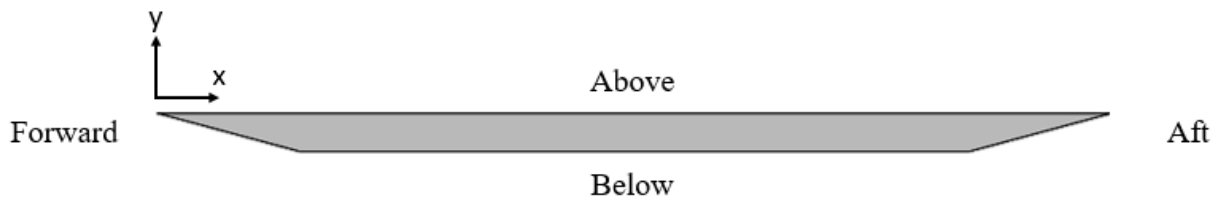


Figure 9: Flat plate coordinate system

Figure 9 shows the coordinate system of the flat plate, as well as the nomenclature used to describe the directions relative to the plate. The span is in the z-direction, but it is not shown since the problem is 2D and the span will not affect the result. Table 7 shows the initial sizes for

these settings. The initial values are based on the work done by J. Wallace in his master’s thesis Investigation of SOLIDWORKS Flow Simulation as a Valid Tool for Analyzing Airfoil Performance Characteristics in Low Reynolds number Flows [17], and were chosen to be larger than anticipated. This is so that the ideal refinement settings could be found without the computational domain being improperly sized.

Initial Computational Domain Settings					
Type	Size (m)				
	Forward	Aft	Above	Below	Span
2D simulation	30	30	15	15	0.0001

Table 7: Initial computational domain settings

The refinement settings are the first settings to be tested, so the values at the beginning are kept low to work up to convergence. The initial values are not intended to be correct since the size of the mesh needed to adequately simulate the heat transfer is not known ahead of time.

Initial Refinement Settings							
Global Mesh			Calculation Control Options				
Type	Initial Refinement Level	Approximate Maximum Cells	Global Domain	Refinement Strategy		Start	Period
Automatic	1	5,000,000	Level = 0	Periodic	Travels	10	2

Figure 10: Initial refinement settings

These are the initial values used to simulate the flow over a flat plate. Although they are likely not the best values to begin with, each value will be tested to determine whether what the appropriate values should be. The type of global mesh is set to automatic as manually defining the mesh adds a lot of complexity and automatic should be sufficient for this study.

Lastly, a surface goal for average heat transfer coefficient was added to the top surface of the flat plate. Since the heat transfer coefficient is the main criteria for determining solution accuracy, it is tracked to make sure it has properly converged on a value.

Once the appropriate settings have been determined, they will be used to analyze the different flow types for the 2D-External-Constant Temperature case. Once compared to theoretical and experimental results, the rest of the general flow cases will be analyzed. For each of the following test cases, the settings used were those found in the Settings section of Chapter IV.

To change the problem from internal to external, a tunnel had to be built around the flat plate model. To keep the settings consistent between test cases, the size of the tunnel is kept the same as the size of the computational domain found for the 2D-External-Constant Temperature case. This tunnel, with half the tunnel hidden so that the plate can be seen, is shown in Figure 11. To run SOLIDWORKS Flow Simulation as internal flow, the tunnel must be airtight. The faces added on each end serve to seal off the tunnel, but the boundary conditions placed on them will make them behave as an inlet and an outlet for the flow.

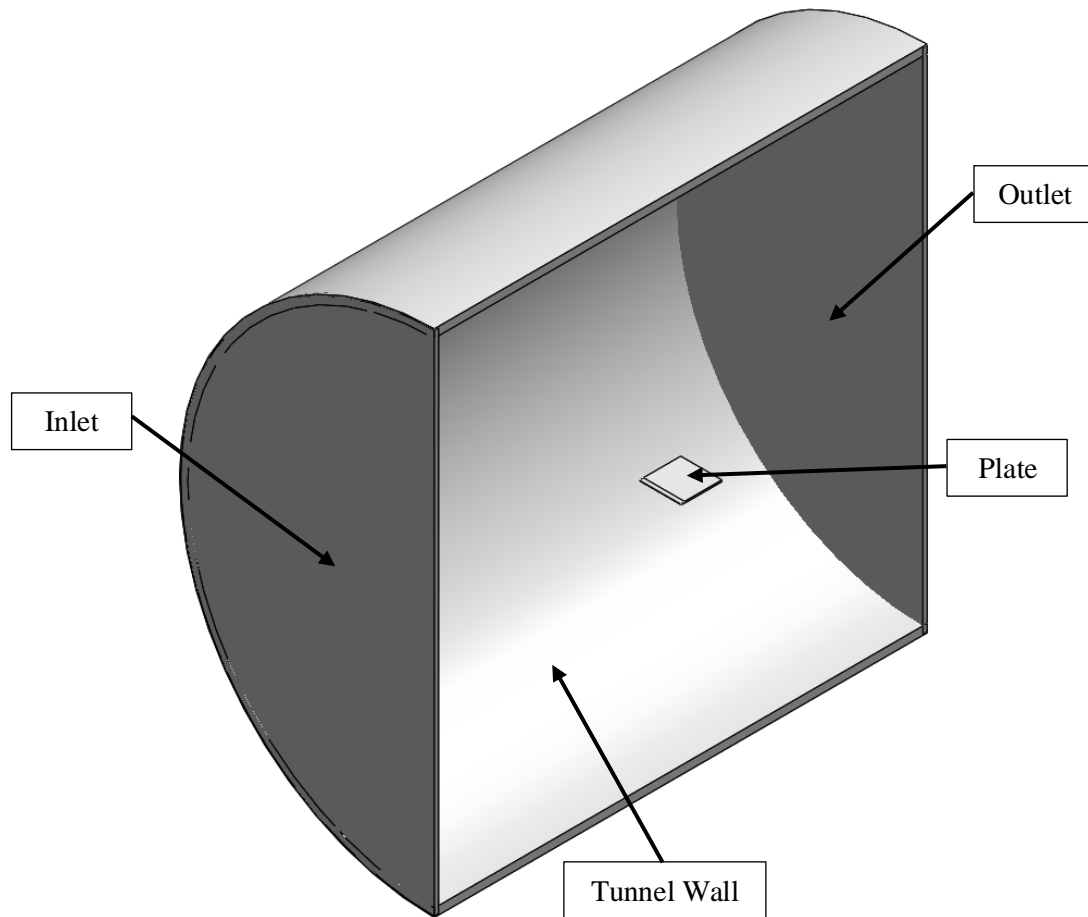


Figure 11: Tunnel design for internal flow test case

Boundary layer conditions needed to be set for the wall, so again the conditions chosen were those that kept the problem as similar the 2D-External-Constant Temperature test case. The boundary conditions added to the tunnel are an ideal wall for the tunnel walls, the velocity at the inlet, and the pressure at the outlet. The boundary condition of ideal wall assumes that the wall is adiabatic and does not apply any shear stress to the fluid, which prevents the tunnel walls from creating any boundary layer that might affect the flow across the flat plate. Since the ideal wall

condition makes the tunnel walls adiabatic, the default wall thermal condition set in the general settings will not apply to them.

For internal analysis type, the velocity of the flow is set using boundary conditions rather than in the general settings. Therefore, a velocity boundary condition is added to the inlet at the appropriate speed for the flow type being tested. In SOLIDWORKS when an inlet velocity boundary condition has been created, the outlet needs to be a pressure opening. [18] The outlet was chosen to be an environmental opening which is treated as a total pressure condition for an inlet and a static pressure condition for an outlet. If, when the environmental opening is selected, there is a vortex at the boundary with flow flowing both in and out, the type of opening will change accordingly between static pressure and total pressure.


Parameter	Value
 Default wall thermal condition	Heat flux
Heat flux	47 W/m ²
Roughness	0 micrometer

Figure 12: Constant heat flux settings change

To change the analysis from constant temperature plate to constant heat flux plate, the Default Wall Thermal Condition in the Wall Settings section of the General Settings was changed from Temperature to Heat flux. The heat fluxes were chosen to keep the plate temperature as close to the constant temperature case as possible. Since the properties of air were obtained assuming the plate would be 303.2 K, maintaining a plate temperature close to this makes it easier to compare the results for each test case.



Figure 13: Changing analysis type from 2D to 3D

To change the analysis type from 2D to 3D, the Computational Domain settings were opened, and the 3D simulation Type was selected. Also, the size of the Computational Domain in the z+ and z- directions were changed to the appropriate size.

RESULT PROCESSING

The main results gathered for processing are the heat transfer coefficient, the number of cells, and the shape factor. These values were chosen to use as the results since the proper settings are a balance of computation time and accuracy. This section describes how these variables are obtained from SOLIDWORKS Flow Simulation.

The heat transfer coefficient is gathered because in the scholarly articles studied in the literature review, this is the parameter used to test the validity of a system for use the heat transfer modeling. Also, the number of cells is recorded as a measure of computation length in order to optimize the time it takes to run the simulation for accurate results. The reason this was chosen over simply measuring the computation time is that the exact time the flow converged is difficult to measure and to keep it consistent. It is far easier to allow the flow to converge, then make note of the number of cells. Also, the computer the simulation runs on has a large effect on how long the computation takes, whereas the number of cells remains consistent across computers.

Both the local and the average heat transfer coefficient were obtained from SOLIDWORKS Flow Simulation. The average heat transfer coefficient is obtained by creating a surface parameter and choosing the top surface as the face, and the heat transfer coefficient as the parameter. The minimum and maximum heat transfer coefficients are also provided, but all that is used for the analysis is the average heat transfer coefficient.

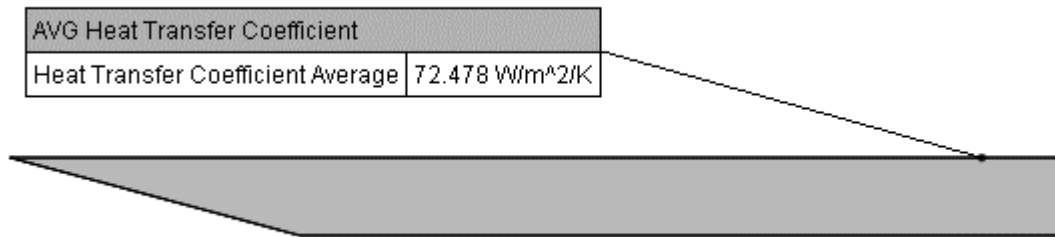


Figure 14: Surface parameter used to obtain average heat transfer coefficient

The average heat transfer coefficient is important, but the local heat transfer coefficient provides more information that can be used to determine if there is something inaccurate in the simulation. To obtain the local heat transfer coefficient along the length of the plate, first a line was drawn down the middle of the top surface parallel with the x-axis. Then a XY Plot was inserted. The line drawn on the top surface was chosen as the selection and again the heat transfer coefficient was chosen as the parameter.

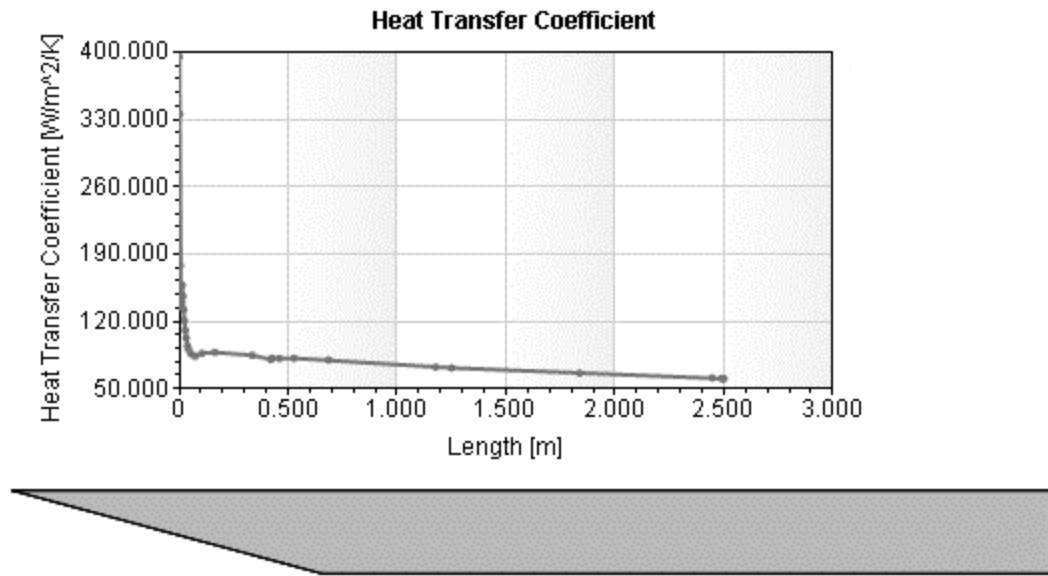


Figure 15: XY Plot of the local heat transfer coefficient along the length of the plate

Despite the air flowing all around the plate, the heat transfer coefficient was taken only on the top surface. This is to keep the problem simple and make it easier to compare to the theoretical and experimental benchmarks shown in the Literature Review section, while also having a model that is similar to the UAS that will be discussed later in the paper.

To determine whether the flow was turbulent, laminar, or transitional in the SOLIDWORKS Flow Simulation calculation, the Shape Factor, H , was used. Shape factor is a measure of the displacement thickness, δ^* , over the momentum thickness, θ . Since SOLIDWORKS Flow Simulation does not have a built-in method for calculating this, the processing was done in excel and the following method was used.

- 1) The velocity vs y was taken from SOLIDWORKS along the length of the plate using an x-y plot

- 2) The boundary layer thickness was determined by analyzing the data to see where the plot reached 99% Max velocity
- 3) The Shape Factor was found in excel using the equations in Figure 17

Although there exists a parameter in SOLIDWORKS Flow Simulation for the boundary layer thickness, it was not found to be reliable. The reason for this seems to be a result of the thickness of the plate. The results show that the velocity vs y never reached the ambient velocity for cases outside of the laminar case, even plotted up to 1 m above the plate. This is believed to be caused by the thickness of the plate and the resulting pressure increase at the leading edge, shown in Figure 16



Figure 16: Pressure increase at leading edge of the plate

Furthermore, the boundary layer velocities were inconsistent, often never reaching 99% of the ambient air velocity. It was decided that the best solution was to find the boundary thickness up to 99% the maximum velocity along the velocity vs y plot for each corresponding x value. This produced values consistent with what was expected. Furthermore, upon investigation the air was moving at approximately this speed throughout the computational domain, which means this was effectively the ambient velocity.

Variable	Equation
Boundary Layer Thickness	$\delta = 0.99 * U_{MAX}$
Displacement Thickness	$\delta^* = \int_0^{\delta} 1 - \frac{u}{U_{MAX}} dy$
Momentum Thickness	$\theta = \int_0^{\delta} \frac{u}{U_{MAX}} \left(1 - \frac{u}{U_{MAX}}\right) dy$
Shape Factor	$H = \frac{\delta^*}{\theta}$

Figure 17: Equations used to calculate Shape Factor

To obtain the boundary layer velocities for the shape factor analysis, a sketch was created using vertical lines that spanned the length of the plate and extended through the boundary layer. This sketch is show in Figure 18. An XY plot was created using Velocity (X) as the parameter and this sketch as the selection. Display boundary layer was also chosen in the Options menu.

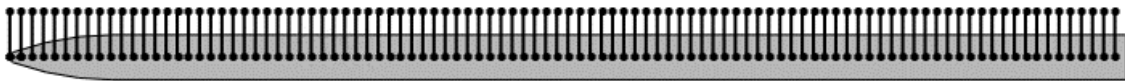


Figure 18: Sketch used to obtain boundary layer velocities

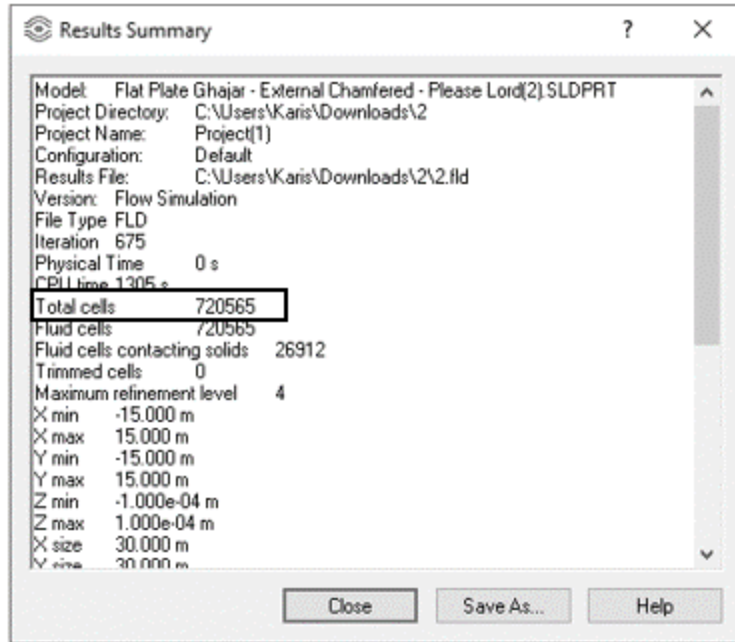


Figure 19: Results summary where Total Cells was obtained

The total number of cells used for the simulation was obtained through the Results Summary page shown in Figure 19. The Results Summary is found by right-clicking on the Results in the tree pane and choosing Summary.

CHAPTER IV

FINDINGS

SETTINGS

To determine if the settings were optimal for testing the flat plate, meaning that an acceptable accuracy was reached without extending the computation time excessively, the settings used were altered, and the average surface heat transfer coefficient and cell count recorded for each iteration. Some settings had a larger effect on the flow while others did not appear to change the results in any meaningful way.

Refinement

The first settings tested were the Initial Refinement Level and the number of Refinements. The Initial Refinement Level changes the size of the initial mesh. As the level increases, the size of the cells in the overall mesh decreases. This is not sufficient to analyze the flow near the plate since the cell size needed is much smaller. To get the cell size needed, the number of Refinements is used. This setting breaks up the mesh into smaller cells when the flow is complex to give a more accurate representation of the flow where it is needed. The results are shown in Figure 20.

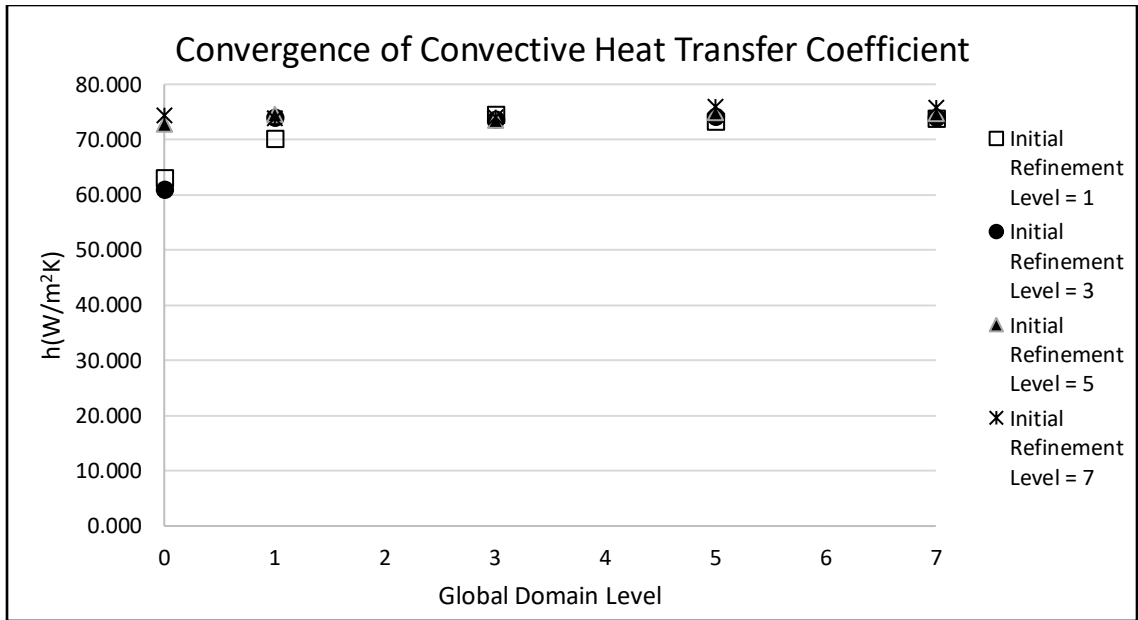


Figure 20: Convergence of the heat transfer coefficient with increase in Initial Refinement Level and Global Domain Level

Both settings have a large effect on the convergence of the flow results. However, The Global Domain Level is generally the more important variable as it can break the mesh down into much smaller cells. Furthermore, it also only decreases the size of the mesh where it is needed, resulting in a more optimized flow model. The results of the refinement are not as dramatic since the ratio factor already refines the cells somewhat as the computational domain approaches the plate. For this study, an Initial Refinement Level of 4 and a Global Domain Level of 4 were chosen as the optimal settings. This was found to be a good balance of cell count and accuracy.

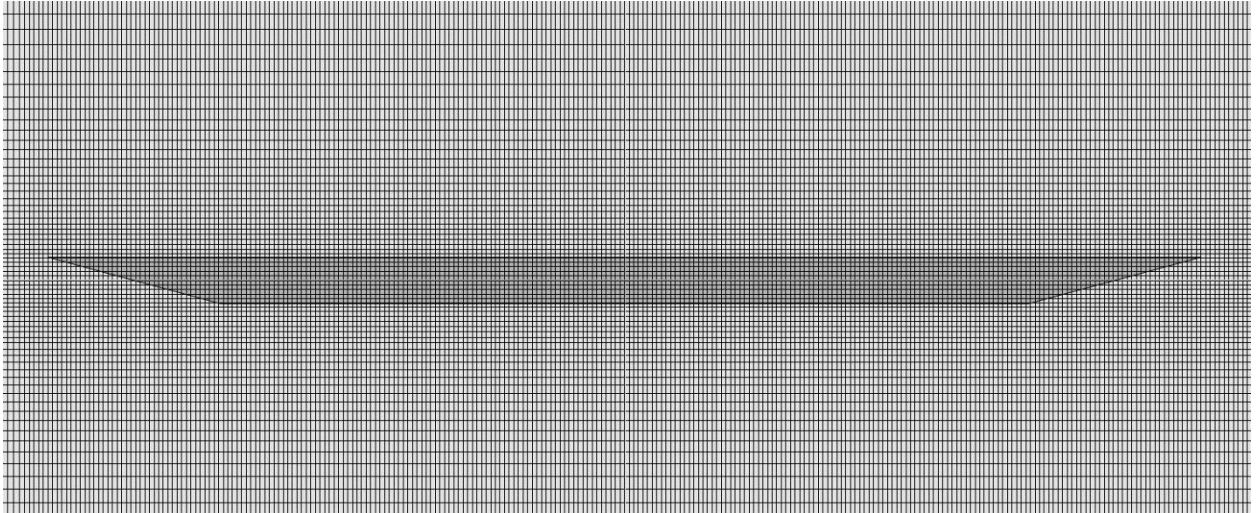


Figure 21: Final Global mesh not including refinements during calculation

The next settings tested were the Refinement Start and Refinement Period. The first setting is the point the first refinement occurs during the calculation and the second is how often after that the refinements will occur again. The goal for finding the proper sizing of these was to make sure that the heat transfer converged on a value before the mesh is further refined to ensure that it is being refined in the locations that need it. The final settings chosen were a Refinement Start of 5 and a Refinement Period of 1. Although a Refinement Period of 2 could have been chosen as a buffer just in case, the flow never took longer than 1 Period to settle. Table 8 shows the final settings used to dynamically refine the flow.

Final Refinement Settings							
Global Mesh			Calculation Control Options				
Type	Initial Refinement Level	Approximate Maximum Cells	Global Domain	Refinement Strategy		Start	Period
Automatic	4	5,000,000	Level = 4	Periodic	Travels	5	1

Table 8: Final refinement settings summary

Transitioning to internal flow the problem was kept mostly the same, only the plate was put inside a large pipe at the same diameter as the computational domain as found in the following section. This allowed most of the settings to remain constant, except for the refinement settings. The refinement settings needed updated because External Flow analysis has an extra setting that helps refine the mesh appropriately called the Ratio Factor. If the settings are not changed when moving to Internal flow, the mesh would be much less refined.

First, the number of Refinements were increased because this type of refinement is more efficient since it only refines the cells where further refinement is needed and not across the whole domain. Once this was maxed out at 7, the Initial Refinement Level was then increased until the cell count was above 2,500,000. This cell count was chosen since it is approximately the cell count of the simulations used in the External Flow analysis. The results of this study are shown in

Refinement Settings Analysis		
Initial refinement Level	Global Domain Level	Cell Count
4	4	35,574
4	5	122,006
4	6	387,190
4	7	1,051,062
5	7	1,134,938
6	7	2,190,881
7	7	3,014,553

Table 9.

Refinement Settings Analysis		
Initial refinement Level	Global Domain Level	Cell Count
4	4	35,574
4	5	122,006
4	6	387,190

4	7	1,051,062
5	7	1,134,938
6	7	2,190,881
7	7	3,014,553

Table 9: Increase in cell count with Initial Refinement Level and Global Domain Level

To reach the same cell count used in previous studies, the Initial refinement Level and Global Domain Level needed to be maxed out at 7 each. This provided a cell count at approximately 3,000,000 which exceeded the desired cell count of 2,500,000. These settings were used for all the internal flow cases.

Computational Domain

To properly size the computational domain, dimensions were increased until increasing them further no longer affected the result. These three dimensions were separated into the computational domain above and below the flat plate and into the computational domain forward and aft of the flat plate, and the computational domain in the Spanwise direction. Although it would be better to do each direction individually, pairing the two together saved time in finding a good enough computational domain, without sacrificing too much computational time in the final product. Increasing the size of the computational domain had a small effect on the overall cell count, since the outer cells did not need refined during the analysis. Once the result converged on a solution, the next dimensions were altered. Until finally increasing in any dimension no longer affected the heat transfer coefficient. The chosen length for the final computation was qualitative and based on using the smallest computational domain size while maximizing the accuracy.

The first computation domain convergence test was performed by testing the convergence of the heat transfer coefficient with an increase in the computational domain in the $y+$ direction and $y-$ direction. These are the directions above and below the flat plate.

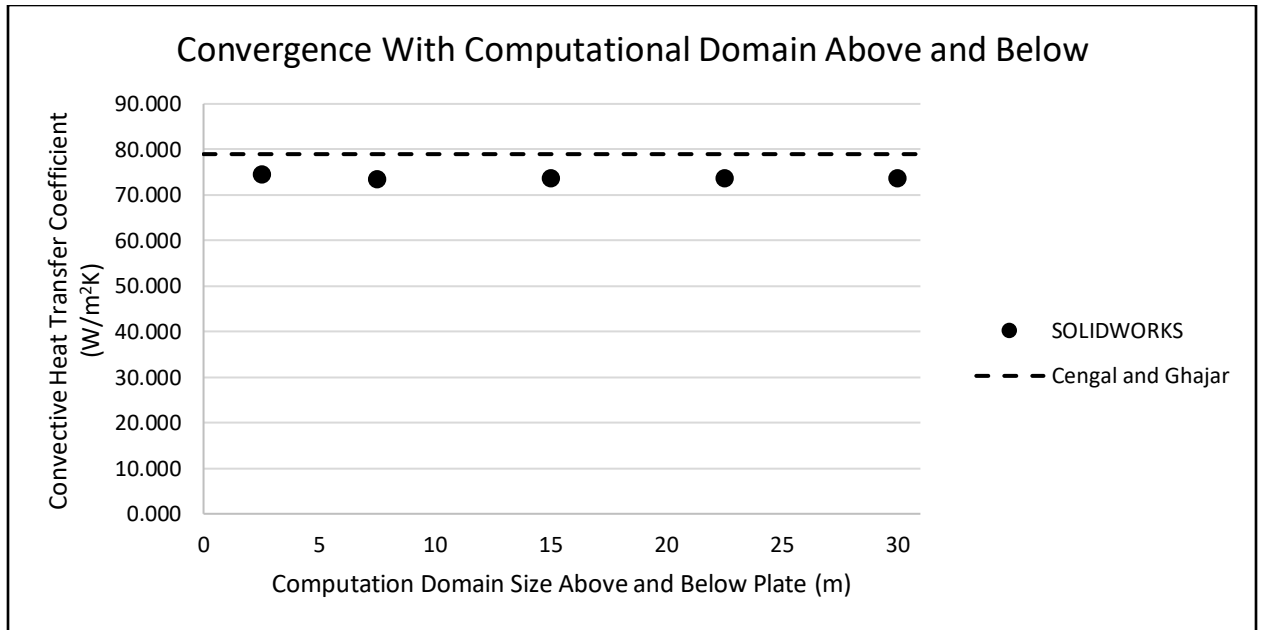


Figure 22: Convergence of heat transfer coefficient with increase in computational domain size in y+ and y- directions

Increasing the computational domain above and below the aircraft converged the flow very quickly. In this case, the flow converges as early as 7.5 m above and below the aircraft. For the final result, 15 m above and below will be used, to add a buffer to ensure that the computational domain is in fact large enough.

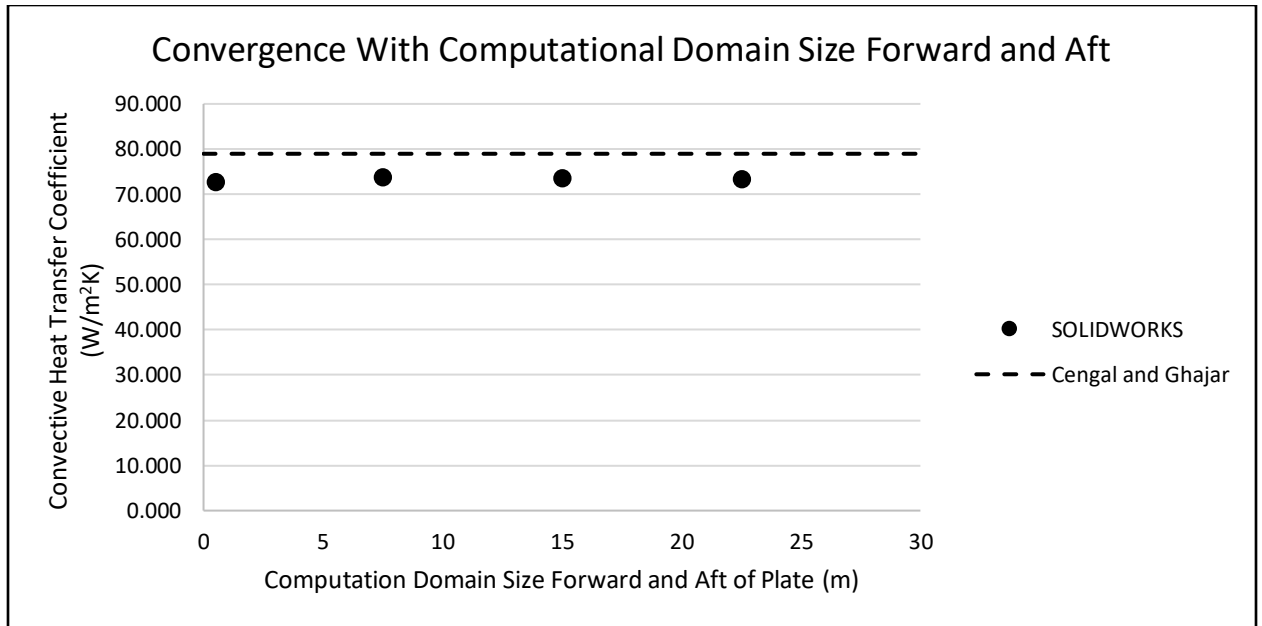


Figure 23: Convergence of heat transfer coefficient with increase in computational domain size in y- direction

Increasing the computational domain size Forward and Aft of the plate resulted in a converged flow nearly as quickly. Although the predicted heat transfer coefficient is still not quite reaching the theoretical value, the error is relatively small and further increases in the computational domain have a negligible effect on the heat transfer coefficient.

Increasing the span of the computational domain in 2D was tested as well, but as expected increasing its size had no significant effect on the resulting heat transfer coefficient. Since increasing the computational domain size had only a small effect on the number of cells in the mesh, the size of the computational domain in the spanwise direction for 3D flow was also assumed to be 15 m in both directions. Table 10 provides a summary of the optimal computational domain settings found through testing.

Final Computational Domain Settings						
Type	Size (m)					
	Forward	Aft	Above	Below	Port	Starboard
2D Simulation	15	15	15	15	0.0001	0.0001
3D Simulation	15	15	15	15	15	15

Table 10: Final computational domain settings summary

General Settings

The final general settings remained unchanged from the initial general settings. The only parameters that were tested were the turbulence intensity and length. Although the turbulence intensity was found to affect the flow at extreme values of 100%, everything under 10% had no significant effect on the flow. However, it should also be noted that this was tested using highly turbulent flow. Increasing the turbulence intensity for the laminar or mixed cases may result in a faster transition to turbulent flow and have a larger effect on the resulting heat transfer coefficient. The turbulence length was found to have no significant effect.

Final General Settings						
Analysis Type	Fluids		Wall Settings		Turbulence Parameters	
	Project Fluids	Flow Type	Default Wall Thermal Condition		Intensity	Length (m)
External	Air	Laminar and Turbulent	Wall Temperature	303.2 K	0.001%	0.01

Table 11: Final general settings summary

In summary, the settings were altered and their effect on the flow was noted. The settings chosen for use in the final computations were those that maximized the accuracy, in this case

meaning that the flow converged to a value and further changing the setting did not affect the value, while minimizing the resources spent on the calculation.

Leading Edge Separation Bubble

Upon finishing the simulations with the sharp edge, it was discovered that there was rotation at the leading edge that was not anticipated. This leading-edge rotation added instabilities to the flow and causing early transition to turbulent flow. This appears to be the same phenomena that is documented in Crompton's Thesis known as a thin airfoil leading edge separation bubble.

[19]

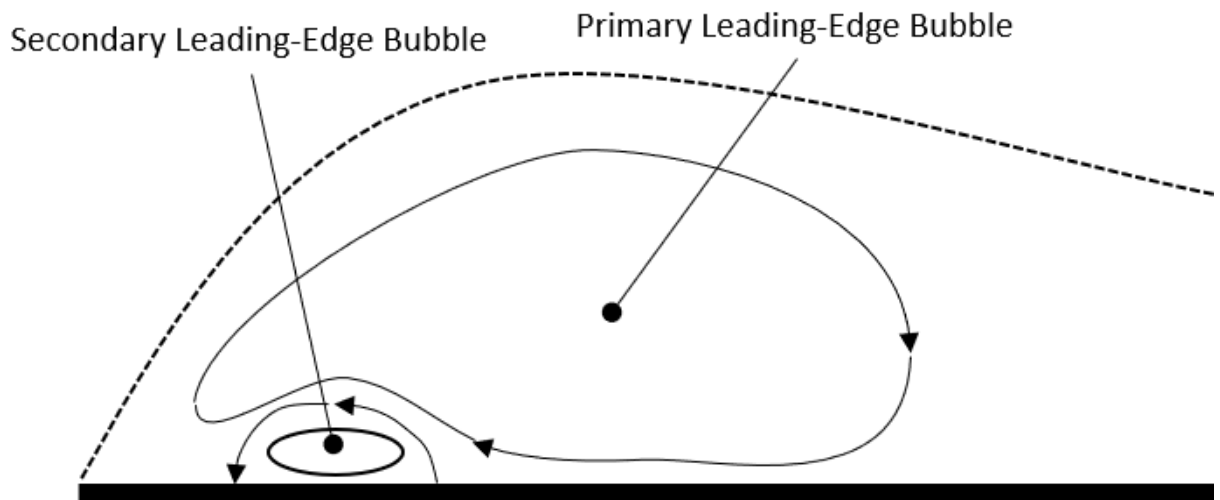


Figure 24: Thin airfoil leading edge separation bubble primary and secondary bubbles

Thin airfoil leading edge separation bubbles are like laminar separation bubbles but are caused by the shape of the leading edge. Specifically, they can be caused by a very sharp leading edge such as the one used in this paper. [19] To make a further argument that this is indeed a thin airfoil leading edge separation bubble, the profile of the leading edge bubble was observed. If it

were the thin airfoil leading edge separation bubble, two rotational regions are expected such as show in Figure 24. [20]

The streamlines were observed at the leading edge of the Laminar case at a Reynolds number of $8.00E+04$. What was found is shown in Figure 25. There are clearly two separate rotational regions as expected, meaning it is very likely that this is the same leading-edge separation bubble as described by Crompton. [19]

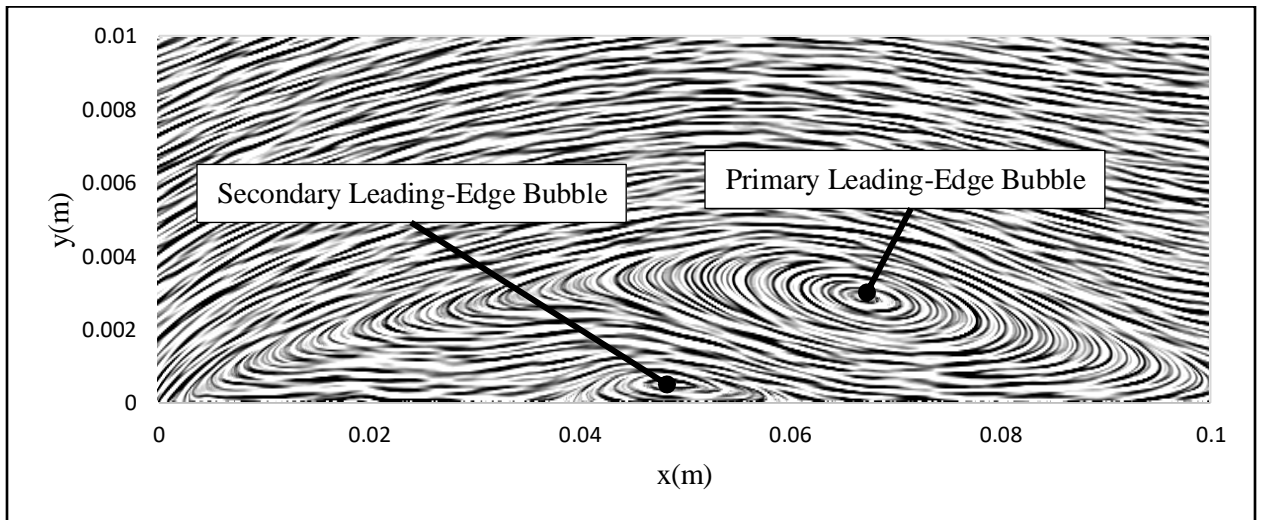


Figure 25: Primary and secondary leading-edge separation bubbles for laminar case at $Re = 8.00E+04$

In order to prevent this separation, the leading edge was modified according to Davis's study, *Design of Flat Plate Leading-Edges to Avoid Flow Separation* [21]. In the paper, Davis optimizes a few common leading edges to minimize the flow separation. The double arc leading-edge was used with the proposed dimensions of $r/t = 0.25$ and $l/t = 4.6$.

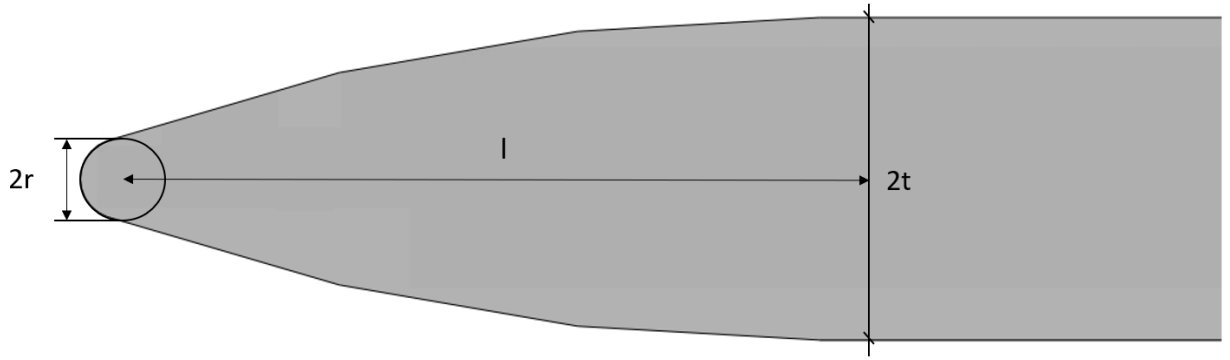


Figure 26: Leading-Edge dimensions to keep flow from separating

Once the proposed adjustments were made, the flow no longer detached from the leading edge. The new streamlines can be seen in Figure 27 and show that there is no longer separation.

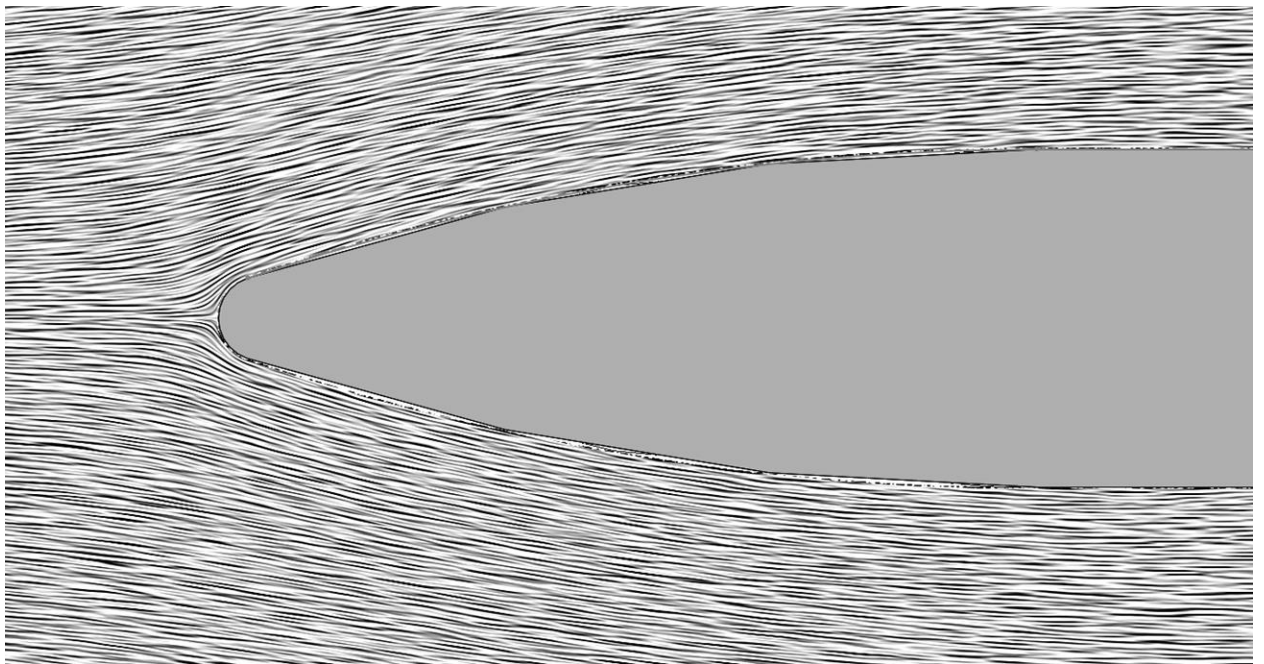


Figure 27: Leading- Edge streamlines after altering the leading edge

Since the airfoil is now symmetrical, some slight changes were made in how the data was obtained from SOLIDWORKS Flow Simulation. The results processing methods that had to be changed slightly were the average heat transfer coefficient, the local heat transfer coefficient, and the boundary layer velocities used for the shape factor.

For the local heat transfer coefficient and boundary layer velocity profiles, only the top surface was still used since only one surface was needed. Either side could have been used, but the top was chosen since the top was used for the first iteration of results processing. A new line, shown in Figure 28, had to be created along the surface. This new line was used for the x-y plots on the new leading edge rather than the straight line used for the original.

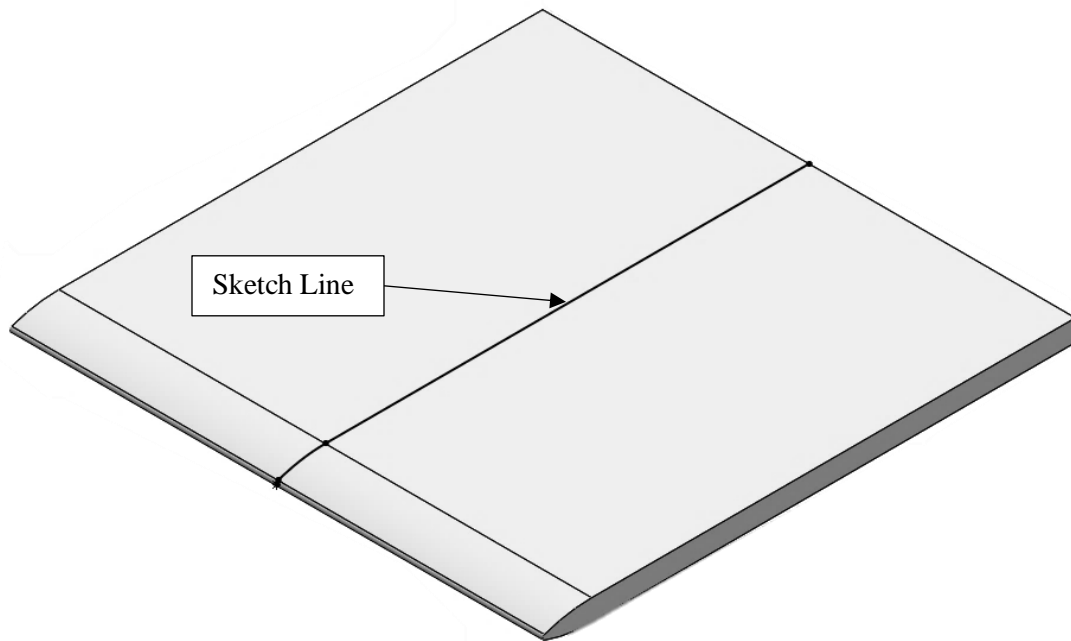


Figure 28: Sketch of line along top surface

For the average heat transfer coefficient, the top, bottom, and leading-edge surfaces were now used both for the Goal Plot and for the Surface Parameter used for the results. The sides and

aft surface were left out. Since the plate is now symmetrical, both top and bottom surfaces should be the same outside of unsteadiness, and since it is averaged using both should have little effect on the outcome.

Although the convergence study was performed on the chamfered plate, it was assumed that the minor modification to the leading edge will not affect the optimal settings. Simulations 48 and on are performed using the modified leading edge.

3D-External

To maintain simplicity, the test cases were designed to only alter one parameter at a time from the base test case (2D, External, with a Constant Plate Temperature) for which the settings were optimized. However, when running three-dimensional simulations with External flow the simulations failed.

The failure is believed to be a result of the cell count being too large. The Approximate Maximum Cells setting was at 5,000,000 as this was found to be around the limit that the computer the simulations were ran on could handle. Increasing beyond this resulted in simulation times that were greater than 48 hours, which was not practical for this study. The initial cell count before refinements for this setting was 20,327,832 cells. This far exceeded the maximum cell count the computer could handle and resulted in SOLIDWORKS Flow Simulation terminating the study before the first iteration.

Parameter	Value
Status	SOLVER ABNORMALLY TERMINATED! Please contact th...
Total cells	20,327,832
Fluid cells	20,327,832
Fluid cells contacting solids	66,720
Iterations	0

Figure 29: SOLIDWORKS Flow Simulation termination during 3D External Flow case

Although this early termination may be the result of the computer having insufficient resources to handle it, even a much more powerful computer probably couldn't handle this flow case. 20,327,832 is the initial cell count and each refinement would exponentially increase the cell count further. For an example of how quickly the cell count can increase with refinements see Figure 4.

These results show that is unlikely the software will be able to properly handle 3D External flow, even if significant time was spent optimizing the initial mesh. However, to fully explore the capabilities of SOLIDWORKS Flow Simulation, a 3D simulation was performed using Internal Analysis. Internal Analysis has a smaller initial cell count since External Flow automatically reduces cell size as the computational domain approaches the plate because of the Ratio Factor setting. This allowed the software to run the 3D simulation without crashing. The actual quality of the analysis is discussed later in the paper.

2D Refinements

Another interesting discovery is that despite having nearly the same number of cells, the mesh for the Internal flow case appeared to be much coarser. Figure 30 shows the mesh after all refinements are finished. The summary shows that the cell count is approximately the same for

both cases, so it is reasonable to assume the cell sizes would be approximately the same size given that the non-refined cell count is negligible.

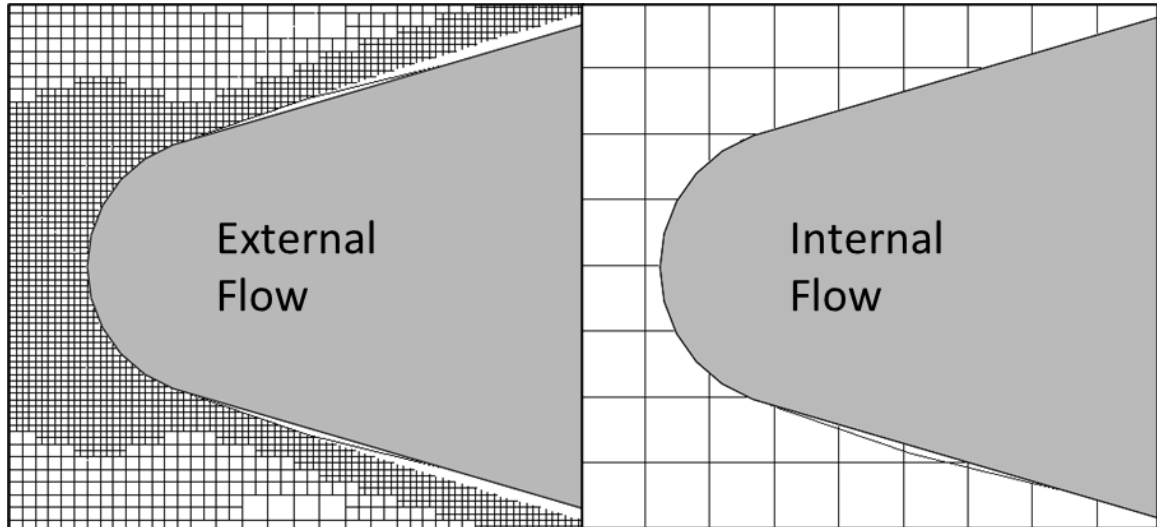


Figure 30: Mesh refinement of External vs Internal Flow leading edge mesh

Furthermore, the mesh appeared coarser throughout the Computational Domain for the External case, not just at the leading edge. Which meant that either the cut plot was not showing an accurate depiction of the mesh, the cell count was not accurate, or, despite being 2D, the Computational Domain was refining the flow considerably more in the spanwise direction for internal flow than for external. It was assumed originally that the cells would not refine in the spanwise direction for 2D analysis, i.e. there would only ever be one cell crossing the spanwise direction, but it was found that this was not true.

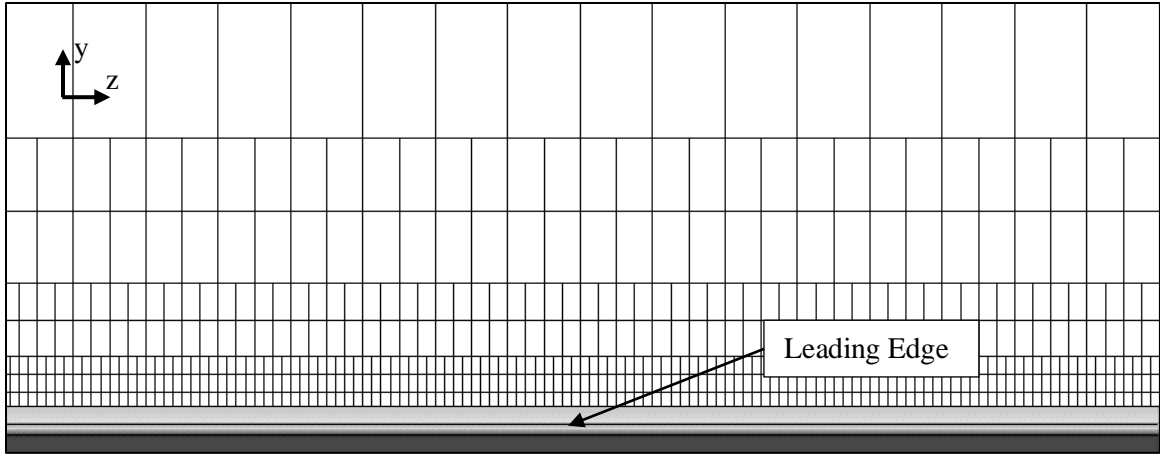


Figure 31: Cell Refinement in spanwise direction for 2D computational domain

As was mentioned in the Settings section of this paper, the Computational Domain is split into eight cells upon refinement. It is split in half by length, width, and span. This means that the cell count increases exponentially when the number of refinements is increased. Since the External flows Ratio Factor already creates a finer mesh near the surface of the plate, fewer refinements are needed to adequately resolve the flow. However, the Internal Flow case used the maximum number of refinements since the initial mesh was very coarse. Therefore, each cell in the Internal flow cases that was refined the maximum number of times resulted in a total of 2^7 or 128 cells across the spanwise direction. Whereas each cell in the External flow cases that was refined the maximum number of times resulted in a total of 2^4 or 16 cells across the spanwise direction. Furthermore, the even when the mesh of the Internal Flow case was refined the maximum number of times, the cell size was still much larger than when the flow was External, meaning the turbulent boundary layer was not being resolved as accurately.

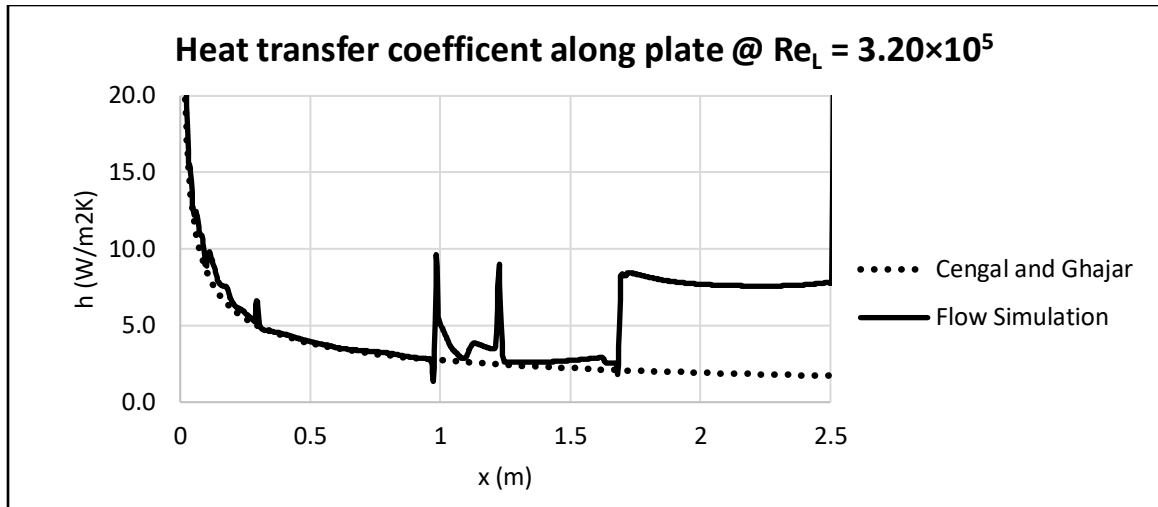


Figure 32: Heat transfer coefficient along plate at $Re_L = 3.20 \times 10^5$ for 2D-Internal-Constant Temperature case

Figure 32 provides an example of the erratic behavior created by the under resolved computational domain. This flow case, which theory predicts should be laminar all along the plate, has occasional spikes in the heat transfer coefficient and appears to transition to turbulent flow at around $x=1.75\text{m}$. Although there is some unsteadiness observed by the External cases, both remain Laminar along the plate and provide results much closer to what is expected.

Because the automatic refinement has such a major impact on the cell count, it is highly recommended that the Basic Mesh be optimized using control panels or by manually increasing the number of cells in the global mesh. Using these tools, while not as precisely target at areas of complex flow as the automatic refinement, can reduce the cells needed for a similar mesh and thus the computation time significantly for 2D flow analysis. If the Basic Mesh is very optimized, it may even be possible to avoid the automatic refinements altogether.

The Internal results gathered are mostly meaningless since mesh was not fine enough to accurately resolve the computational domain and will be left out of a lot of the discussion in the results. Although an optimized initial mesh would likely be able to gather better data, this was outside the scope of this paper and will be left for future studies to analyze and determine.

FLUID FLOW AND HEAT TRANSFER

SOLIDWORKS Flow Simulation average heat transfer coefficient results mostly agreed with theoretical predictions. The External flow cases were within 20% of the theoretical values for all cases except when the Reynolds number was 1.28×10^6 . Some differences in values were expected here since a significant portion of the plate is in a transitional state from laminar to turbulence, which is not accurately captured by the theory used in this paper and is very difficult for CFD to properly resolve. The Internal case showed similar trends but has much greater differences from theoretical since the mesh was not fine enough to accurately resolve the computational domain as was determined by the settings analysis. The 3D analysis is left out altogether since the 3D-External cases had no results due to the software terminating the study before it began. The 3D-Internal case will be examined in its own section.

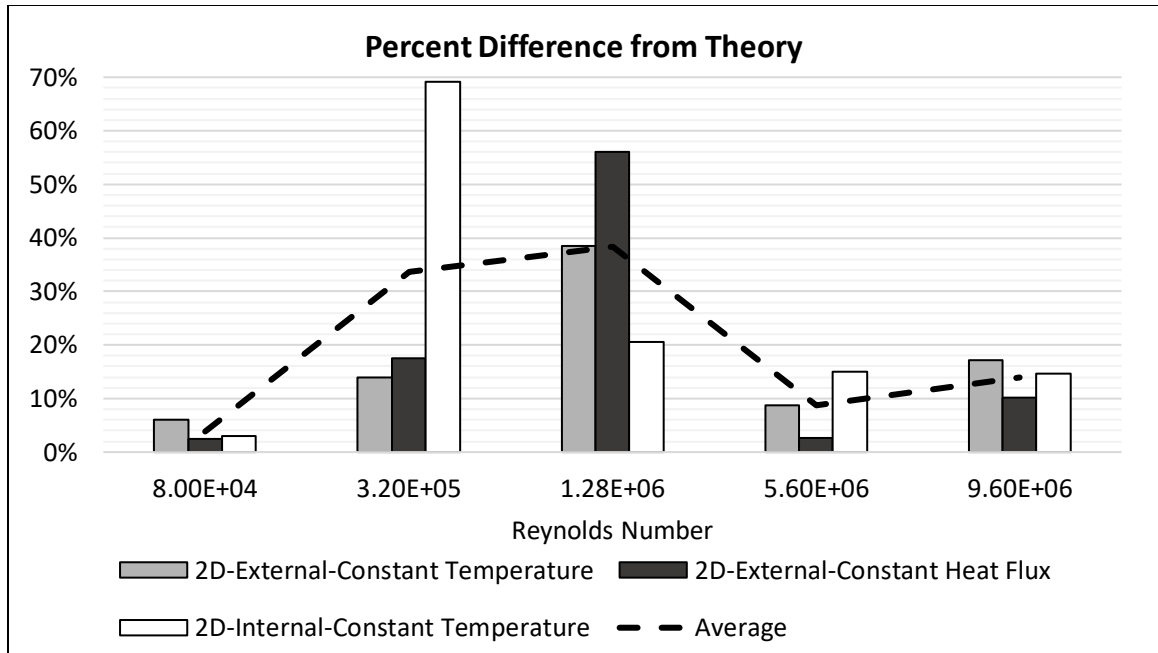


Figure 33: Average heat transfer coefficient's percent difference from theoretical predictions by Reynolds number

It is in the mixed flow regions that the SOLIDWORKS Flow Simulation predictions deviated from theory the most. However, the External Flow case agrees very well with the experimental data, as seen in Figure 34, in this region, suggesting that the difference may from the theoretical solutions not being able to fully capture the mixed region rather than the software not resolving the flow correctly. There is not enough data to really confirm this given that the Internal data is not reliable, so more experimental comparisons could be performed in the future.

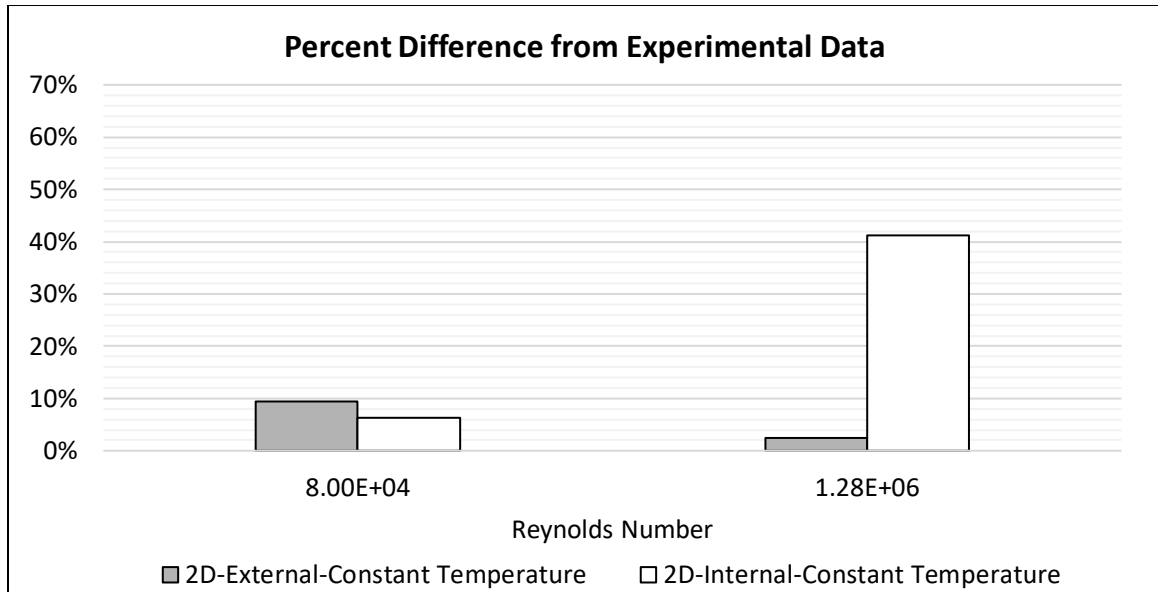


Figure 34: Average heat transfer coefficient's percent difference from experimental data by Reynolds number

The average heat transfer coefficient does not provide the whole picture. To understand where the differences were coming from, the local heat transfer coefficients and shape factors were analyzed. The following sections highlight some of the noteworthy trends from the data both positive and negative.

Leading Edge

In all studies that had a Reynolds number of 1.28×10^6 and higher, there was a “bump” in the heat transfer coefficient at the leading edge that seemed to trip the flow into turbulent flow prematurely or at least created a higher heat transfer coefficient than theoretical predictions at the leading edge. In the constant heat flux case, there was a lot of unsteadiness as well.

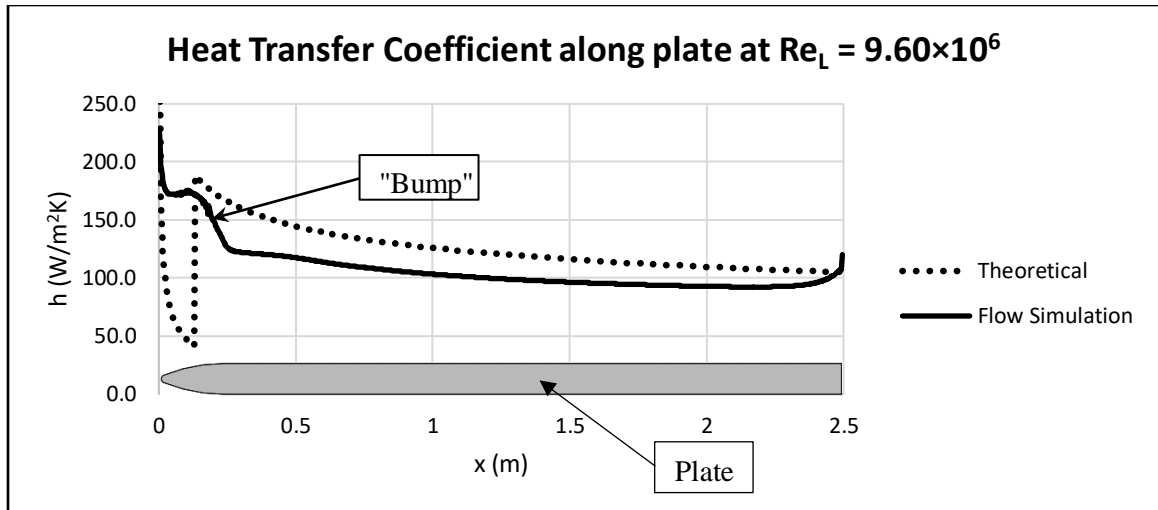


Figure 35: Heat transfer coefficient along plate at $Re_L = 9.60 \times 10^6$ for 2D-External-Constant Temperature case

Figure 35 highlights the bump in heat transfer coefficient near the leading edge of the plate. This rise in the local heat transfer coefficient is believed to be caused by effects of the leading edge. Although the leading edge was designed to keep the flow attached at the leading edge and prevent the leading-edge separation bubble, it does still appear to cause flow simulation to differ from theoretical predictions slightly. The theoretical analysis assumes that the plate is flat however, so some difference is not concerning.

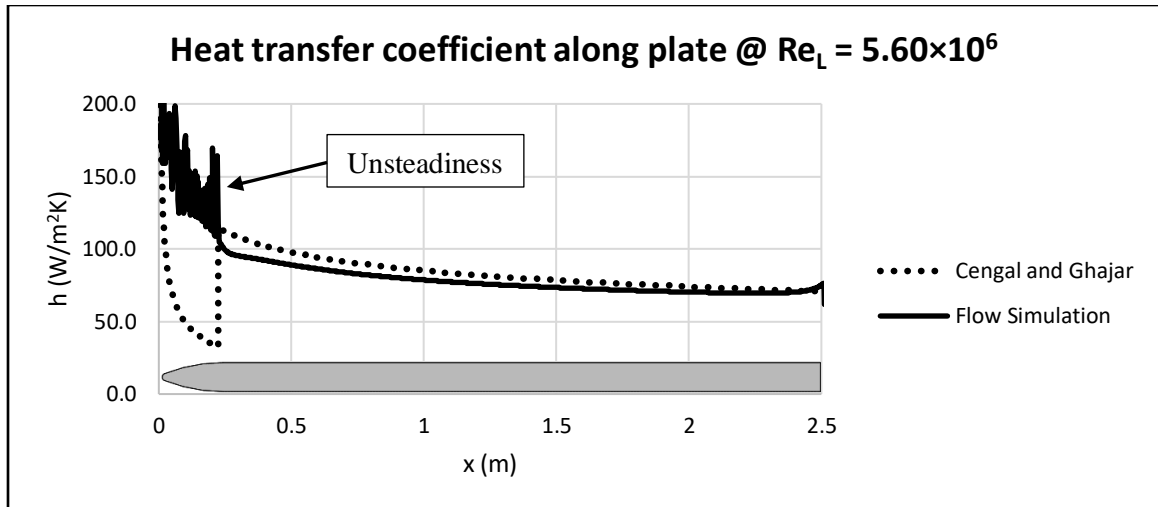


Figure 36: Heat transfer coefficient along plate at $Re_L = 5.60 \times 10^6$ for 2D-Internal-Constant Heat Flux case

In contrast with Figure 42, Figure 36 shows some unsteadiness at the leading edge. It is not obvious why there is erratic behavior present in the Heat Flux case and not in the Constant Temperature case, but it is possible that the constant heat flux setting adds complexity that requires further refinement of the computational domain to be adequately resolved.

Early Turbulence Transition

The effects at the leading edge appear to have ramifications downstream as well. The transitioned from laminar to turbulent earlier than predicted and even began transitioning in flow cases where it should have been totally laminar.

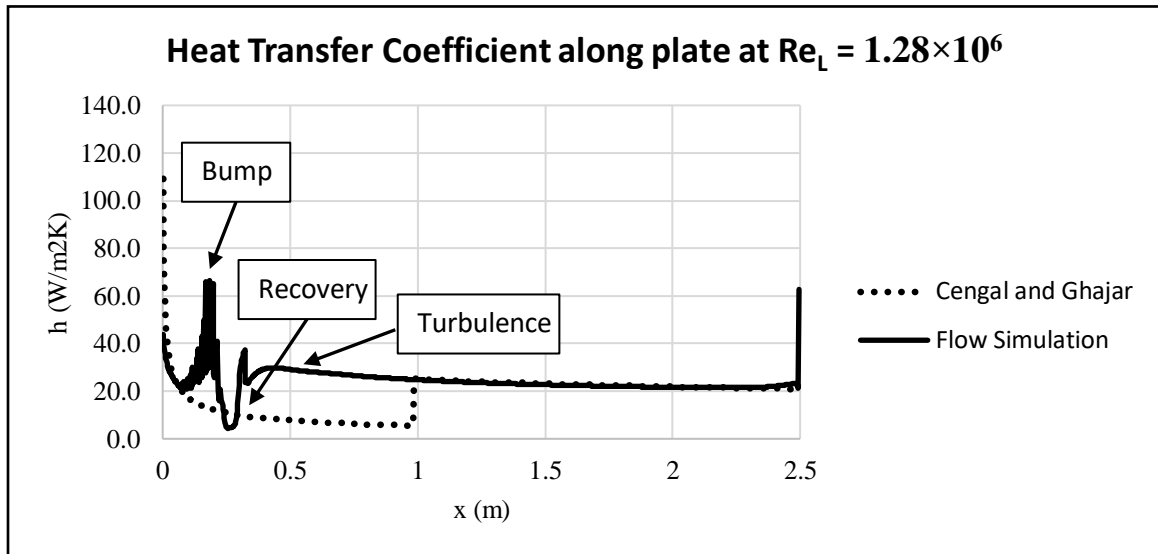


Figure 37: Heat transfer coefficient along plate at $Re_L = 1.28 \times 10^6$ for 2D-External-Constant Temperature case

In Figure 37 the bump at the leading edge is still present, is followed by a recovery back to laminar flow, and a quick transition to turbulent flow. This transition happens at a Reynolds number of about 1.2×10^5 , which theory predicts that there may be some transitioning happening, but not that it should be fully turbulent. [8]

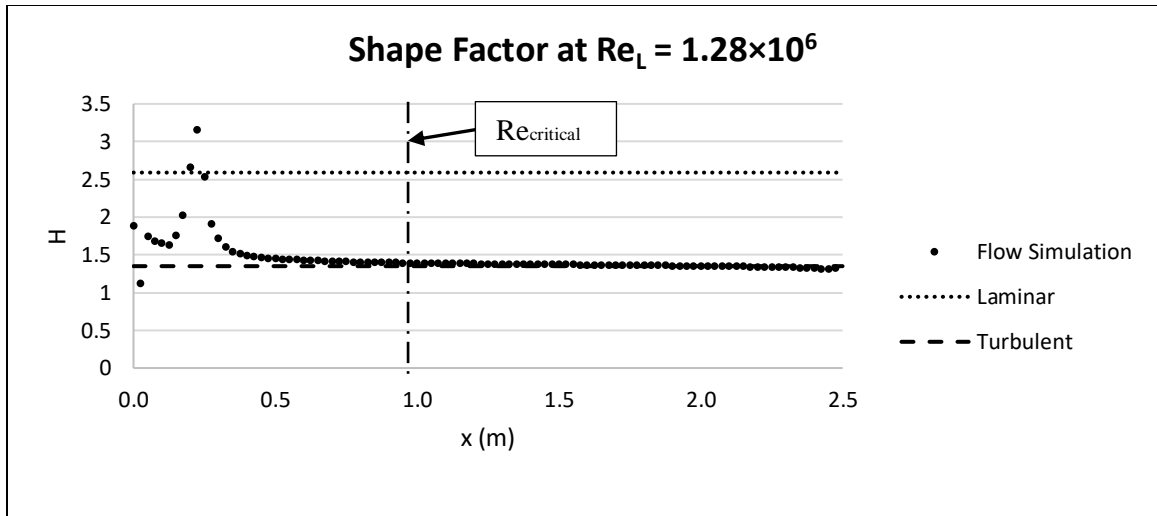


Figure 38: Shape factor along plate at $Re_L = 1.28 \times 10^6$ for 2D-External-Constant Temperature case

The shape factor analysis shown in Figure 38 confirms what appears to be true, that the flow starts in a transitional phase, briefly becomes laminar, then becomes fully turbulent well before the critical Reynolds number. Similar effects can even be seen in flow that never reaches a Reynolds number where the flow should start to transition, or a Reynolds number of 1.0×10^5 . [8]

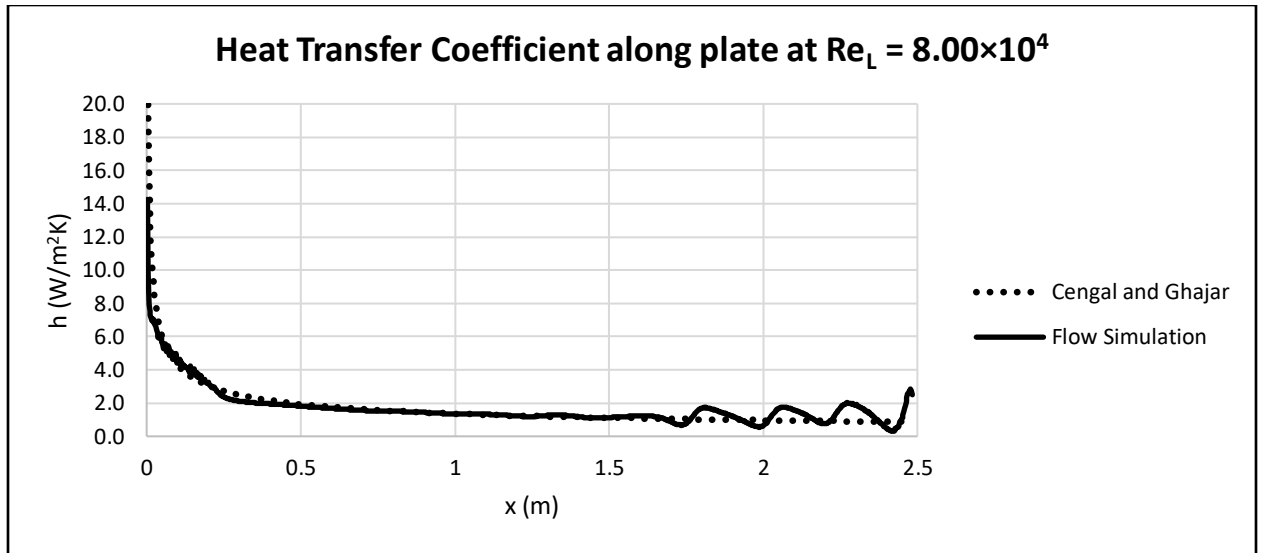


Figure 39: Heat transfer coefficient along plate at $Re_L = 8.00 \times 10^4$ for 2D-External-Constant Temperature case

With a Reynolds number of 8.00×10^4 the heat transfer coefficient starts to become unsteady and looks to be entering a transitional phase towards the trailing edge of the plate. Again, the shape factor analysis confirms this to be true in Figure 40. Although most of the plate is clearly laminar, the shape factor starts to waver towards the trailing edge and dip down towards turbulence.

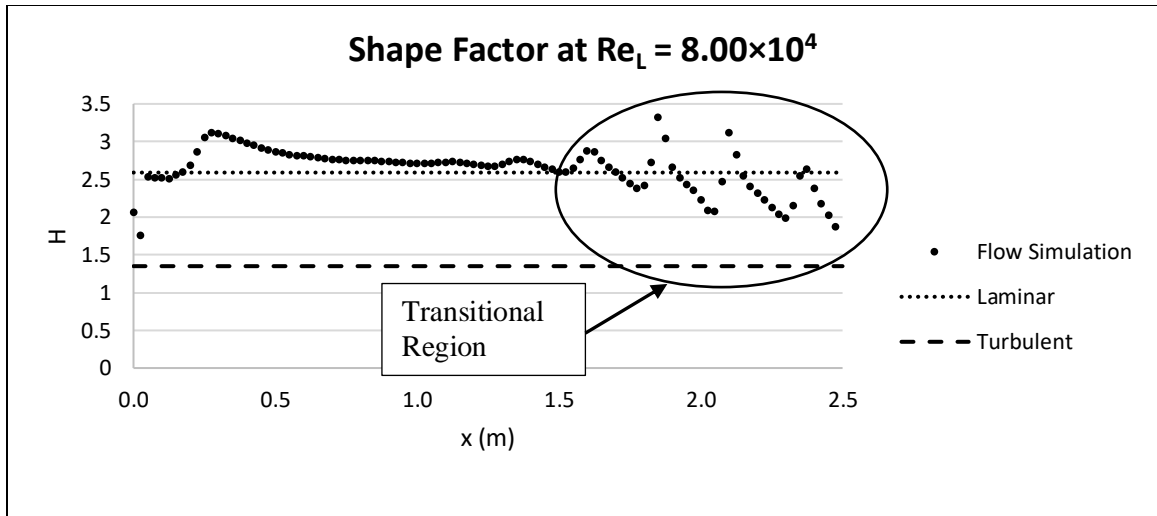


Figure 40: Shape factor along plate at $Re_L = 8.00 \times 10^4$ for 2D-External-Constant Temperature case

It seems that the leading-edge shape, although necessary to prevent the leading-edge separation bubble, produces results that differ from theory in other ways. However, the early turbulence transition and increased heat transfer coefficient at the leading-edge likely aren't caused by inaccuracy in the software but happen because the model used for the theoretical analysis is not exactly the same as the model created in SOLIDWORKS Flow Simulation.

High Reynolds Number Discrepancies

Another interesting phenomenon is that the percent difference between Flow Simulation and theoretical values increased as the maximum Reynolds number increased. For example, comparing the turbulent region of the 2D-Internal-Constant Heat Flux case at a Reynolds number of 1.28×10^6 in Figure 41 to turbulent region of the 2D-External-Constant Temperature case at a Reynolds number of 9.60×10^6 in Figure 42, the gap between Flow Simulation's predicted heat transfer coefficient and the theoretical heat transfer coefficient becomes noticeably larger.

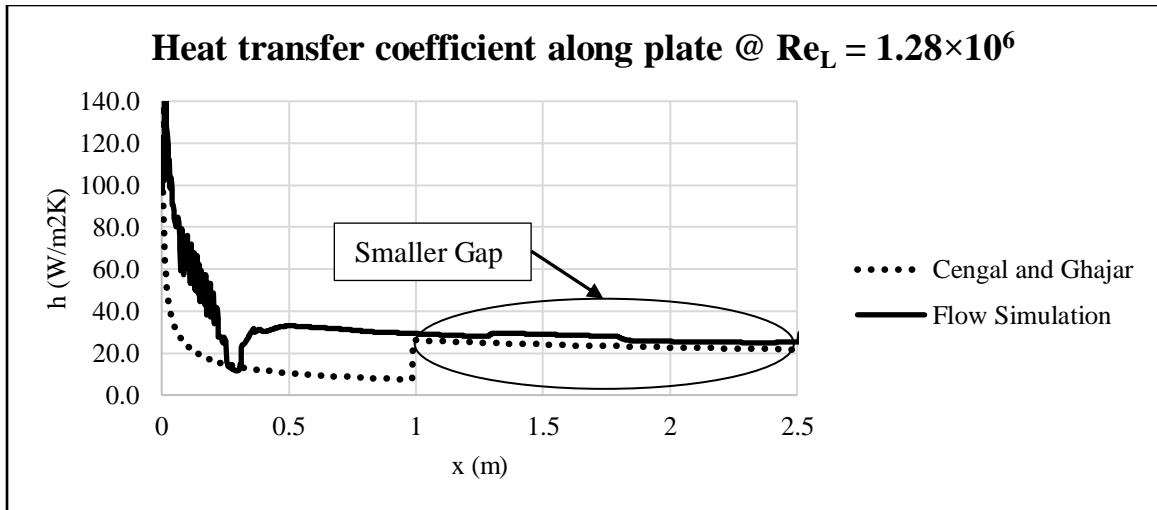


Figure 41: Heat transfer coefficient along plate at $Re_L = 1.28 \times 10^6$ for 2D-Internal-Constant Heat Flux case

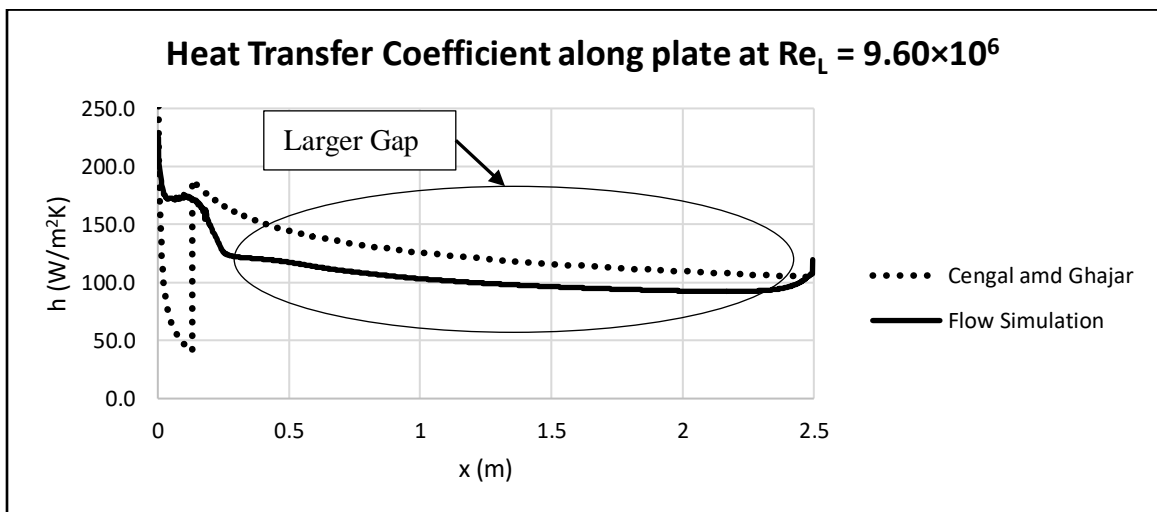


Figure 42: Heat transfer coefficient along plate at $Re_L = 9.60 \times 10^6$ for 2D-External-Constant Temperature case

It is difficult to pinpoint the discrepancies on either SOLIDWORKS Flow Simulation or on the theoretical equations. The turbulent equations themselves are only stated to be effective up to a Reynolds number of 10^7 . To be sure, either experimental data for flat plates is needed at these

Reynolds number or new theoretical equations need to be produced or found that are more accurate in this higher Reynolds number zone.

3D-Internal

SOLIDWORKS Flow Simulation was able to run Internal analysis because of the decreased cell count of the initial mesh and the software performed better than expected. Figure 43 and Figure 44 show that the percent differences between the average heat transfer coefficient for Flow Simulation and theoretical or experimental values is similar to the percent differences of the other cases.

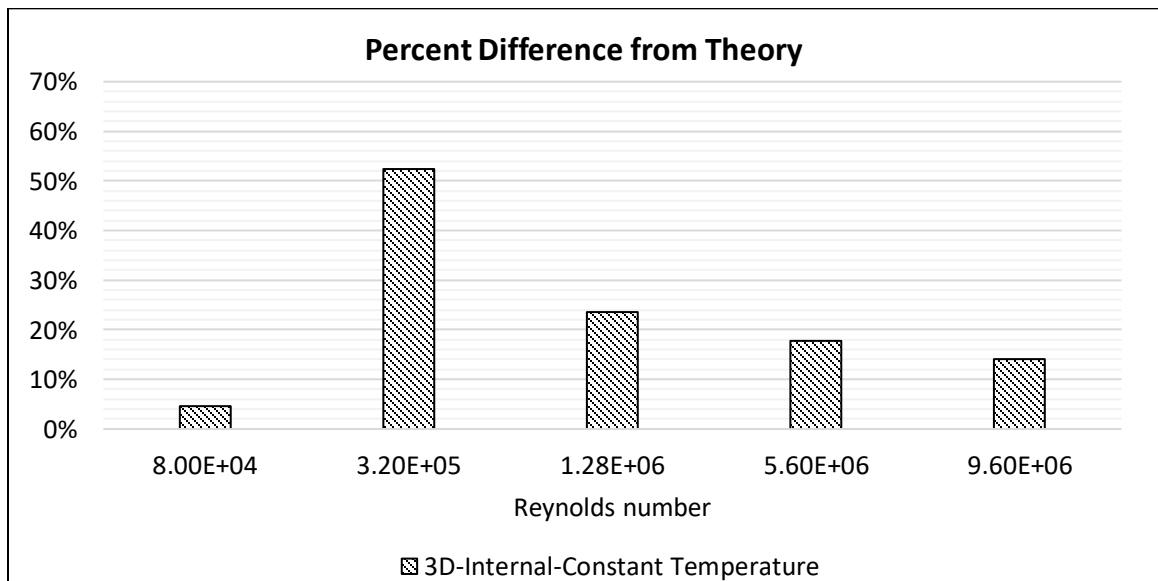


Figure 43: Average heat transfer coefficient's percent difference from theoretical predictions by Reynolds number for 3D-Internal-Constant Temperature case

Although the 3D results do not agree as well with theory as 2D cases, the results are still reasonable. Especially for Reynolds numbers further away from the transitional regions. The most concerning Reynolds number is 3.20×10^5 , which also differed greatly from theory for the 2D

analysis: suggesting that the 3D analysis is not refining the flow well enough like was the case for the Internal study.

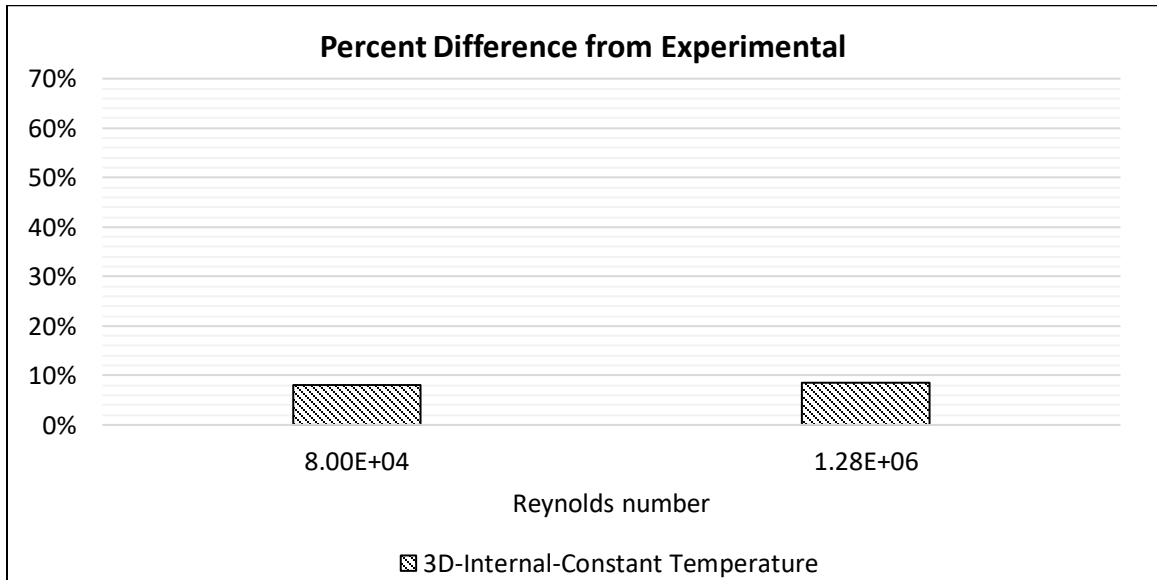


Figure 44: Average heat transfer coefficient's percent difference from experimental data by Reynolds number for 3D-Internal-Constant Temperature case

Although there was some erratic behavior in the predicted heat transfer coefficient such as seen in Figure 45, most of the data actually agreed well with theory as it does in Figure 46. Since the mesh is much coarser for this case, the software is likely simplifying the turbulent boundary layer and is still producing reasonable results.

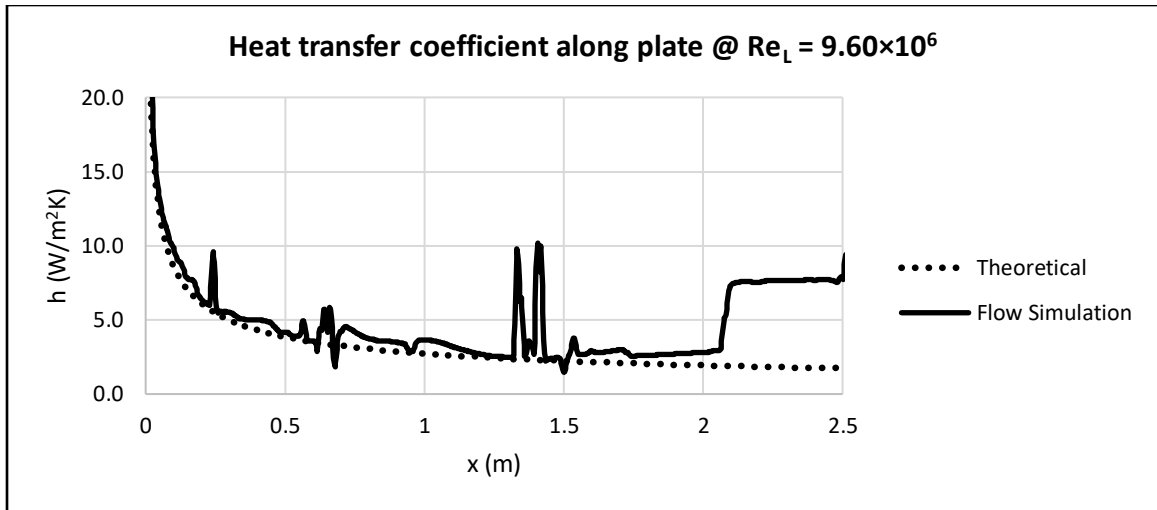


Figure 45: Heat transfer coefficient along plate at $Re_L = 3.20 \times 10^5$ for 3D- Internal -Constant Temperature case

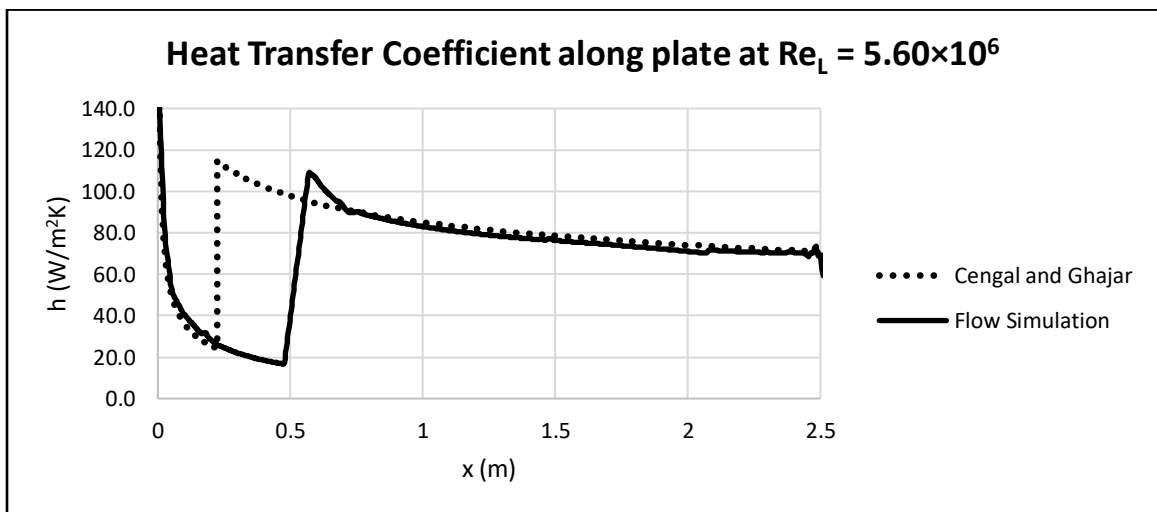


Figure 46: Heat transfer coefficient along plate at $Re_L = 5.60 \times 10^6$ for 3D-Internal-Constant Temperature case

These results are promising and show that the software could potentially qualitatively handle 3D simulations so long as the initial mesh size is not too large. Manually optimizing the mesh and mirroring the computational domain across symmetrical planes could potentially

produce results as detailed in the 2D cases. However, the model used in this paper would have produced very little flow in the z-direction and was not very complex. For actual UAVs, with complex surfaces, the results may not be as close to reality. Also, the leading-edge effects seen in the 2D cases are no longer present, which indicates that the software is not accurately prediction some of the physical phenomena that is present in real flows.

CHAPTER V

CONCLUSION

This paper aims to validate SOLIDWORKS Flow Simulation's ability to analyze the thermal management of UAVs both qualitatively and quantitatively by comparing the software's prediction for basic heat transfer problems to theoretical and experimental data. Although no hard conclusions are drawn, this paper provides many findings that will help lay the foundation for future thermal management studies and similar heat transfer problems.

Although SOLIDWORKS Flow Simulation provided heat transfer values that agreed with theoretical and experimental data, what is perhaps more impressive than that is that it was able to predict real life physical phenomena that was not even anticipated when beginning the study. The main example of this is the leading-edge separation bubbles. The sharp leading edge that was originally designed to prevent leading edge effects on the top surface of the plate actually resulted in a turbulent region at the leading edge of the plate. After reviewing the literature on sharp leading edges, it was found that this was not an artifact of the software but a physical phenomenon that had been studied. [19] The leading edge was changed to minimize this effect after it was discovered, but this was very promising and shows the power of SOLIDWORKS Flow Simulations capabilities.

However, SOLIDWORKS Flow Simulation did not always perform this well. It was found that for internal flow the software did not produce a mesh that was fine enough to produce the accuracy seen in the external flow case. This is because the software needed more refinements for the internal case since the ratio factor was only default for external flow and the software refined the mesh in the spanwise direction despite being a 2D analysis. This drastically increased the cell count in the spanwise direction and limited the number of useful cells in the x-y plane. It is likely that an optimized initial mesh would prevent the need for the refinements and allow improve the results of the internal flow case, but this falls outside the scope for this study. Furthermore, the constant heat flux case showed erratic predictions for the local heat transfer coefficient. The problem only appeared in transitional regions and the results still agreed well with the data, but it is not known why the constant heat flux setting displayed this behavior, and caution is recommended with this setting because of it.

3D flow provided mixed results. 3D flow terminated without running the simulation for external flow since the initial mesh had over 20,000,000 cells and the approximate maximum cell count setting was set at 5,000,000 since the computer used for the simulations was not powerful enough. An additional test case was added using internal analysis to see if the software could run with the reduced initial cell count. Not only did the internal 3D simulation run, but it provided results that were much closer to theory and experimental data than expected. However, the results were no longer able to predict some of the leading-edge effects seen in the 2D cases, and therefore should be used with caution but may be able to provide results good enough for qualitative analysis.

SUGGESTIONS AND FUTURE WORK

Since SOLIDWORKS Flow Simulation's refinements during simulation are very inefficient for 2D flow, properly optimizing the initial mesh would be very valuable. This kind of study would help more than just the heat transfer studies like seen in this paper but could drastically improve all 2D studies performed in SOLIDWORKS Flow Simulation. An area of particular importance for UASs would be to optimize the initial mesh for airfoils. The benefits are not as great for 3D analysis, but more optimized initial mesh may improve the accuracy of SOLIDWORKS Flow Simulation enough to pick up on more of the physical phenomena like the leading-edge effects on the plate in this study.

To further validate that the leading-edge effects seen in the analysis would be present in real flow, an experiment could be modeled using the plate from the simulation and heat transfer coefficient values measured accordingly. This would also reveal if the discrepancies at higher Reynolds numbers and the early turbulence transitions are due to inaccuracies in the software or the theoretical model. Experimental data was used in the analysis, but it was formulas derived from experimental data not experimental data modeled after the simulation.

There were many shortcomings in the software found in this study, but there are likely more. To push the boundary of what this software can and can't do, there needs to be more studies with increasingly complex cases leading up to studies on actual models of UASs with experimental data taken on the real aircraft.

No matter how many studies are done, the results should always be interpreted with caution. CFD is complex and requires careful setup and consideration. Although the results are

fast and accurate when it is used correctly, a small careless error may provide believable results that are incorrect and interfere with what would otherwise be good design.

REFERENCES

- [1] H. B. S. M. B. P. Donald R. Lowe, *U.S. ARMY UNMANNED AIRCRAFT SYSTEMS (UAS)—A HISTORICAL PERSPECTIVE TO IDENTIFYING AND UNDERSTANDING STAKEHOLDER RELATIONSHIPS*, MONTEREY, CALIFORNIA: NAVAL POSTGRADUATE SCHOOL, 2014.
- [2] B. C. Preble, "A case for drones," *Technology and engineering teacher*, vol. 74, no. 7, pp. 24-29, 2015.
- [3] U.S. Department of Defense, "UNMANNED AIRCRAFT SYSTEMS (UAS)," [Online]. Available: <https://dod.defense.gov/UAS/>. [Accessed 20 February 2021].
- [4] Federal Aviation Administration, "UAS by the Numbers," 18 February 2021. [Online]. Available: https://www.faa.gov/uas/resources/by_the_numbers/. [Accessed 20 February 2021].

- [5] Teal Group, "Teal Group Predicts Worldwide Civil Drone Production Will Almost Triple Over the Next Decade," 16 June 2019. [Online]. Available: <https://www.tealgroup.com/index.php/pages/press-releases/60-teal-group-predicts-worldwide-civil-drone-production-will-almost-triple-over-the-next-decade>. [Accessed 20 February 2021].
- [6] D. D. D. Rory A. Roberts, "Control Architecture Study Focused on Energy Savings of an Aircraft Thermal Management System," *Journal of Dynamic Systems, Measurement, and Control*, vol. 136, 2014.
- [7] E. N. T. N. J. Y. Forrester T. Johnson, "THIRTY YEARS OF DEVELOPMENT AND APPLICATION OF CFD AT BOEING COMMERCIAL AIRPLANES, SEATTLE," *AIAA*, vol. 34, no. 10, pp. 1115-1151, 2005.
- [8] A. J. Ghajar and Y. A. Cengel, *Heat and Mass Transfer: Fundamentals & Applications*, New York: McGraw-Hill, 1997.
- [9] Jürges, "Der Wärmübergang an einer ebenen Wand," *Gesundheits-Ingenieur*, vol. 19, no. 1, 1924.
- [10] J. Watmuff, W. Charters and D. Proctor, "Solar and wind induced external coefficients - Solar collectors," *Cooperation Méditerranéenne pour l'Energie Solaire*, p. 56, 1977.
- [11] S. Sharples and P. S. Charlesworth, "FULL-SCALE MEASUREMENTS OF WIND-INDUCED CONVECTIVE HEAT TRANSFER FROM A ROOF-MOUNTED FLAT PLATE SOLAR COLLECTOR," *Solar Energy*, vol. 62, no. 2, pp. 69-77, 1998.

- [12] E. Sartori, "Convection coefficient equations for forced airflow over flat surfaces," *Solar Energy*, vol. 80, no. 9, pp. 1063-1071, 2006.
- [13] A. Edwards and B. N. Furber, "THE INFLUENCE OF FREE-STREAM TURBULENCE ON HEAT TRANSFER BY CONVECTION FROM AN ISOLATED REGION OF A PLANE SURFACE IN PARALLEL AIR FLOW," *Proceedings of the Institute of Mechanical engineers*, pp. 941-954, 1956.
- [14] B. C. a. M. M. Tien-Yu Tom Lee, "Application of CFD Technology to Electronic Thermal Management," *IEEE TRANSACTIONS ON COMPONENTS, PACKAGING, AND MANUFACTURING TECHNOLOGY*, vol. 18, no. 3, pp. 511-520, 1995.
- [15] M. S. . P. F. . A. D. . J. B. iotr Łapka, "Simplified Thermo-Fluid Model of an Engine Cowling in a Small Airplane," *Aircraft Engineering and Aerospace Technology*, vol. 86, no. 3, pp. 242-249, 2014.
- [16] O. M. D. D. M. M. M. S. A. Zied Driss, "Numerical simulation and experimental validation of the turbulent flow around a small incurved Savonius wind rotor," *Energy*, vol. 74, pp. 506-517, 2014.
- [17] J. Wallace, "Investigation of SOLIDWORKS Flow Simulation as a Valid Tool for Analyzing Airfoil Performance Characteristics in Low Reynolds Number Flow," Oklahoma State University, 2017.
- [18] SOLIDWORKS, "Flow Simulation 2018 Technical Reference," SOLIDWORKS, 2018.

- [19] M. J. Crompton, "The Thin Airfoil Leading Edge Separation Bubble," *University of Bristol*, 2001.
- [20] S. Collie, M. Gerritsen and P. Jackson, "Performance of Two-Equation Turbulence Models for Flat Plate Flows With Leading Edge Bubbles," *ASME*, 2008.
- [21] M. R. Davis, "Design of Flat Plate Leading Edges to Avoid Flow Separation," *AIAA Journal*, vol. 18, no. 5, pp. 598-600.
- [22] P. G. Huang and G. N. Coleman, "Van Driest Transformation and Compressible Wall-Bounded Flows," *AIAA JOURNAL*, vol. 32, no. 10, pp. 2110-2113, 1994.
- [23] J. Ala-Juusela, "CFD Simulations of a Turbulent Flow over a Flat Plate," Aalto University, 2001.
- [24] W. Reynolds, W. Kays and S. Kline, "Heat Transfer in the Turbulent Incompressible Boundary Layer," National Aeronautics and Space Administration, Washington, DC, 1958.
- [25] S. Whitaker, "Forced Convection Heat Transfer Correlations for Flow in Pipes, Past Flat Plates, Single Cylinders, Single Spheres, and for Flow in Packed Beds and Tube Bundles," *AIChE Journal*, vol. 18, no. 2, pp. 361-371, 1972.
- [26] SOLIDWORKS, "Flow Simulation 2018 Tutorial," SOLIDWORKS, 2018.
- [27] SOLIDWORKS, "Flow Simulation 2018 Validation Examples," SOLIDWORKS, 2018.
- [28] Dassault Systems, "Enhanced Turbulence Modeling in SOLIDWORKS Flow Simulation," Dassault Systems, 2013.

- [29] B. L. Alberto Sigala, "Applications of Unmanned Aerial Systems (UAS): A Delphi Study Projecting Future UAS Missions and Relevant Challenges," *Drones*, vol. 4, no. 8, 2020.

APPENDICES

Results		
Simulation number	h (W/(m ² K))	number of Cells
1	63.14	33,851
2	61.015	62,340
3	72.769	122,499
4	74.402	235,677
5	70.232	48,345
6	74.54	272,603
7	73.36	3,992,513
8	73.8418	4,705,688
9	73.99	86,463
10	73.67	3,828,216
11	74.128	4,823,032
12	73.976	4,825,005
13	74.614	177,042
14	73.4336	1,614,998
15	74.85	4,901,188
16	74.79	4,902,526
17	73.914	342,577
18	74.0287	970,312
19	75.96	4,819,883
20	75.804	4,757,629
21	73.6773	2,555,382
22	73.7048	2,562,011
23	73.719	2,663,328
24	73.512	2,092,747

25	74.611	2,864,197
26	73.461	2,578,709
27	73.8799	2,627,181
28	72.8352	2,972,379
29	73.6704	2,299,539
30	73.714	2,749,788
31	73.8316	2,583,612
32	73.768	2,633,251
33	73.786	2,549,406
34	73.873	2,991,957
35	74.001	2,987,596
36	59.7683	3,002,464
37	73.582	3,015,472
38	74.03	3,015,470
39	73.192	1,942,304
40	73.4503	2,474,488
41	73.417	2,468,573
42	73.666	2,238,810
43	24.616	1,218,850
44	4.253	3,284,601
45	1.938	4,810,217
46	1.905	4,512,892
47	101.9	3,286,112
48	1.83	4,797,494
49	3.619	3,331,981
50	25.105	1,257,883
51	77.729	2,436,408

52	108.51	3,753,356
53	57.88	35,574
54	58.384	122,006
55	58.771	387,190
56	56.528	1,051,062
57	57.514	1,134,938
58	59.67	2,190,881
59	58.59	3,014,553
60	1.778	2,584,319
61	5.84	2,688,567
62	14.413	2,603,368
63	72.396	2,681,799
64	111.902	2,347,815
65	2.412	2,879,563
66	5.536	2,320,406
67	31.629	1,032,646
68	83.747	2,497,191
69	116.302	2,450,844
70	N/A	20,327,832
71	N/A	20,327,832
72	N/A	20,327,832
73	N/A	20,327,832
74	N/A	20,327,832
75	1.806	4,598,210
76	5.259	4,669,279
77	22.401	4,329,963
78	69.96	4,557,480
79	112.53	4,534,679

Table 12: General simulation results

Flat Plate Parameters			
Simulation number	V (m/s)	Length (m)	Reynolds number
1	35	2.5	5,637,887
2	35	2.5	5,640,000
3	35	2.5	5,640,000
4	35	2.5	5,640,000

5	35	2.5	5,640,000
6	35	2.5	5,640,000
7	35	2.5	5,640,000
8	35	2.5	5,640,000
9	35	2.5	5,640,000
10	35	2.5	5,640,000
11	35	2.5	5,640,000
12	35	2.5	5,640,000
13	35	2.5	5,640,000
14	35	2.5	5,640,000
15	35	2.5	5,640,000
16	35	2.5	5,640,000
17	35	2.5	5,640,000
18	35	2.5	5,640,000
19	35	2.5	5,640,000
20	35	2.5	5,640,000
21	35	2.5	5,640,000
22	35	2.5	5,640,000
23	35	2.5	5,640,000
24	35	2.5	5,640,000
25	35	2.5	5,640,000
26	35	2.5	5,640,000
27	35	2.5	5,640,000
28	35	2.5	5,640,000
29	35	2.5	5,640,000
30	35	2.5	5,640,000
31	35	2.5	5,640,000
32	35	2.5	5,640,000
33	35	2.5	5,640,000
34	35	2.5	5,640,000
35	35	2.5	5,640,000
36	35	2.5	5,640,000
37	35	2.5	5,640,000
38	35	2.5	5,640,000
39	35	2.5	5,640,000
40	35	2.5	5,640,000
41	35	2.5	5,640,000
42	35	2.5	5,640,000

43	8	2.5	1,080,000
44	2	2.5	322,000
45	0.5	2.5	322,000
46	0.5	2.5	322,000
47	60	2.5	322,000
48	0.5	2.5	322,000
49	2	2.5	322,000
50	8	2.5	322,000
51	35	2.5	322,000
52	60	2.5	322,000
53	35	2.5	322,000
54	35	2.5	322,000
55	35	2.5	322,000
56	35	2.5	322,000
57	35	2.5	322,000
58	35	2.5	322,000
59	35	2.5	322,000
60	0.5	2.5	322,000
61	2	2.5	322,000
62	8	2.5	322,000

63	35	2.5	322,000
64	60	2.5	322,000
65	0.5	2.5	322,000
66	2	2.5	322,000
67	8	2.5	322,000
68	35	2.5	322,000
69	60	2.5	322,000
70	0.5	2.5	322,000
71	2	2.5	322,000
72	8	2.5	322,000
73	35	2.5	322,000
74	60	2.5	322,000
75	0.5	2.5	322,000
76	2	2.5	322,000
77	8	2.5	322,000
78	35	2.5	322,000
79	60	2.5	322,000

Table 13: Flat plate parameters by simulation number

Computational Domain Settings						
Simulation number	Type	Forward Length (m)	Aft Length (m)	Above Length (m)	Below Length (m)	Span (m)
1	2D	30	30	15	15	0.0001
2	2D	30	30	15	15	0.0001
3	2D	30	30	15	15	0.0001
4	2D	30	30	15	15	0.0001
5	2D	30	30	15	15	0.0001
6	2D	30	30	15	15	0.0001
7	2D	30	30	15	15	0.0001
8	2D	30	30	15	15	0.0001
9	2D	30	30	15	15	0.0001
10	2D	30	30	15	15	0.0001
11	2D	30	30	15	15	0.0001
12	2D	30	30	15	15	0.0001
13	2D	30	30	15	15	0.0001
14	2D	30	30	15	15	0.0001

15	2D	30	30	15	15	0.0001
16	2D	30	30	15	15	0.0001
17	2D	30	30	15	15	0.0001
18	2D	30	30	15	15	0.0001
19	2D	30	30	15	15	0.0001
20	2D	30	30	15	15	0.0001
21	2D	30	30	15	15	0.0001
22	2D	22.5	22.5	15	15	0.0001
23	2D	15	15	15	15	0.0001
24	2D	7.5	7.5	15	15	0.0001
25	2D	2.5	2.5	15	15	0.0001
26	2D	30	30	22.5	22.5	0.0001
27	2D	30	30	7.5	7.5	0.0001
28	2D	30	30	0.5	0.5	0.0001
29	2D	15	15	15	15	0.0001
30	2D	15	15	15	15	0.001
31	2D	15	15	15	15	0.01
32	2D	15	15	15	15	0.1
33	2D	15	15	15	15	1
34	2D	15	15	15	15	0.0001
35	2D	15	15	15	15	0.0001
36	2D	15	15	15	15	0.0001
37	2D	15	15	15	15	0.0001
38	2D	15	15	15	15	0.0001
39	2D	15	15	15	15	0.0001
40	2D	15	15	15	15	0.0001
41	2D	15	15	15	15	0.0001
42	2D	15	15	15	15	0.0001
43	2D	15	15	15	15	0.0001
44	2D	15	15	15	15	0.0001
45	2D	15	15	15	15	0.0001
46	2D	15	15	15	15	0.0001
47	2D	15	15	15	15	0.0001
48	2D	15	15	15	15	0.0001
49	2D	15	15	15	15	0.0001
50	2D	15	15	15	15	0.0001
51	2D	15	15	15	15	0.0001
52	2D	15	15	15	15	0.0001

53	2D	15	15	15	15	7.12
54	2D	15	15	15	15	7.12
55	2D	15	15	15	15	7.12
56	2D	15	15	15	15	7.12
57	2D	15	15	15	15	7.12
58	2D	15	15	15	15	7.12
59	2D	15	15	15	15	7.12
60	2D	15	15	15	15	0.0001
61	2D	15	15	15	15	0.0001
62	2D	15	15	15	15	0.0001
63	2D	15	15	15	15	0.0001
64	2D	15	15	15	15	0.0001
65	2D	15	15	15	15	0.0001
66	2D	15	15	15	15	0.0001
67	2D	15	15	15	15	0.0001
68	2D	15	15	15	15	0.0001
69	2D	15	15	15	15	0.0001
70	3D	15	15	15	15	0.0001
71	3D	15	15	15	15	0.0001
72	3D	15	15	15	15	0.0001
73	3D	15	15	15	15	0.0001
74	3D	15	15	15	15	0.0001
75	3D	15	15	15	15	0.0001
76	3D	15	15	15	15	0.0001
77	3D	15	15	15	15	0.0001
78	3D	15	15	15	15	0.0001
79	3D	15	15	15	15	0.0001

Table 14: Computational domain settings by simulation number

Mesh Settings			
Simulation number	Refinement Type	Refinement Level	Ratio Factor
1	Automatic	1	1
2	Automatic	3	1
3	Automatic	5	1
4	Automatic	7	1
5	Automatic	1	1

6	Automatic	1	1
7	Automatic	1	1
8	Automatic	1	1
9	Automatic	3	1
10	Automatic	3	1
11	Automatic	3	1
12	Automatic	3	1
13	Automatic	5	1
14	Automatic	5	1
15	Automatic	5	1
16	Automatic	5	1
17	Automatic	7	1
18	Automatic	7	1
19	Automatic	7	1
20	Automatic	7	1
21	Automatic	4	1
22	Automatic	4	1
23	Automatic	4	1
24	Automatic	4	1
25	Automatic	4	1
26	Automatic	4	1
27	Automatic	4	1
28	Automatic	4	1
29	Automatic	4	1
30	Automatic	4	1
31	Automatic	4	1
32	Automatic	4	1
33	Automatic	4	1
34	Automatic	4	1
35	Automatic	4	1
36	Automatic	4	1
37	Automatic	4	1
38	Automatic	4	1
39	Automatic	4	1
40	Automatic	4	1
41	Automatic	4	1
42	Automatic	4	1
43	Automatic	4	1

44	Automatic	4	1
45	Automatic	4	1
46	Automatic	4	1
47	Automatic	4	1
48	Automatic	4	1
49	Automatic	4	1
50	Automatic	4	1
51	Automatic	4	1
52	Automatic	4	1
53	Automatic	4	N/A
54	Automatic	4	N/A
55	Automatic	4	N/A
56	Automatic	4	N/A
57	Automatic	5	N/A
58	Automatic	6	N/A
59	Automatic	7	N/A
60	Automatic	7	N/A
61	Automatic	7	N/A
62	Automatic	7	N/A
63	Automatic	7	N/A
64	Automatic	7	N/A
65	Automatic	4	N/A
66	Automatic	4	N/A
67	Automatic	4	N/A
68	Automatic	4	N/A
69	Automatic	4	N/A
70	Automatic	7	N/A
71	Automatic	7	N/A
72	Automatic	7	N/A
73	Automatic	7	N/A
74	Automatic	7	N/A
75	Automatic	7	N/A
76	Automatic	7	N/A
77	Automatic	7	N/A
78	Automatic	7	N/A
79	Automatic	7	N/A

Table 15: Global Mesh settings by simulation number

Refinement Settings				
Simulation number	number of Refinements	Approximate Max Cells	Start (Travels)	Period (Travels)
1	0	5,000,000	293.2	303.2
2	0	5,000,000	293.2	303.2
3	0	5,000,000	293.2	303.2
4	0	5,000,000	293.2	303.2
5	1	5,000,000	293.2	303.2
6	3	5,000,000	293.2	303.2
7	5	5,000,000	293.2	303.2
8	7	5,000,000	293.2	303.2
9	1	5,000,000	293.2	303.2
10	3	5,000,000	293.2	303.2
11	5	5,000,000	293.2	303.2
12	7	5,000,000	293.2	303.2
13	1	5,000,000	293.2	303.2
14	3	5,000,000	293.2	303.2
15	5	5,000,000	293.2	303.2
16	7	5,000,000	293.2	303.2
17	1	5,000,000	293.2	303.2
18	3	5,000,000	293.2	303.2
19	5	5,000,000	293.2	303.2
20	7	5,000,000	293.2	303.2
21	4	5,000,000	293.2	303.2
22	4	5,000,000	293.2	303.2
23	4	5,000,000	293.2	303.2
24	4	5,000,000	293.2	303.2
25	4	5,000,000	293.2	303.2
26	4	5,000,000	293.2	303.2
27	4	5,000,000	293.2	303.2
28	4	5,000,000	293.2	303.2
29	4	5,000,000	293.2	303.2
30	4	5,000,000	293.2	303.2
31	4	5,000,000	293.2	303.2
32	4	5,000,000	293.2	303.2
33	4	5,000,000	293.2	303.2
34	4	5,000,000	293.2	303.2

35	4	5,000,000	293.2	303.2
36	4	5,000,000	293.2	303.2
37	4	5,000,000	293.2	303.2
38	4	5,000,000	293.2	303.2
39	4	5,000,000	293.2	303.2
40	4	5,000,000	293.2	303.2
41	4	10,000,000	293.2	303.2
42	4	5,000,000	293.2	303.2
43	4	5,000,000	293.2	303.2
44	4	5,000,000	293.2	303.2
45	4	5,000,000	293.2	303.2
46	4	5,000,000	293.2	303.2
47	4	5,000,000	293.2	303.2
48	4	5,000,000	293.2	303.2
49	4	5,000,000	293.2	303.2
50	4	5,000,000	293.2	303.2
51	4	5,000,000	293.2	303.2
52	4	5,000,000	293.2	303.2
53	4	5,000,000	293.2	816
54	5	5,000,000	293.2	816
55	6	5,000,000	293.2	816
56	7	5,000,000	293.2	816
57	7	5,000,000	293.2	816
58	7	5,000,000	293.2	816
59	7	5,000,000	293.2	816
60	7	3,000,000	293.2	303.2
61	7	3,000,000	293.2	303.2
62	7	3,000,000	293.2	303.2
63	7	3,000,000	293.2	303.2
64	7	3,000,000	293.2	303.2
65	4	3,000,000	293.2	-
66	4	3,000,000	293.2	-
67	4	3,000,000	293.2	-
68	4	3,000,000	293.2	-
69	4	3,000,000	293.2	-
70	7	5,000,000	293.2	303.2
71	7	5,000,000	293.2	303.2
72	7	5,000,000	293.2	303.2

73	7	5,000,000	293.2	303.2
74	7	5,000,000	293.2	303.2
75	7	5,000,000	293.2	303.2
76	7	5,000,000	293.2	303.2
77	7	5,000,000	293.2	303.2
78	7	5,000,000	293.2	303.2
79	7	5,000,000	293.2	303.2

Table 16: Refinement settings by simulation number

General Settings - Part 1					
Simulation number	Wall Roughness (micrometers)	Air Pressure (atm)	Air Temperature (K)	Turbulence Intensity (%)	Turbulence Length (m)
1	0	1	293.2	0.1%	0.01
2	0	1	293.2	0.1%	0.01
3	0	1	293.2	0.1%	0.01
4	0	1	293.2	0.1%	0.01
5	0	1	293.2	0.1%	0.01
6	0	1	293.2	0.1%	0.01
7	0	1	293.2	0.1%	0.01
8	0	1	293.2	0.1%	0.01
9	0	1	293.2	0.1%	0.01
10	0	1	293.2	0.1%	0.01
11	0	1	293.2	0.1%	0.01
12	0	1	293.2	0.1%	0.01
13	0	1	293.2	0.1%	0.01
14	0	1	293.2	0.1%	0.01
15	0	1	293.2	0.1%	0.01
16	0	1	293.2	0.1%	0.01
17	0	1	293.2	0.1%	0.01
18	0	1	293.2	0.1%	0.01
19	0	1	293.2	0.1%	0.01
20	0	1	293.2	0.1%	0.01
21	0	1	293.2	0.1%	0.01
22	0	1	293.2	0.1%	0.01
23	0	1	293.2	0.1%	0.01
24	0	1	293.2	0.1%	0.01

25	0	1	293.2	0.1%	0.01
26	0	1	293.2	0.1%	0.01
27	0	1	293.2	0.1%	0.01
28	0	1	293.2	0.1%	0.01
29	0	1	293.2	0.1%	0.01
30	0	1	293.2	0.1%	0.01
31	0	1	293.2	0.1%	0.01
32	0	1	293.2	0.1%	0.01
33	0	1	293.2	0.1%	0.01
34	0	1	293.2	1.0%	0.01
35	0	1	293.2	10.0%	0.01
36	0	1	293.2	100.0%	0.01
37	0	1	293.2	0.1%	0.001
38	0	1	293.2	0.1%	0.1
39	0	1	293.2	0.1%	0.01
40	0	1	293.2	0.1%	0.01
41	0	1	293.2	0.1%	0.01
42	0	1	293.2	0.1%	0.01
43	0	1	293.2	0.1%	0.01
44	0	1	293.2	0.1%	0.01
45	0	1	293.2	0.1%	0.01
46	0	1	293.2	0.1%	0.01
47	0	1	293.2	0.1%	0.01
48	0	1	293.2	0.1%	0.01
49	0	1	293.2	0.1%	0.01
50	0	1	293.2	0.1%	0.01
51	0	1	293.2	0.1%	0.01
52	0	1	293.2	0.1%	0.01
53	0	1	293.2	0.1%	0.01
54	0	1	293.2	0.1%	0.01
55	0	1	293.2	0.1%	0.01
56	0	1	293.2	0.1%	0.01
57	0	1	293.2	0.1%	0.01
58	0	1	293.2	0.1%	0.01
59	0	1	293.2	0.1%	0.01
60	0	1	293.2	0.1%	0.01
61	0	1	293.2	0.1%	0.01
62	0	1	293.2	0.1%	0.01

63	0	1	293.2	0.1%	0.01
64	0	1	293.2	0.1%	0.01
65	0	1	293.2	0.1%	0.01
66	0	1	293.2	0.1%	0.01
67	0	1	293.2	0.1%	0.01
68	0	1	293.2	0.1%	0.01
69	0	1	293.2	0.1%	0.01
70	0	1	293.2	0.1%	0.01
71	0	1	293.2	0.1%	0.01
72	0	1	293.2	0.1%	0.01
73	0	1	293.2	0.1%	0.01
74	0	1	293.2	0.1%	0.01
75	0	1	293.2	0.1%	0.01
76	0	1	293.2	0.1%	0.01
77	0	1	293.2	0.1%	0.01
78	0	1	293.2	0.1%	0.01
79	0	1	293.2	0.1%	0.01

Table 17: General settings by simulation number part 1

General Settings - Part 2			
Simulation number	Analysis Type	Fluid	Flow Type
1	External	Air	Laminar and Turbulent
2	External	Air	Laminar and Turbulent
3	External	Air	Laminar and Turbulent
4	External	Air	Laminar and Turbulent
5	External	Air	Laminar and Turbulent
6	External	Air	Laminar and Turbulent
7	External	Air	Laminar and Turbulent

8	External	Air	Laminar and Turbulent
9	External	Air	Laminar and Turbulent
10	External	Air	Laminar and Turbulent
11	External	Air	Laminar and Turbulent
12	External	Air	Laminar and Turbulent
13	External	Air	Laminar and Turbulent
14	External	Air	Laminar and Turbulent
15	External	Air	Laminar and Turbulent
16	External	Air	Laminar and Turbulent
17	External	Air	Laminar and Turbulent
18	External	Air	Laminar and Turbulent
19	External	Air	Laminar and Turbulent
20	External	Air	Laminar and Turbulent
21	External	Air	Laminar and Turbulent
22	External	Air	Laminar and Turbulent
23	External	Air	Laminar and Turbulent
24	External	Air	Laminar and Turbulent
25	External	Air	Laminar and Turbulent
26	External	Air	Laminar and Turbulent

27	External	Air	Laminar and Turbulent
28	External	Air	Laminar and Turbulent
29	External	Air	Laminar and Turbulent
30	External	Air	Laminar and Turbulent
31	External	Air	Laminar and Turbulent
32	External	Air	Laminar and Turbulent
33	External	Air	Laminar and Turbulent
34	External	Air	Laminar and Turbulent
35	External	Air	Laminar and Turbulent
36	External	Air	Laminar and Turbulent
37	External	Air	Laminar and Turbulent
38	External	Air	Laminar and Turbulent
39	External	Air	Laminar and Turbulent
40	External	Air	Laminar and Turbulent
41	External	Air	Laminar and Turbulent
42	External	Air	Laminar and Turbulent
43	External	Air	Laminar and Turbulent
44	External	Air	Laminar and Turbulent
45	External	Air	Laminar and Turbulent

46	External	Air	Laminar Only
47	External	Air	Laminar and Turbulent
48	External	Air	Laminar and Turbulent
49	External	Air	Laminar and Turbulent
50	External	Air	Laminar and Turbulent
51	External	Air	Laminar and Turbulent
52	External	Air	Laminar and Turbulent
53	External	Air	Laminar and Turbulent
54	External	Air	Laminar and Turbulent
55	External	Air	Laminar and Turbulent
56	External	Air	Laminar and Turbulent
57	External	Air	Laminar and Turbulent
58	External	Air	Laminar and Turbulent
59	External	Air	Laminar and Turbulent
60	External	Air	Laminar and Turbulent
61	External	Air	Laminar and Turbulent
62	External	Air	Laminar and Turbulent
63	External	Air	Laminar and Turbulent
64	External	Air	Laminar and Turbulent

65	External	Air	Laminar and Turbulent
66	External	Air	Laminar and Turbulent
67	External	Air	Laminar and Turbulent
68	External	Air	Laminar and Turbulent
69	External	Air	Laminar and Turbulent
70	External	Air	Laminar and Turbulent
71	External	Air	Laminar and Turbulent
72	External	Air	Laminar and Turbulent
73	External	Air	Laminar and Turbulent
74	External	Air	Laminar and Turbulent
75	External	Air	Laminar and Turbulent
76	External	Air	Laminar and Turbulent
77	External	Air	Laminar and Turbulent
78	External	Air	Laminar and Turbulent
79	External	Air	Laminar and Turbulent

Table 18: General settings by simulation number part 2

General Solid Settings			
Simulation number	Thermal Condition	Wall Temperature (K)	Wall Heat Flux (K)

1	Constant Temperature	303.2	-
2	Constant Temperature	303.2	-
3	Constant Temperature	303.2	-
4	Constant Temperature	303.2	-
5	Constant Temperature	303.2	-
6	Constant Temperature	303.2	-
7	Constant Temperature	303.2	-
8	Constant Temperature	303.2	-
9	Constant Temperature	303.2	-
10	Constant Temperature	303.2	-
11	Constant Temperature	303.2	-
12	Constant Temperature	303.2	-
13	Constant Temperature	303.2	-
14	Constant Temperature	303.2	-
15	Constant Temperature	303.2	-
16	Constant Temperature	303.2	-
17	Constant Temperature	303.2	-
18	Constant Temperature	303.2	-
19	Constant Temperature	303.2	-

20	Constant Temperature	303.2	-
21	Constant Temperature	303.2	-
22	Constant Temperature	303.2	-
23	Constant Temperature	303.2	-
24	Constant Temperature	303.2	-
25	Constant Temperature	303.2	-
26	Constant Temperature	303.2	-
27	Constant Temperature	303.2	-
28	Constant Temperature	303.2	-
29	Constant Temperature	303.2	-
30	Constant Temperature	303.2	-
31	Constant Temperature	303.2	-
32	Constant Temperature	303.2	-
33	Constant Temperature	303.2	-
34	Constant Temperature	303.2	-
35	Constant Temperature	303.2	-
36	Constant Temperature	303.2	-
37	Constant Temperature	303.2	-
38	Constant Temperature	303.2	-

39	Constant Temperature	303.2	-
40	Constant Temperature	303.2	-
41	Constant Temperature	303.2	-
42	Constant Temperature	303.2	-
43	Constant Temperature	303.2	-
44	Constant Temperature	303.2	-
45	Constant Temperature	303.2	-
46	Constant Temperature	303.2	-
47	Constant Temperature	303.2	-
48	Constant Temperature	303.2	-
49	Constant Temperature	303.2	-
50	Constant Temperature	303.2	-
51	Constant Temperature	303.2	-
52	Constant Temperature	303.2	-
53	Constant Heat Flux	816	-
54	Constant Heat Flux	816	-
55	Constant Heat Flux	816	-
56	Constant Heat Flux	816	-
57	Constant Heat Flux	816	-

58	Constant Heat Flux	816	-
59	Constant Heat Flux	816	-
60	Constant Temperature	303.2	-
61	Constant Temperature	303.2	-
62	Constant Temperature	303.2	-
63	Constant Temperature	303.2	-
64	Constant Temperature	303.2	-
65	Constant Heat Flux	-	23.5
66	Constant Heat Flux	-	47.1
67	Constant Heat Flux	-	203
68	Constant Heat Flux	-	816
69	Constant Heat Flux	-	1294
70	Constant Temperature	303.2	-
71	Constant Temperature	303.2	-
72	Constant Temperature	303.2	-
73	Constant Temperature	303.2	-
74	Constant Temperature	303.2	-
75	Constant Temperature	303.2	-
76	Constant Temperature	303.2	-

77	Constant Temperature	303.2	-
78	Constant Temperature	303.2	-
79	Constant Temperature	303.2	-

Table 19: General solid settings by simulation number

2D-External-Constant Temperature Results Summary						
Flow Type	Reynolds Number	Average Heat Transfer Coefficient (W/m ² K)			Percent Difference	
		SOLIDWORKS	Cengal and Ghajar	Furber	Cengal and Ghajar	Edwards and Furber
Laminar	8.00E+04	1.8	1.7	1.7	6.1%	9.5%
Mixed	3.20E+05	4.4	3.8	N/A	14.0%	N/A
Mixed	1.28E+06	25.1	18.1	24.5	38.4%	2.5%
Turbulent	5.60E+06	77.7	85.1	N/A	8.7%	N/A
Turbulent	9.60E+06	108.5	131.0	N/A	17.2%	N/A

Table 20: Comparison of predicted heat transfer coefficients for 2D-External-Constant Temperature

2D-External-Constant Heat Flux Results Summary						
Flow Type	Reynolds Number	Average Heat Transfer Coefficient (W/m ² K)			Percent Difference	
		SOLIDWORKS	Cengal and Ghajar	Furber	Cengal and Ghajar	Edwards and Furber
Laminar	8.00E+04	2.4	2.4	N/A	2.4%	N/A
Mixed	3.20E+05	5.5	4.7	N/A	17.6%	N/A
Mixed	1.28E+06	31.6	20.3	N/A	56.1%	N/A
Turbulent	5.60E+06	83.7	81.6	N/A	2.6%	N/A
Turbulent	9.60E+06	116.3	129.4	N/A	10.1%	N/A

Table 21: Comparison of predicted heat transfer coefficients for 2D-External-Constant Heat Flux case

2D-Internal-Constant Temperature Results Summary						
Flow Type	Reynolds Number	Average Heat Transfer Coefficient (W/m ² K)			Percent Difference	
		SOLIDWORKS	Cengal and Ghajar	Furber	Cengal and Ghajar	Edwards and Furber
Laminar	8.00E+04	1.8	1.7	1.7	3.0%	6.4%
Mixed	3.20E+05	5.8	3.5	N/A	69.2%	N/A
Mixed	1.28E+06	14.4	18.1	24.5	20.5%	41.1%
Turbulent	5.60E+06	72.4	85.1	N/A	14.9%	N/A
Turbulent	9.60E+06	111.9	131.0	N/A	14.6%	N/A

Table 22: Comparison of predicted heat transfer coefficients for 2D-Internal-Constant Temperature case

3D-Internal-Constant Temperature Results Summary						
Flow Type	Reynolds Number	Average Heat Transfer Coefficient (W/m ² K)			Percent Difference	
		SOLIDWORKS	Cengal and Ghajar	Furber	Cengal and Ghajar	Edwards and Furber
Laminar	8.00E+04	1.8	1.7	1.7	4.7%	8.1%
Mixed	3.20E+05	5.3	3.5	N/A	52.4%	N/A
Mixed	1.28E+06	22.4	18.1	24.5	23.5%	8.5%
Turbulent	5.60E+06	70.0	85.1	N/A	17.8%	N/A
Turbulent	9.60E+06	112.5	131.0	N/A	14.1%	N/A

Table 23: Comparison of predicted heat transfer coefficients for 3D-Internal-Constant Temperature case

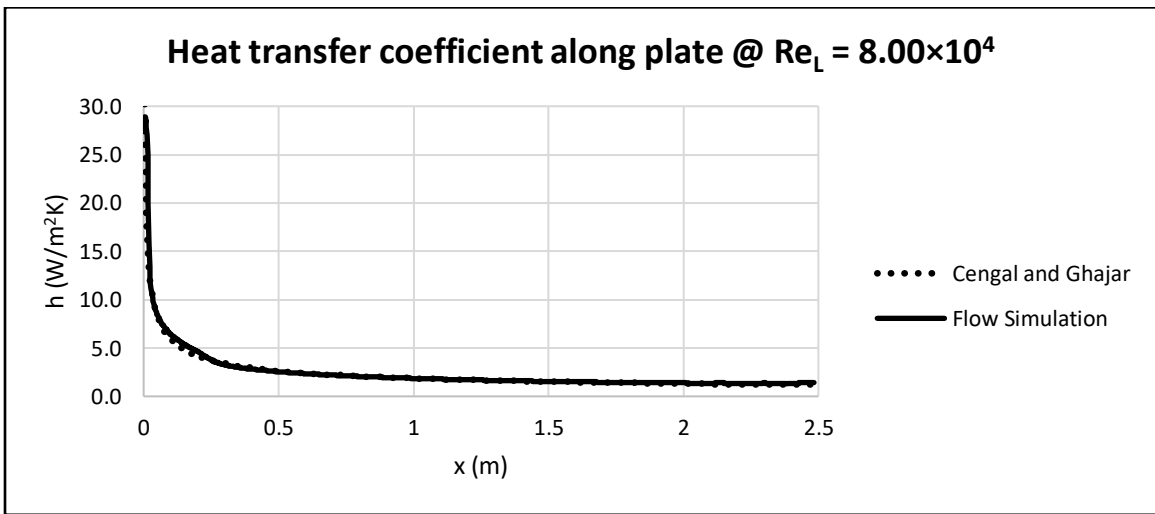


Figure 47: Heat transfer coefficient along plate at $Re_L = 8.00 \times 10^4$ for 2D-Internal-Constant Heat Flux case

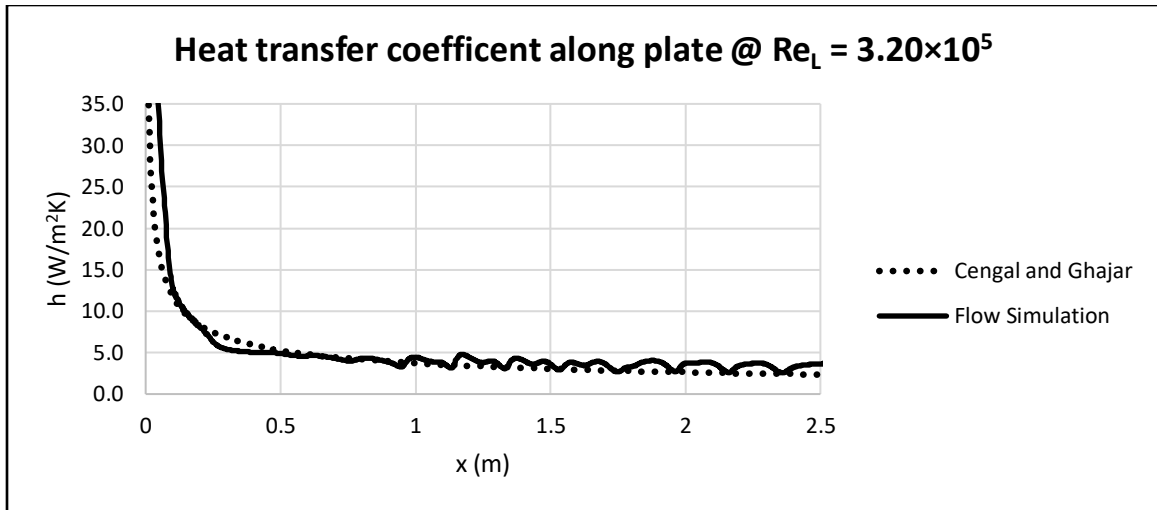


Figure 48: Heat transfer coefficient along plate at $Re_L = 3.20 \times 10^5$ for 2D-Internal-Constant Heat Flux case

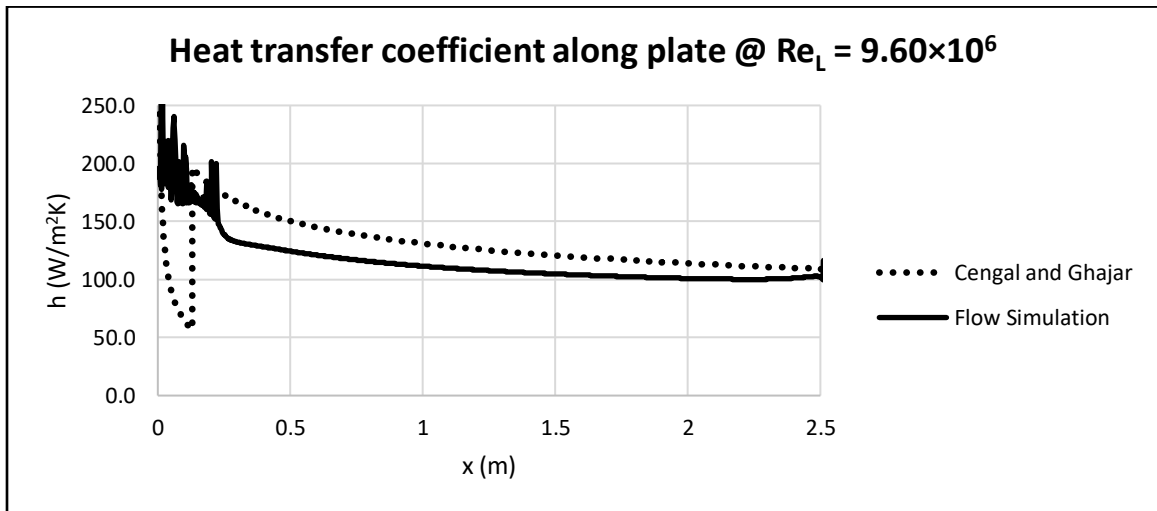


Figure 49: Heat transfer coefficient along plate at $Re_L = 9.60 \times 10^6$ for 2D-Internal-Constant Heat Flux case

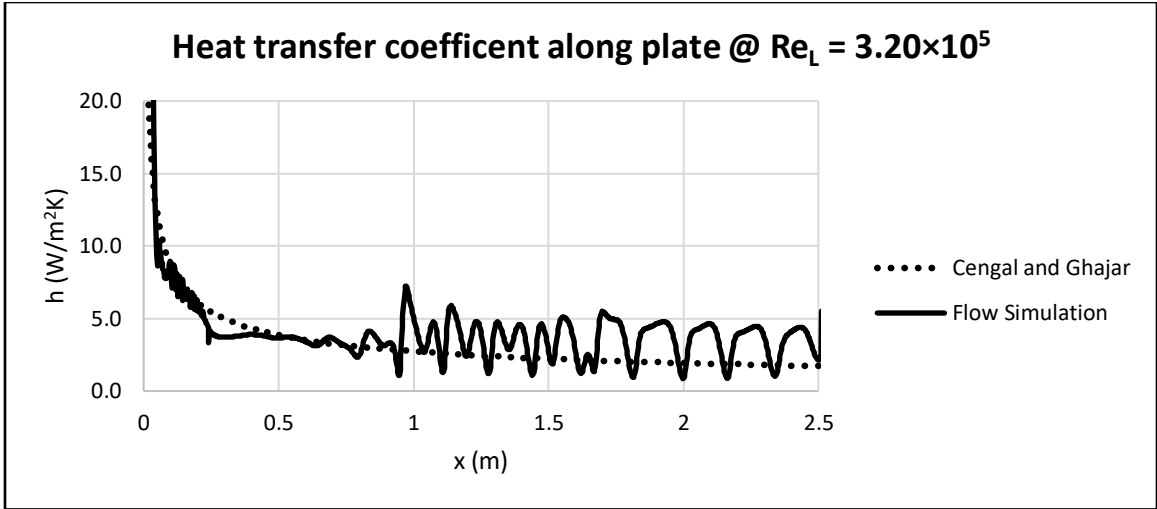


Figure 50: Heat transfer coefficient along plate at $Re_L = 3.20 \times 10^5$ for 2D-External-Constant Temperature case

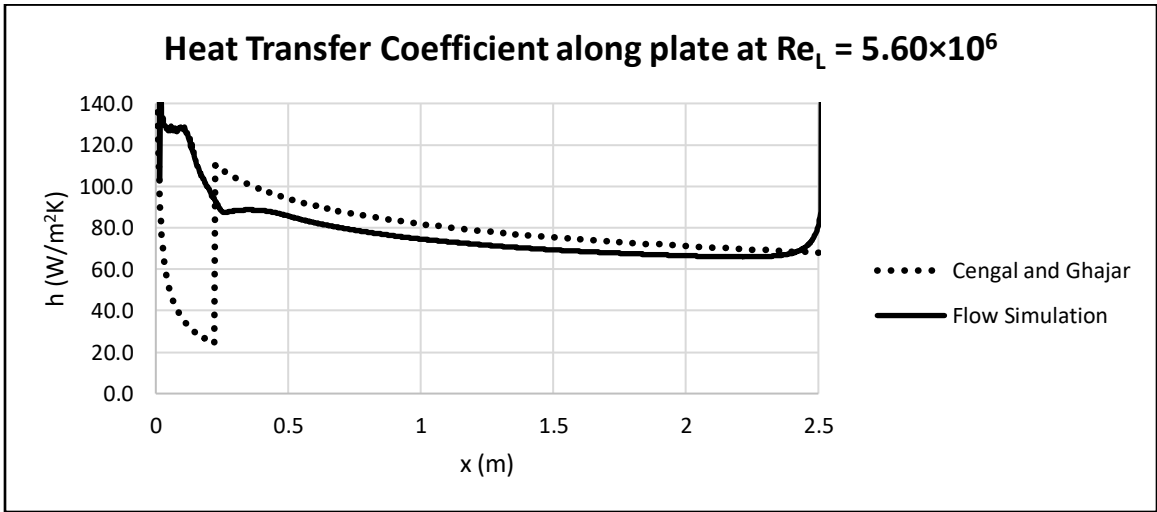


Figure 51: Heat transfer coefficient along plate at $Re_L = 5.60 \times 10^6$ for 2D-External-Constant Temperature case

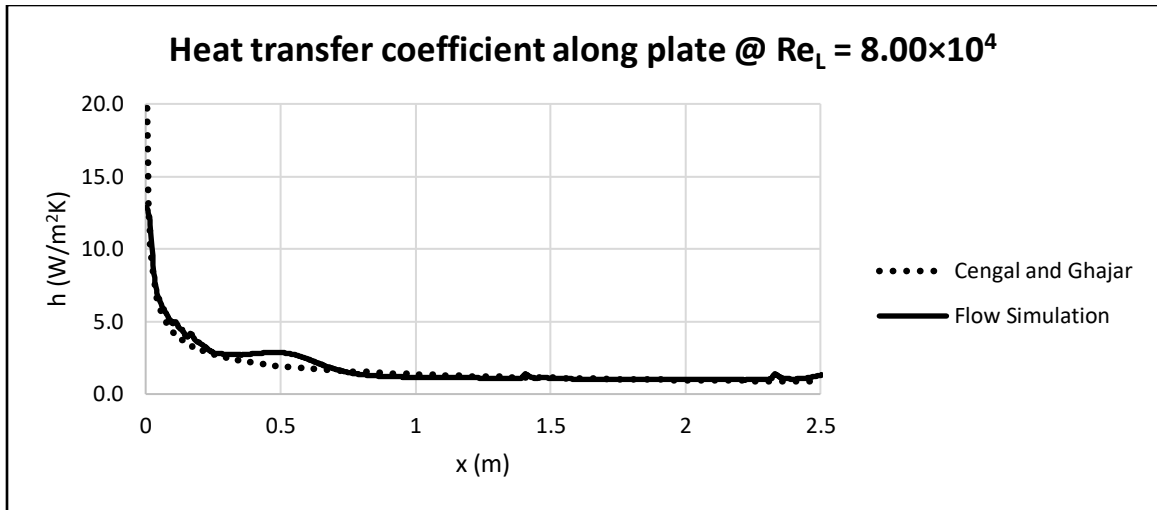


Figure 52: Heat transfer coefficient along plate at $Re_L = 8.00 \times 10^4$ for 2D-Internal-Constant Temperature case

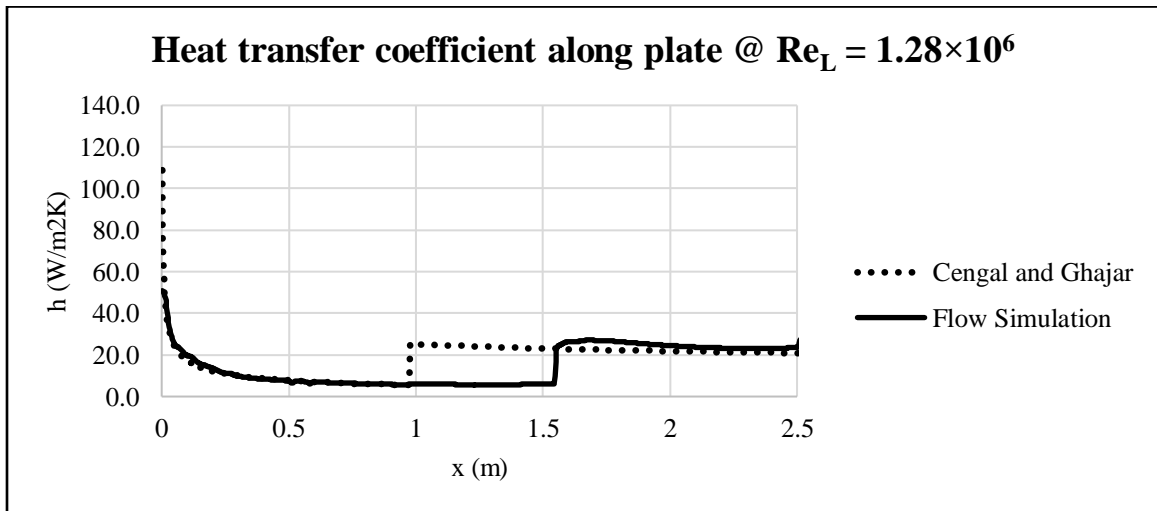


Figure 53: Heat transfer coefficient along plate at $Re_L = 1.28 \times 10^6$ for 2D-Internal-Constant Temperature case

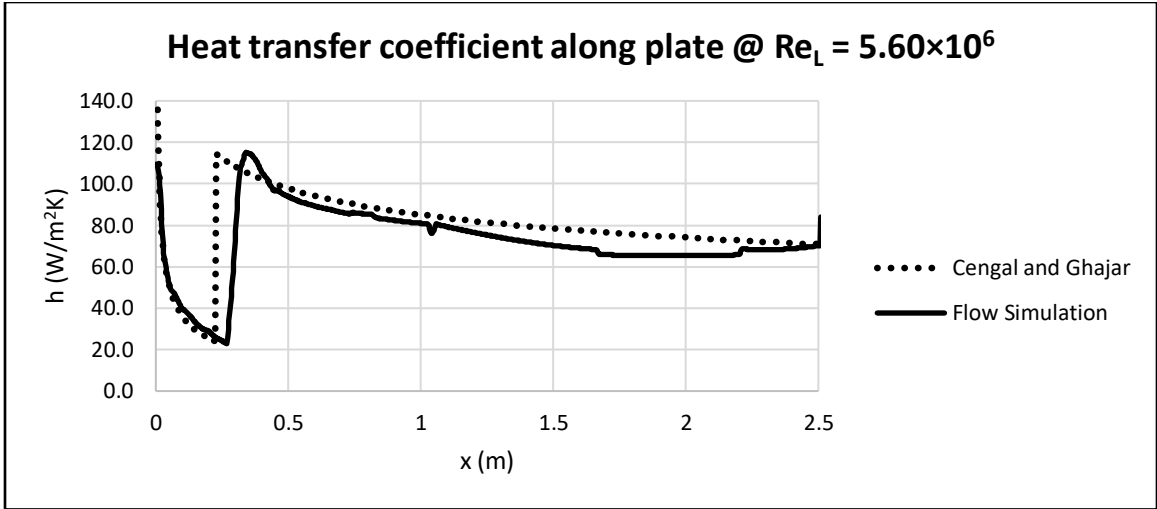


Figure 54: Heat transfer coefficient along plate at $Re_L = 5.60 \times 10^6$ for 2D-Internal-Constant Temperature case

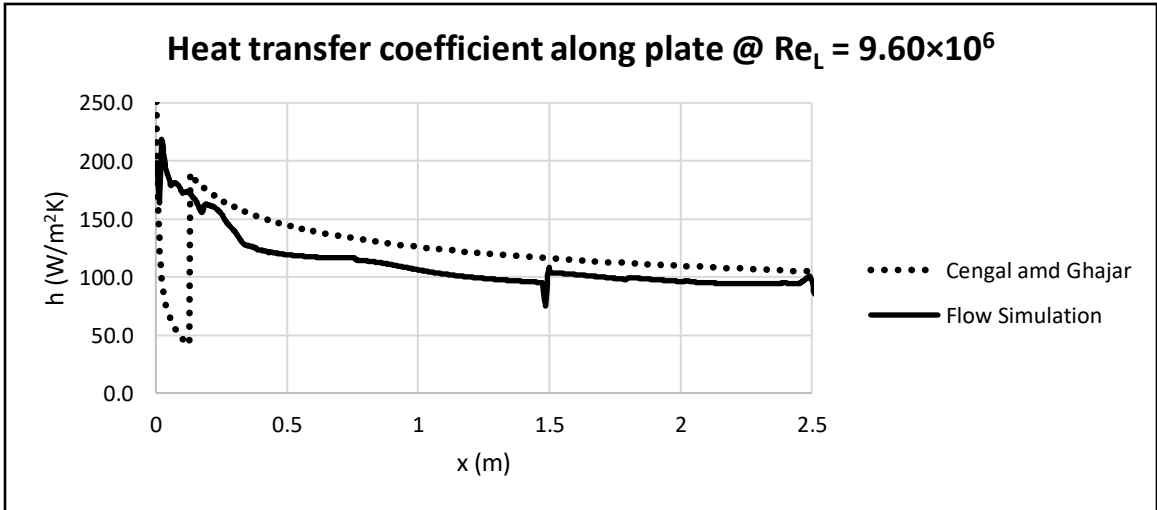


Figure 55: Heat transfer coefficient along plate at $Re_L = 9.60 \times 10^6$ for 2D-Internal-Constant Temperature case

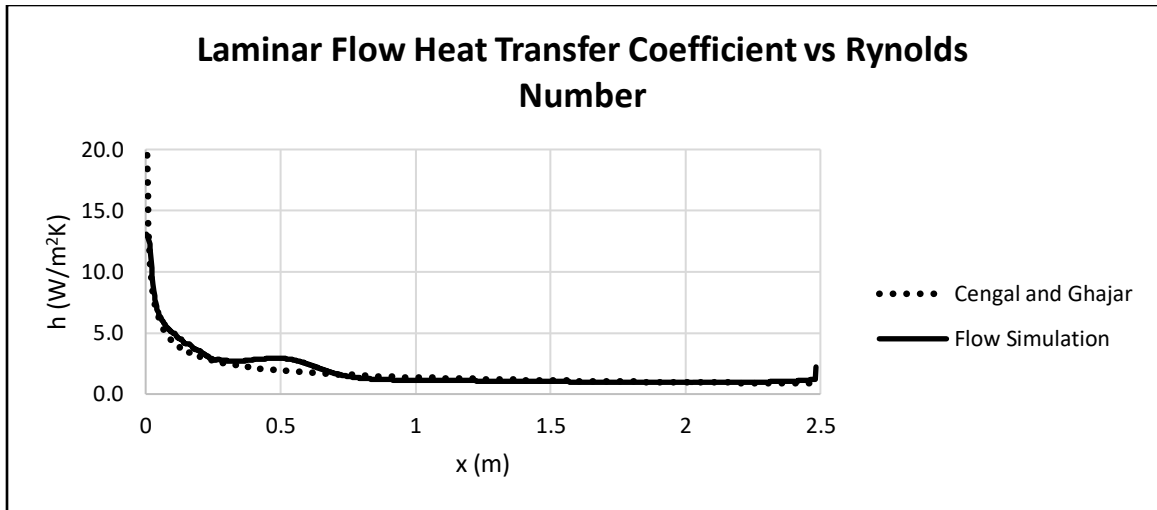


Figure 56: Heat transfer coefficient along plate at $Re_L = 8.00 \times 10^4$ for 3D-Internal-Constant Temperature case

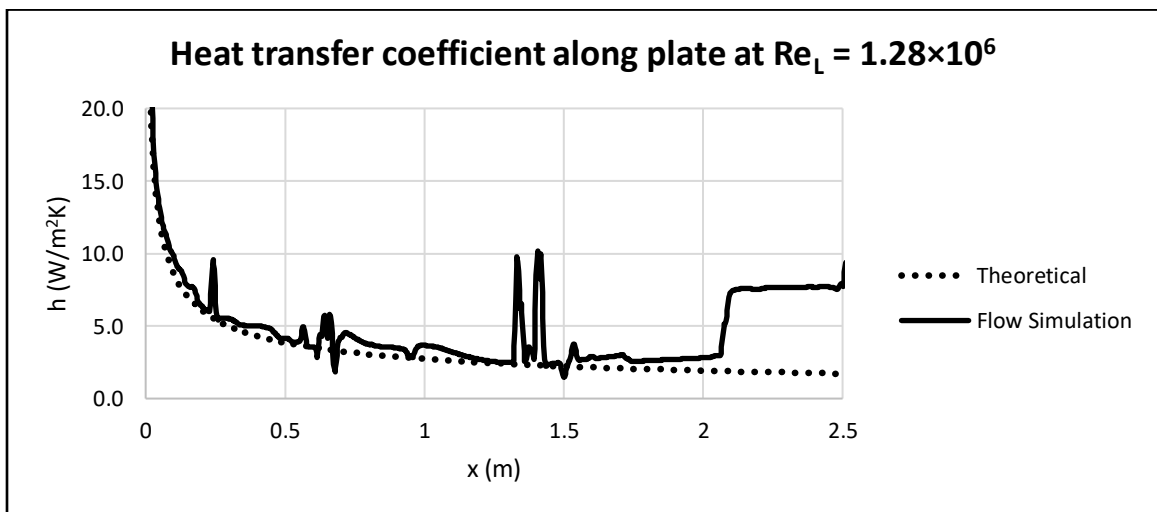


Figure 57: Heat transfer coefficient along plate at $Re_L = 3.20 \times 10^6$ for 3D-Internal-Constant Temperature case

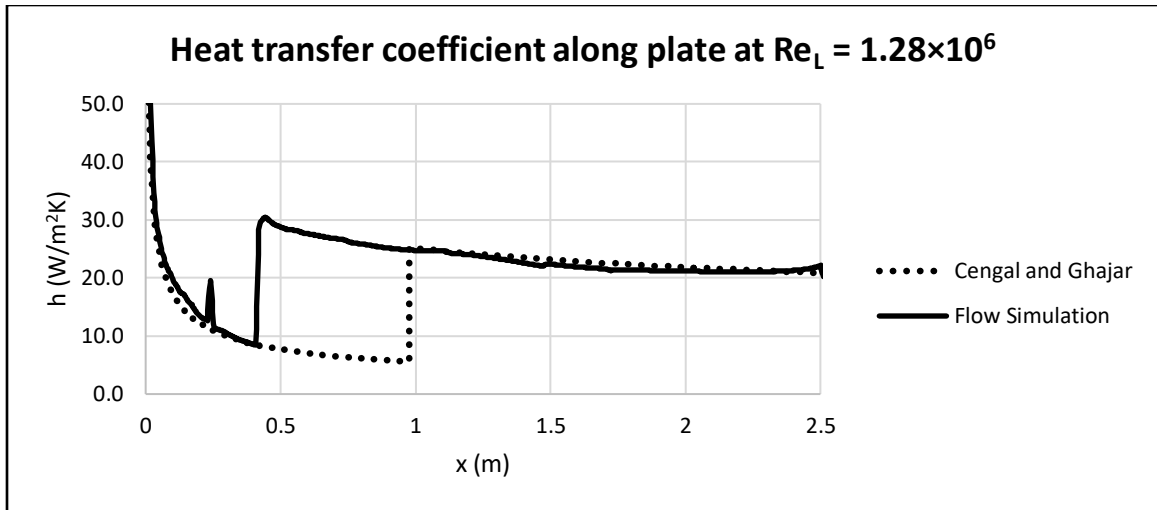


Figure 58: Heat transfer coefficient along plate at $Re_L = 1.28 \times 10^6$ for 3D-Internal-Constant Temperature case

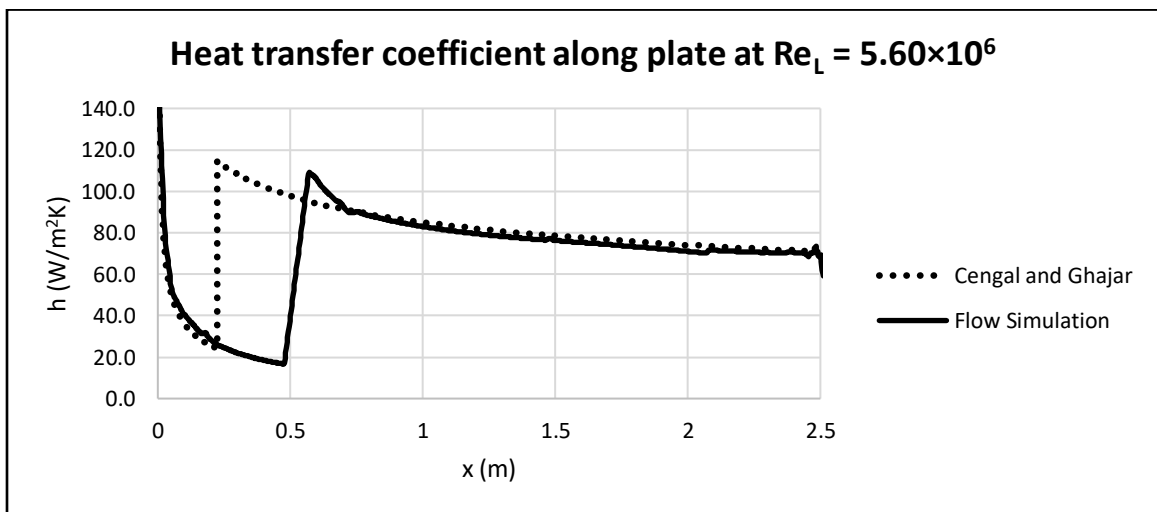


Figure 59: Heat transfer coefficient along plate at $Re_L = 5.60 \times 10^6$ for 3D-Internal-Constant Temperature case

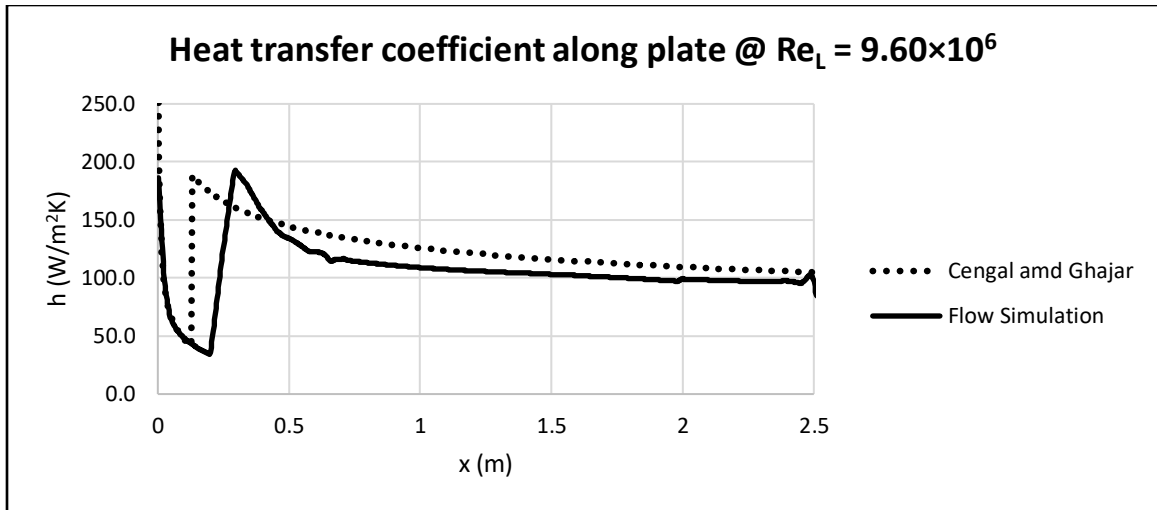


Figure 60: Heat transfer coefficient along plate at $Re_L = 9.60 \times 10^6$ for 3D-Internal-Constant Temperature case

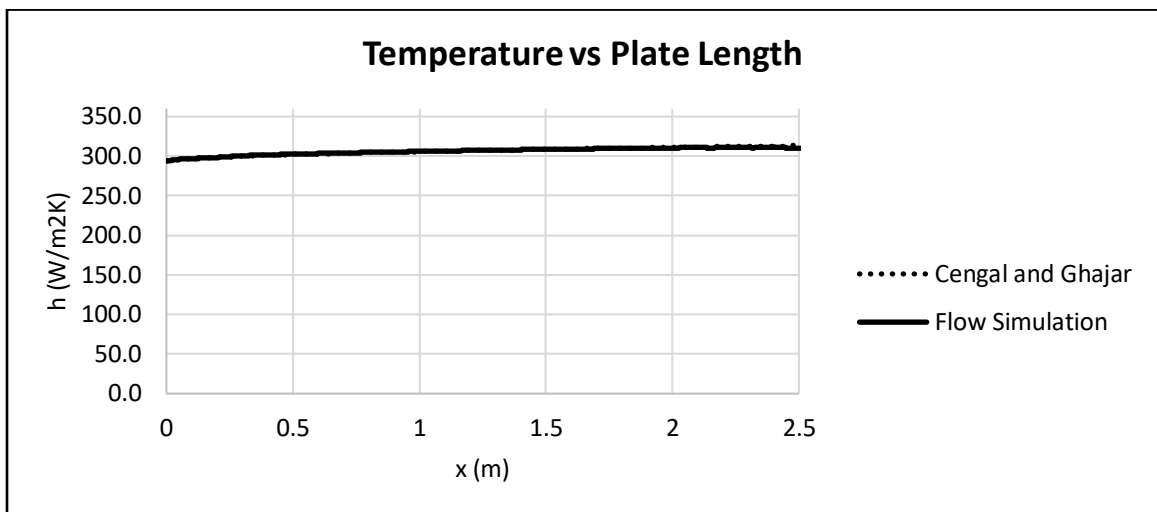


Figure 61: Temperature along plate at $Re_L = 8.00 \times 10^4$ for 2D-Internal-Constant Heat Flux case

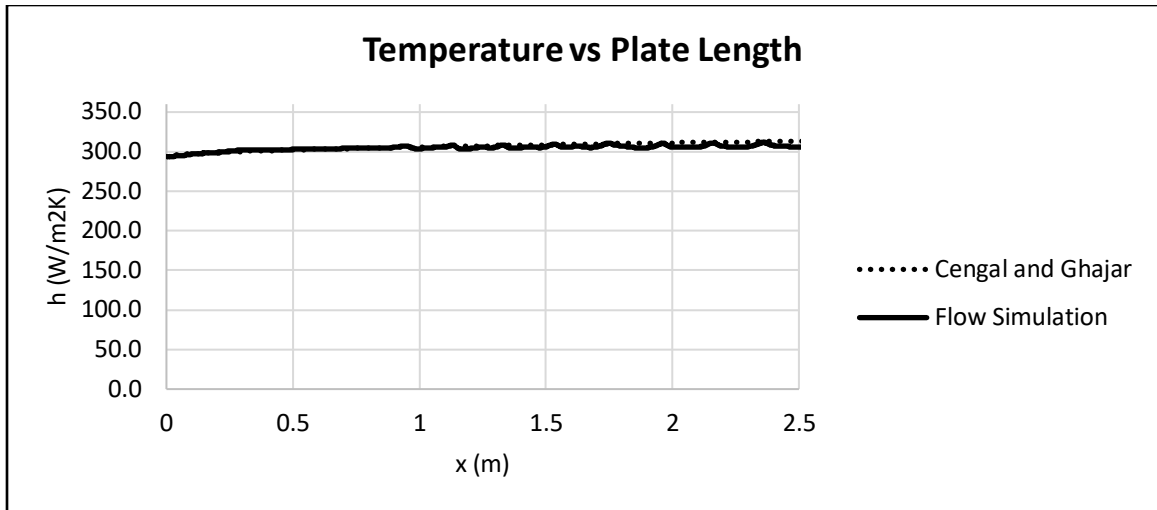


Figure 62: Temperature along plate at $Re_L = 3.20 \times 10^5$ for 2D-Internal-Constant Heat Flux case

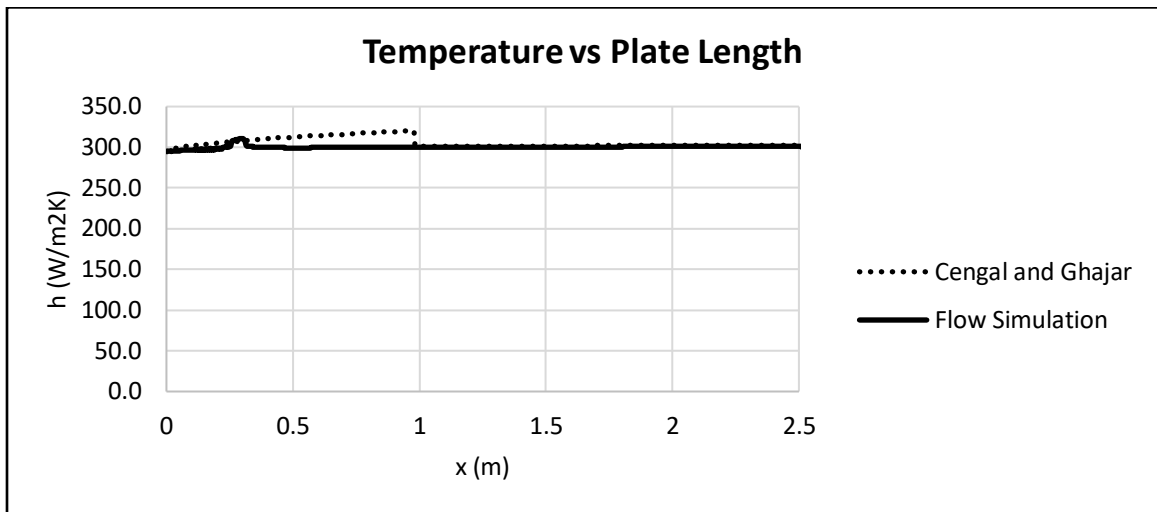


Figure 63: Temperature along plate at $Re_L = 1.28 \times 10^6$ for 2D-Internal-Constant Heat Flux case

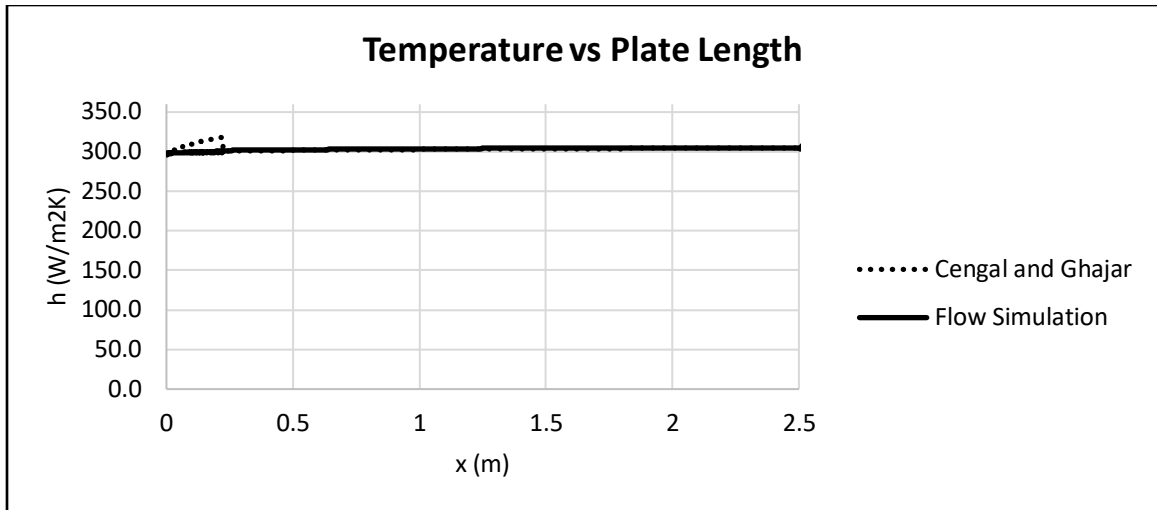


Figure 64: Temperature along plate at $Re_L = 5.60 \times 10^6$ for 2D-Internal-Constant Heat Flux case

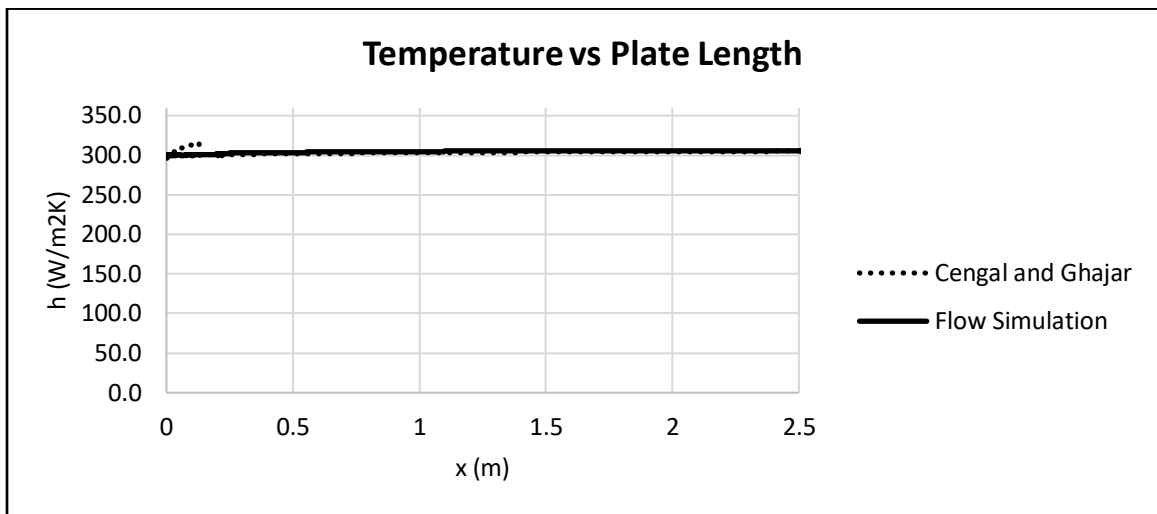


Figure 65: Temperature along plate at $Re_L = 9.60 \times 10^6$ for 2D-Internal-Constant Heat Flux case

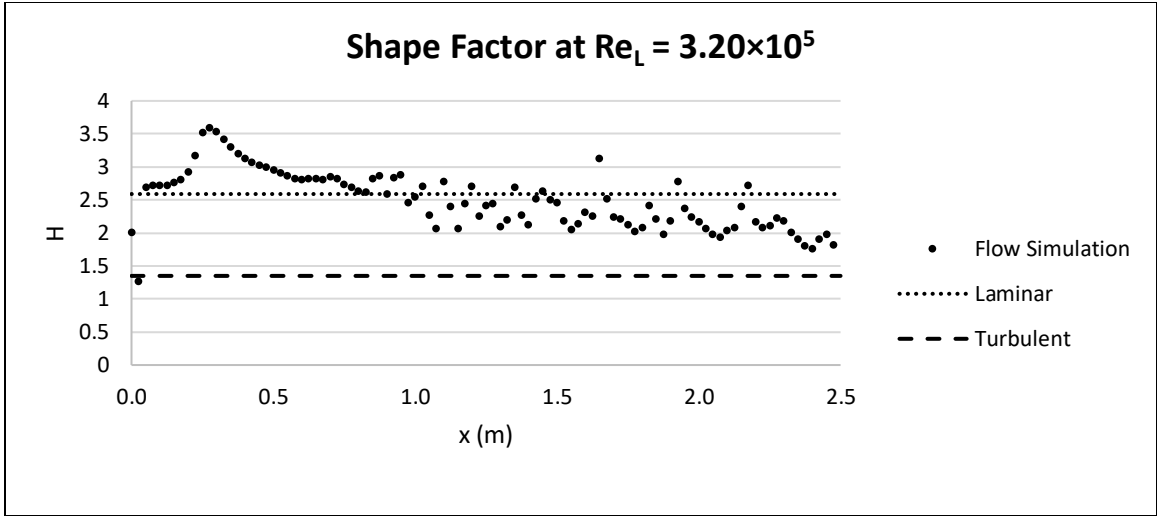


Figure 66: Shape factor along plate at $Re_L = 3.20 \times 10^5$ for 2D-External-Constant Temperature case

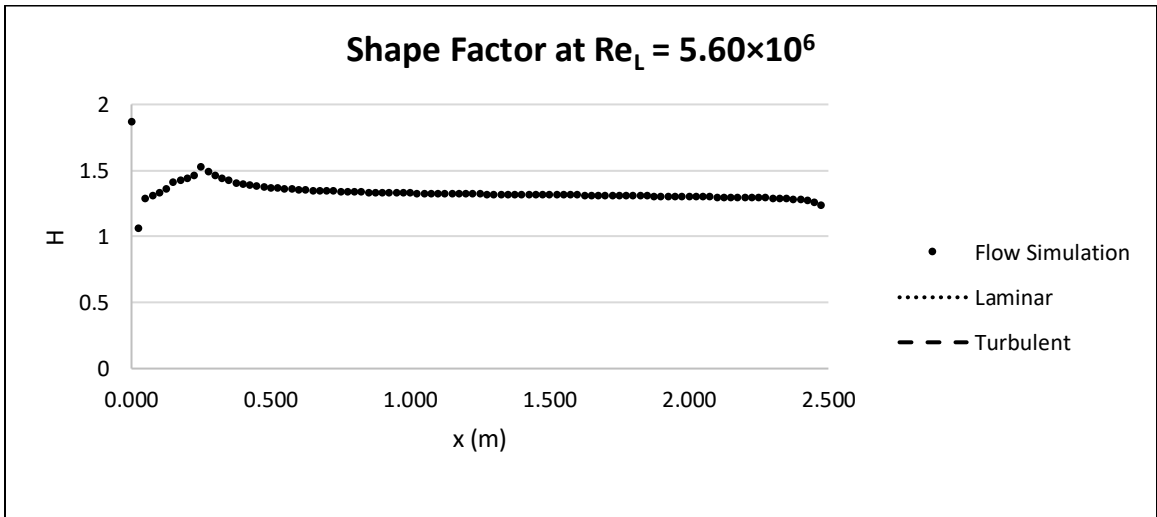


Figure 67: Shape factor along plate at $Re_L = 5.60 \times 10^6$ for 2D-External-Constant Temperature case

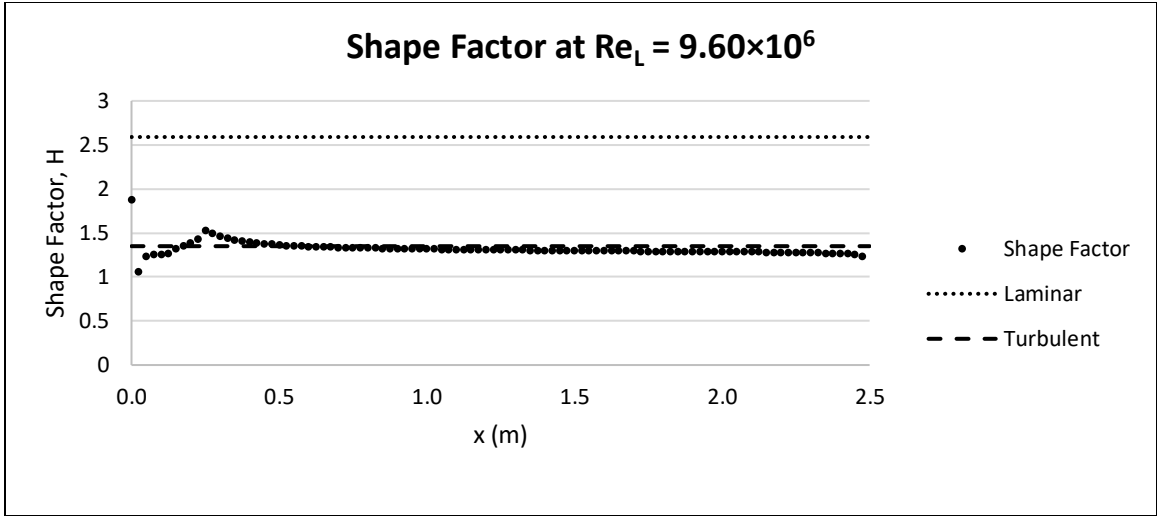


Figure 68: Shape factor along plate at $Re_L = 9.60 \times 10^6$ for 2D-External-Constant Temperature case

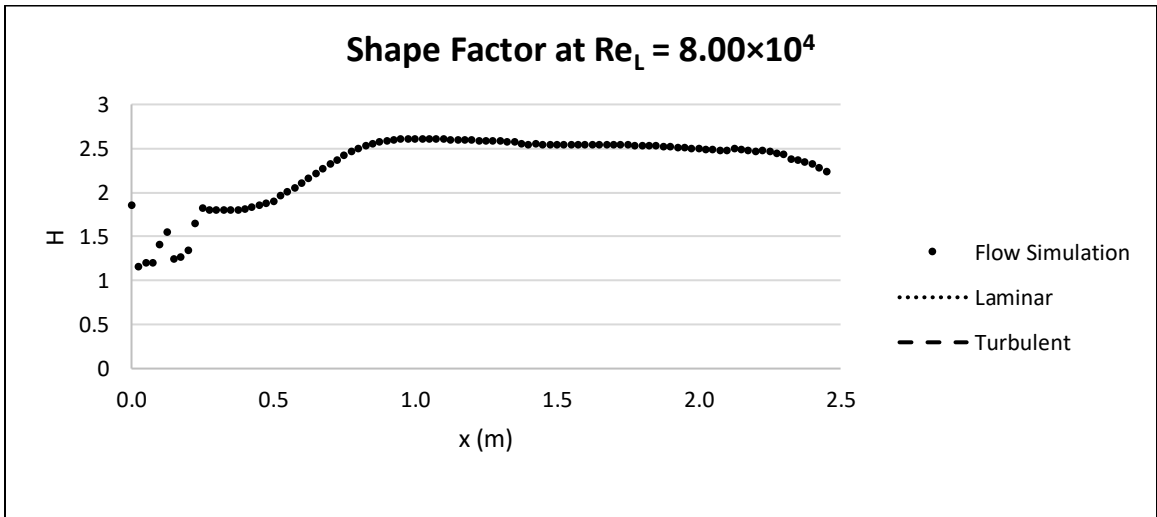


Figure 69: Shape factor along plate at $Re_L = 8.00 \times 10^4$ for 2D-External-Constant Temperature case

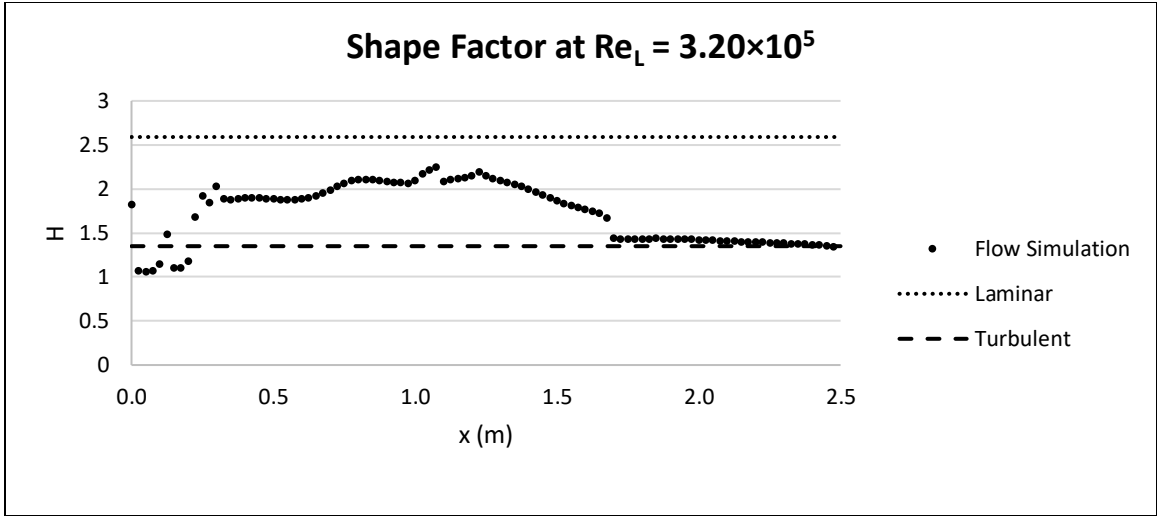


Figure 70: Shape factor along plate at $Re_L = 3.20 \times 10^5$ for 2D-External-Constant Temperature case

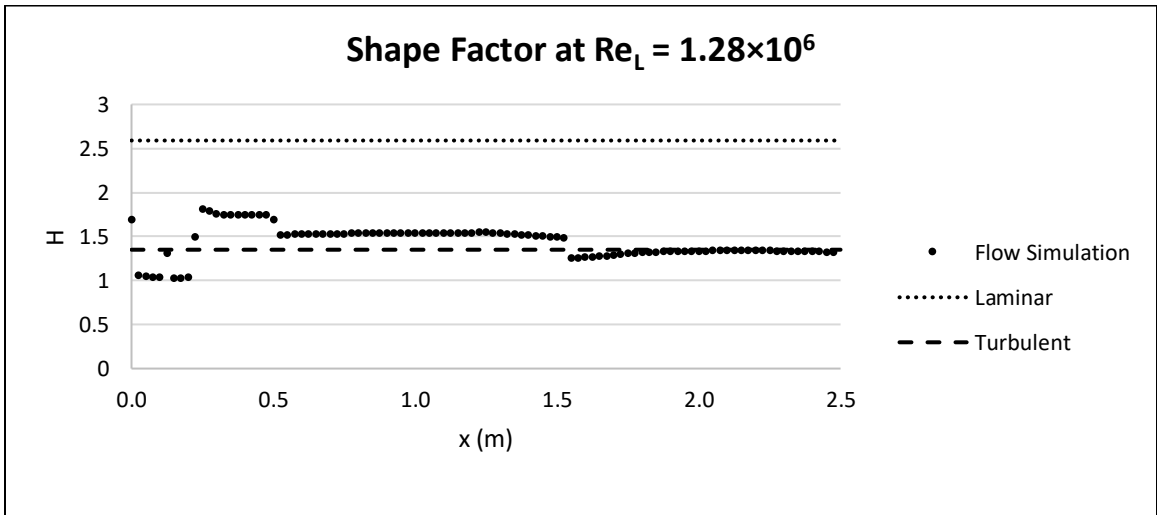


Figure 71: Shape factor along plate at $Re_L = 5.60 \times 10^6$ for 2D-Internal-Constant Temperature case

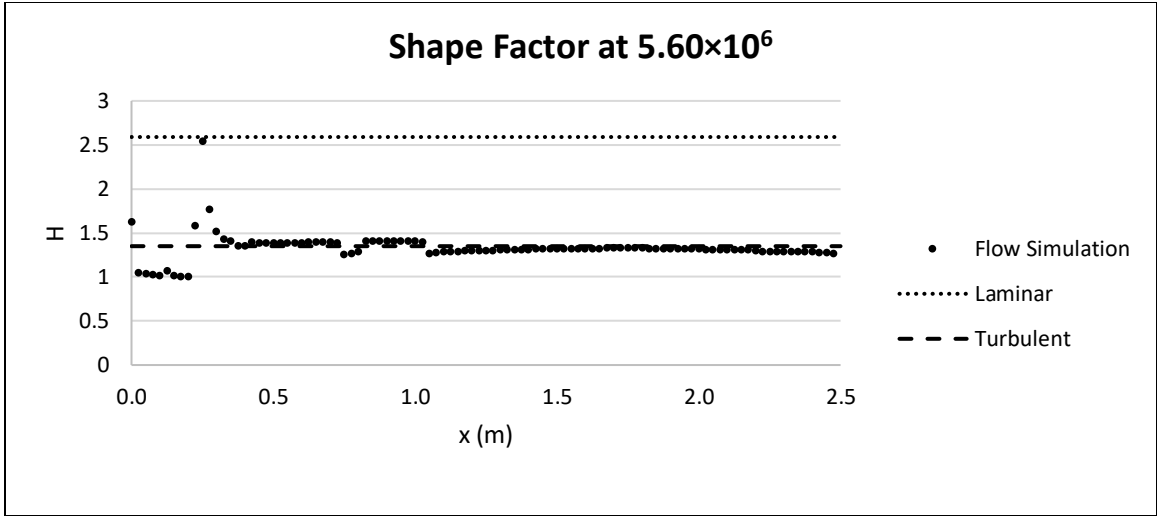


Figure 72: Shape factor along plate at $Re_L = 5.60 \times 10^6$ for 2D-Internal-Constant Temperature case

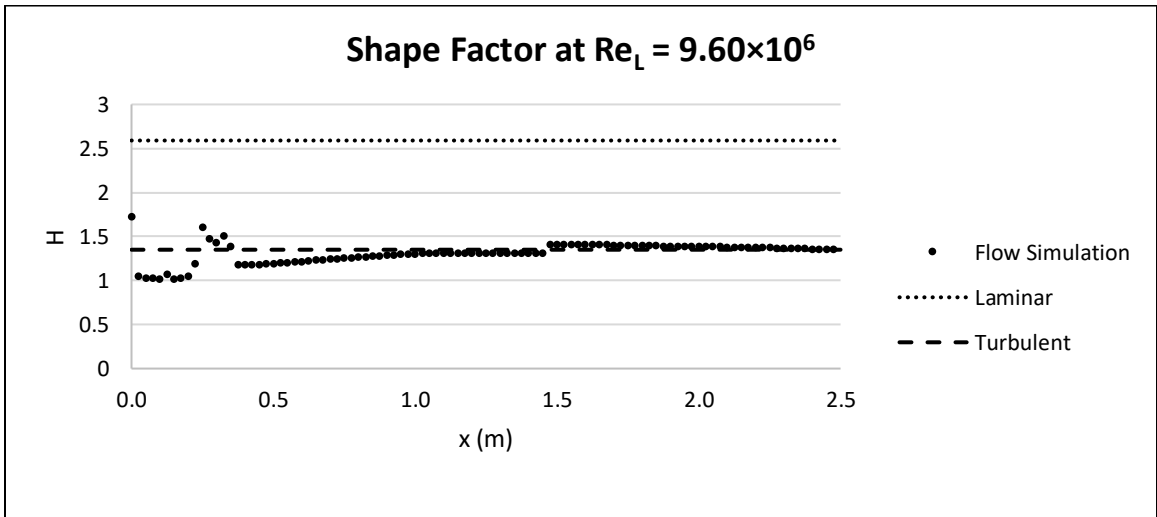


Figure 73: Shape factor along plate at $Re_L = 9.60 \times 10^6$ for 2D-Internal-Constant Temperature case

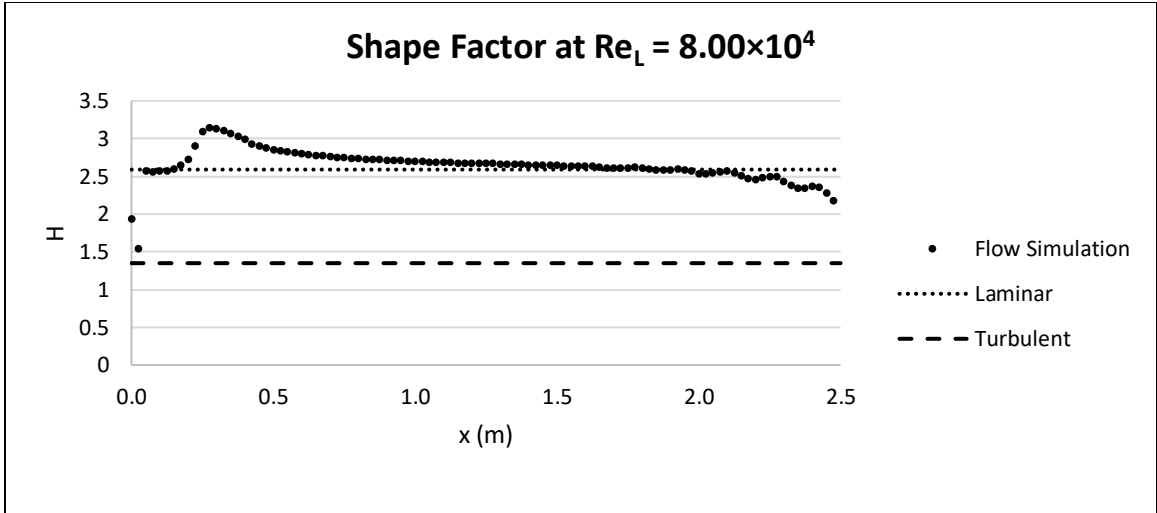


Figure 74: Shape factor along plate at $Re_L = 8.00 \times 10^4$ for 2D-External-Constant Heat Flux case

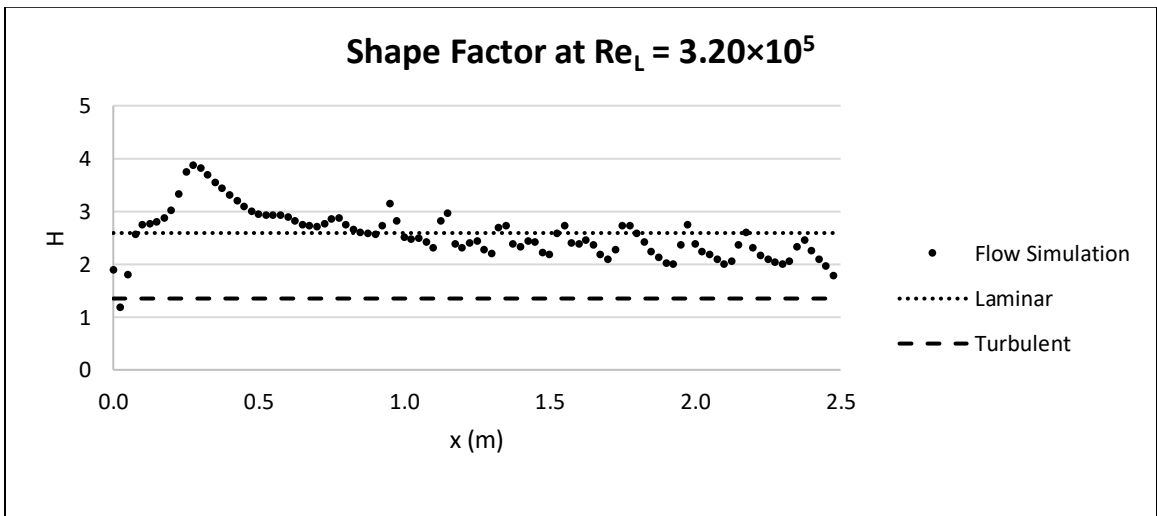


Figure 75: Shape factor along plate at $Re_L = 3.20 \times 10^5$ for 2D-External-Constant Heat Flux case

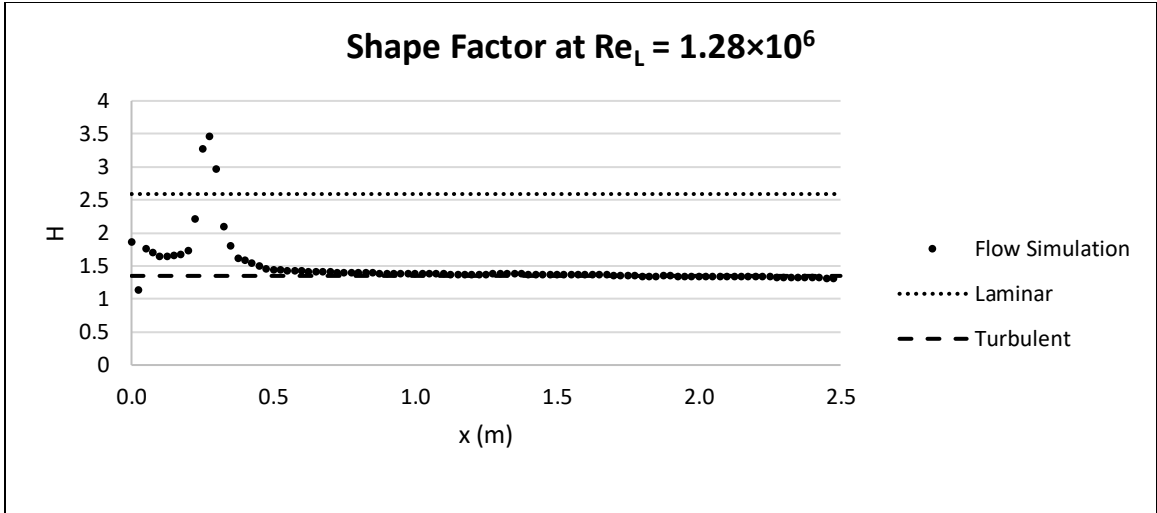


Figure 76: Shape factor along plate at $Re_L = 1.28 \times 10^6$ for 2D-External-Constant Heat Flux case

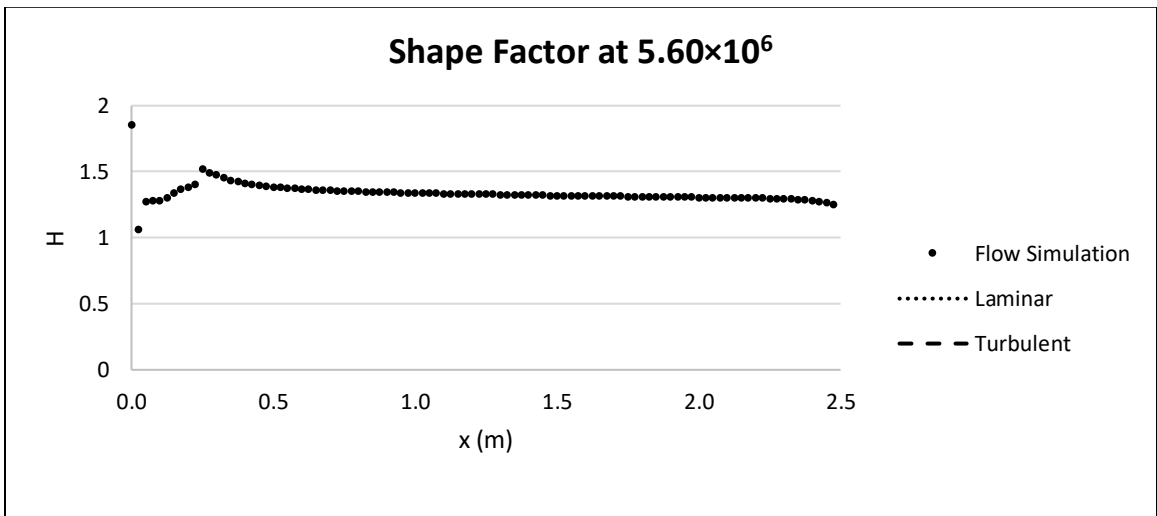


Figure 77: Shape factor along plate at $Re_L = 5.60 \times 10^6$ for 2D-External-Constant Heat Flux case

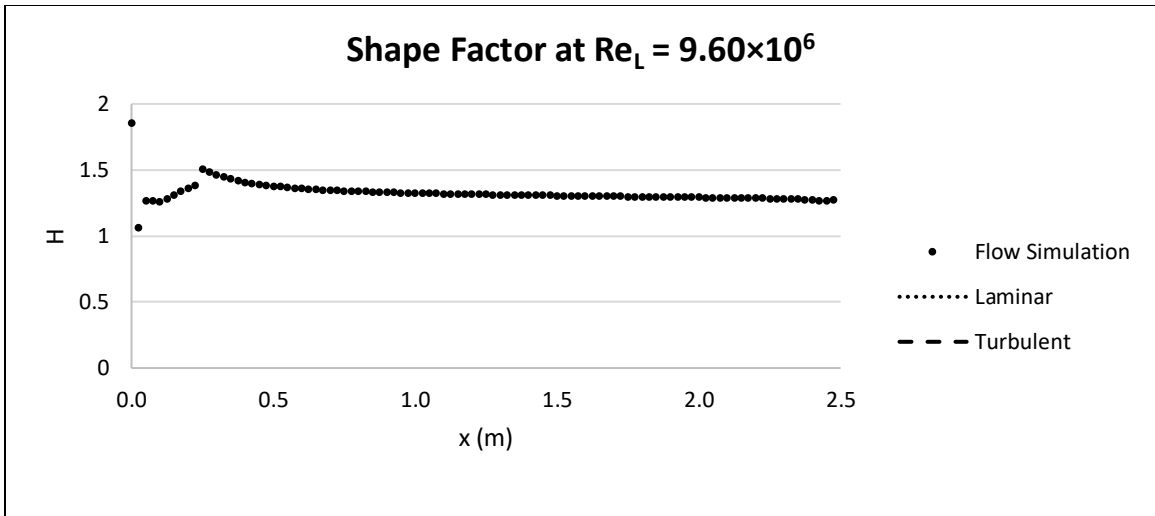


Figure 78: Shape factor along plate at $Re_L = 9.60 \times 10^6$ for 2D-External-Constant Heat Flux case

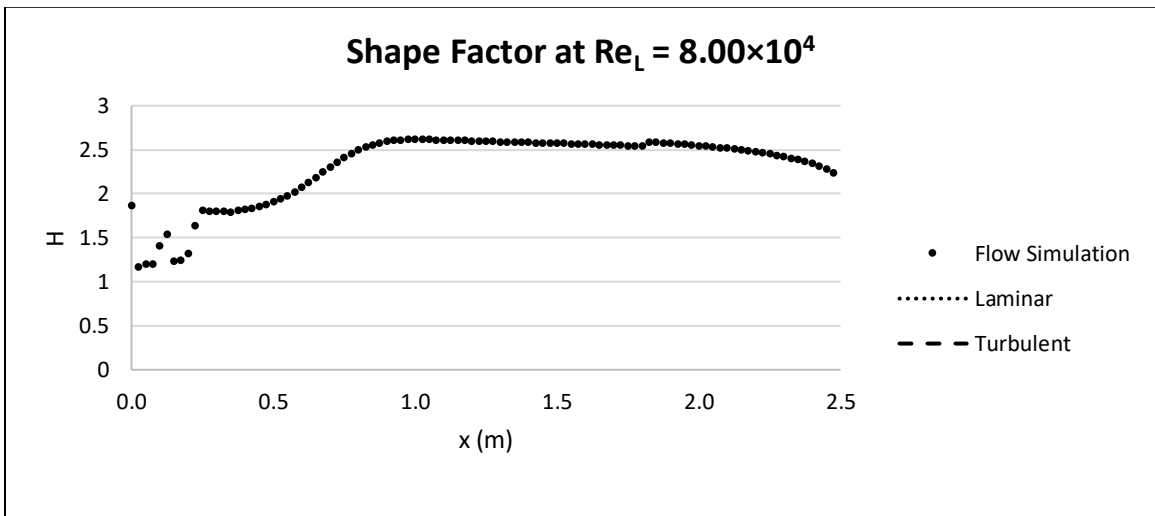


Figure 79: Shape factor along plate at $Re_L = 8.00 \times 10^4$ for 3D-Internal-Constant Temperature case

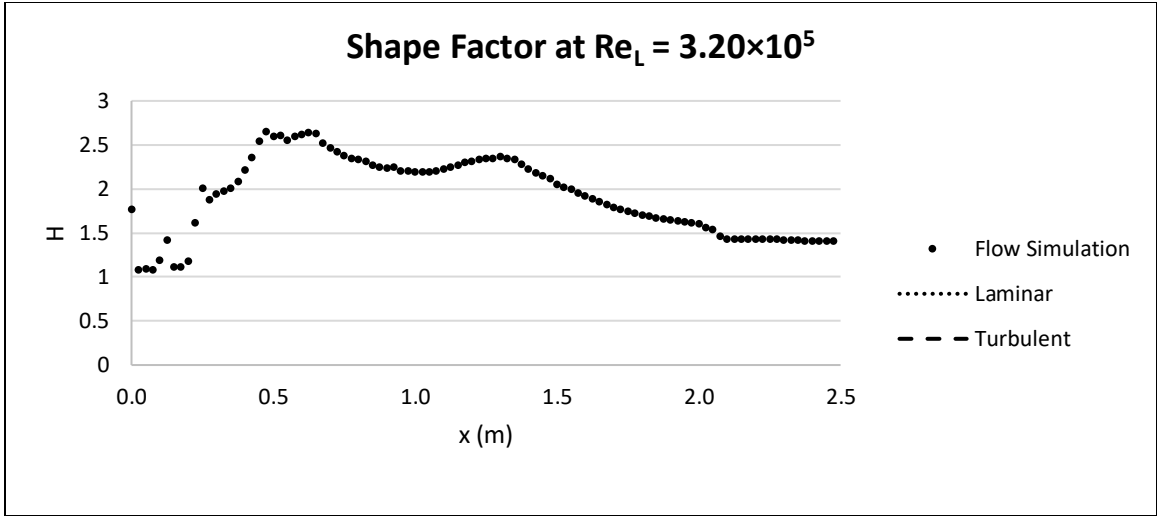


Figure 80: Shape factor along plate at $Re_L = 3.20 \times 10^5$ for 3D-Internal-Constant Temperature case

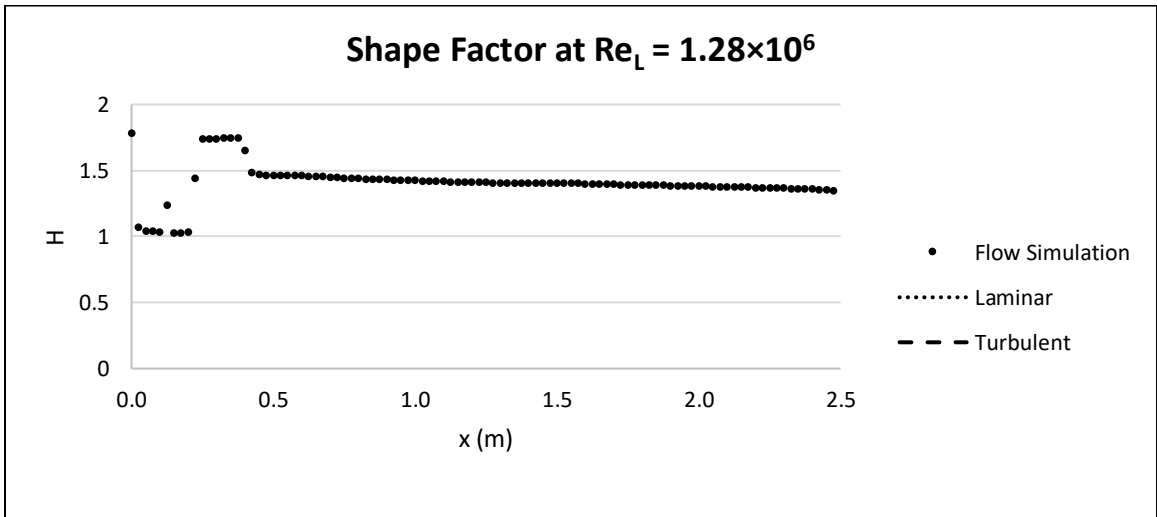


Figure 81: Shape factor along plate at $Re_L = 1.28 \times 10^6$ for 3D-Internal-Constant Temperature case

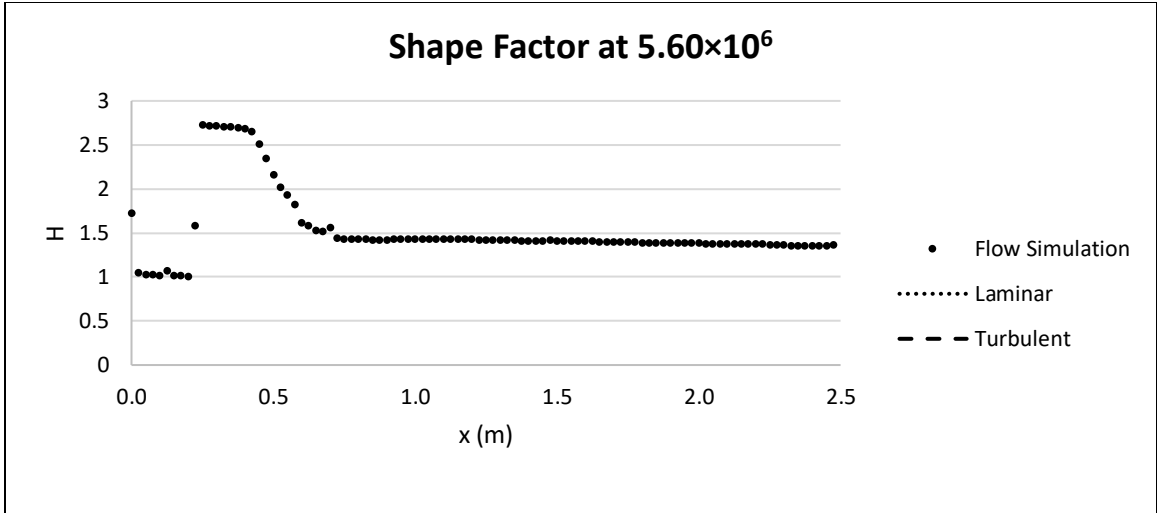


Figure 82: Shape factor along plate at $Re_L = 5.60 \times 10^6$ for 3D-Internal-Constant Temperature case

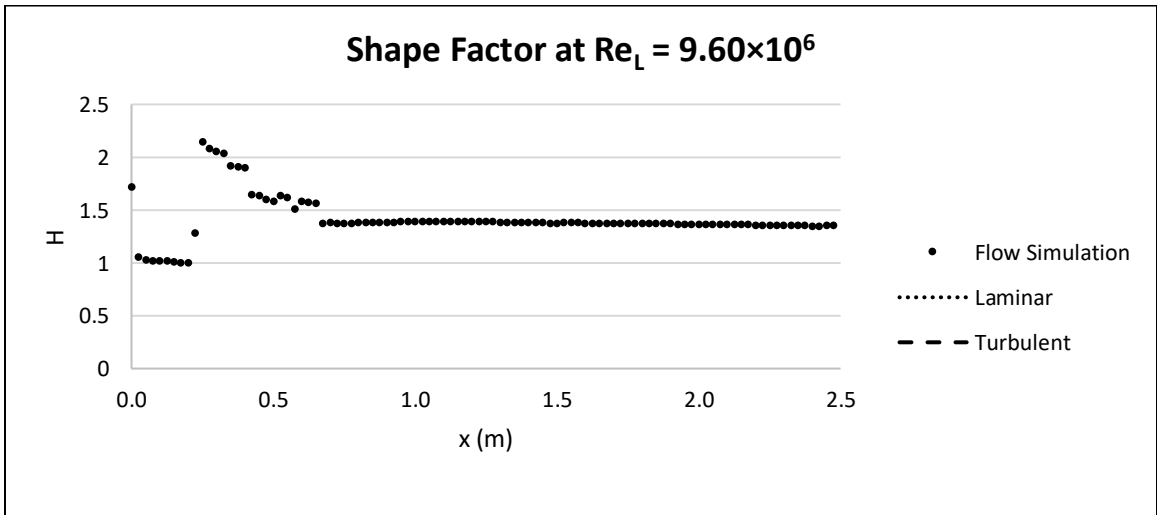


Figure 83: Shape factor along plate at $Re_L = 9.60 \times 10^6$ for 3D-Internal-Constant Temperature case

VITA

Karis L. Reavis

Candidate for the Degree of

Master of Science

Thesis: EFFICACY OF SOLIDWORKS FLOW SIMULATION FOR USE IN
THERMAL MANAGEMENT AND PROPULSION SYSTEMS COOLING OF
UNMANNED AIRCRAFT SYSTEMS

Major Field: Mechanical and Aerospace Engineering

Biographical:

Education:

Completed the requirements for the Master of Science in Mechanical and
Aerospace Engineering at Oklahoma State University, Stillwater, Oklahoma May
2021.

Completed the requirements for the Bachelor of Science in Mechanical and
Aerospace Engineering at Oklahoma State University, Stillwater, Oklahoma May
2017.

Experience:

Applications Engineer at NI

Orange Team CAD Lead for Speedfest 2017 at Oklahoma State University

Teacher's Assistant for Heat Transfer at Oklahoma State University